The Dissertation Committee for Andrew Marcus Hunter
certifies that this is the approved version of the following dissertation:

Capacity of Multi-Antenna Ad Hoc Networks via Stochastic Geometry

Committee:

Jeffrey G. Andrews, Supervisor

Gustavo de Veciana

Robert W. Heath, Jr.

Peter Stone

Martin Haenggi

Capacity of Multi-Antenna Ad Hoc Networks via Stochastic Geometry

by

Andrew Marcus Hunter, B.S., M.S.

DISSERTATION

Presented to the Faculty of the Graduate School of

The University of Texas at Austin

in Partial Fulfillment

of the Requirements

for the Degree of

DOCTOR OF PHILOSOPHY

THE UNIVERSITY OF TEXAS AT AUSTIN

December 2012

To Dinilawi Kanati, whoever *he* is.

Capacity of Multi-Antenna Ad Hoc Networks via Stochastic Geometry

Publication No. _____

Andrew Marcus Hunter, Ph.D.
The University of Texas at Austin, 2012

Supervisor: Jeffrey G. Andrews

This thesis takes as its objective quantifying, comparing, and optimizing multiple-antenna (MIMO) physical layer techniques in dense ad hoc wireless networks. A framework is developed from the spatial shot noise interference model for packet radio network analysis. The framework captures the behavior of a wide variety of signal and interference distributions, which permit inspection of a number of signal processing methods including representatives from most of the major MIMO techniques. Multi-antenna systems for point-to-point are becoming mature and being developed and deployed in many wireless communication systems due to their potential to combat fading, increase spectral efficiency, and overcome interference.

The framework permits an algorithm or system designer to view the network from the perspective of a typical user, to optimize performance in the midst of a given environment, or to view the network as a whole, to determine behavior

that maximizes network performance. In particular, it enables questions to be answered quantitatively, such as which MIMO techniques perform best in a given environment? Or what rate and power settings should be used across the available spatial modes? Or what is the maximum benefit of channel state information? Or what gain should an individual device, or the network as a whole expect to see given a particular physical layer strategy?

The dissertation begins by developing the framework for a generic set of assumptions on network behavior and signal and interference distributions. It then presents a progression of applications to representative MIMO techniques. Broad and intuitive scaling laws are developed as well as detailed exact results for careful comparison. Capacity scaling with the number of antennas is given for systems employing beamforming, selection combining, space-time block coding, and spatial multiplexing. These applications are used as the basis for developing simple distributed algorithms for optimizing MIMO settings with QoS constraints and in heterogeneous networks. Lastly, the framework is expanded to permit comparison and optimization of MIMO performance under alternative medium access strategies. In general it is found that significant performance gains can be reaped with multi-antenna physical layers, provided the proper techniques are employed. It is also shown that the availability of multiple spatial channels impacts the inherent tradeoff between per-link throughput and spatial reuse.

Table of Contents

List of Tables

List of Figures

Chapter 1

Introduction

The final chapter of L. R. Ford and D. R. Fulkerson's landmark text *Flows in Networks* from 1962 opens with the following (excerpted) summary:

"The primary concern [of this chapter] will be with certain problems that arise when attention is shifted to all pairs of nodes. For example, how does one determine maximal flow values between all pairs of nodes in a network with capacity constraints on arcs? Does this necessitate solving all pairs of flow problems, or will something simpler suffice? Or what are necessary and sufficient conditions for a given set of numbers to represent maximal flow values between pairs of nodes in some network? In addition, [we have the problem] of synthesizing a network which meets specified lower bounds on all maximal flow values, and at minimal total network capacity. Concise and elegant answers [have been given] to all of these questions."

This sweeping statement seems somewhat at odds with the voluminous literature on network information theory over the succeeding half century. The above passage notwithstanding, and in spite of a great deal of technical expertise expended in its pursuit, the capacity of distributed wireless networks remains an elusive, but relevant and fascinating, problem.

In its simplest —most abstract and most static —form, the problem of the capacity of a network can be solved with relative ease, given link capacities for servicing a single steady-state source-destination pair. Furthermore, the calculation is based on the max-flow min-cut theorem, itself a special case of duality in linear programs, and initially implemented via the Ford-Fulkerson algorithm. But stating the capacity of a general network, particularly a *wireless* network, is more difficult for many reasons.

The first is that there are typically many competing source-destination relationships, which is true also of a wired medium, and hence the capacity is no longer a single number, but a high-dimensional region. And the second is like it, that the link capacities themselves are no longer single numbers, but regions dependent upon, in the worst case, every other device in the network. These facts indicate that in addition to the capacity region, it is necessary to have metrics with which to trade off performance along one dimension against another. Examples of such metrics have included in practice sum rate, minimax rate, transport throughput (information rate weighted by the distance transported), as well as families of utility maximization formulae. Unfortunately, there is no reason any metric should be preferred in all cases. Thus, the scope of the problem is large even when all information describing a network is available, and even then, the (Shannon) capacity region under arbitrary, known, static channels has not been completely characterized for more than two participants.

All this is compounded by the fact that a wireless network is rarely static, because of fluctuating propagation channels, mobility of devices, and changing

traffic patterns. Network dynamics raise the cost of obtaining information about the structure of the network, a cost which can be greater than the total traffic carried by the network. And when this information is available, determining optimum network behavior, such as an optimal schedule, can be computationally expensive, even NP-hard in some cases.

The pages that follow will not lay the question of information network capacity to rest, but they will advance understanding of a particular model of wireless networks. The model, which originated with the packet radio network analysis of Norman Abramson and Leonard Kleinrock, is the power-law shot noise model which takes, from a theoretical perspective, a traditional view of what wireless devices are capable. In brief, communication is primarily between pairs of devices, a transmitter and receiver, with energy emitted by other communicating pairs treated as interference. While there are a number of techniques being considered theoretically at present that are not restricted by this paradigm, including cooperative and hierarchical MIMO and interference alignment as prominent examples, virtually all devices produced to date are of the "traditional" type.

Section 1.1 provides a high-level view of the modern understanding of wireless network capacity. Section 1.2 contains the thesis statement and expected contributions, and outlines the following chapters. It also provides a list of acronym and symbol definitions.

1.1 The State of the Art

So what is known of wireless network capacity? First, there has been progress on the fundamental building blocks of networks, such as the broadcast and multiple access channels [95], and the interference channel [17]. The concept of interference alignment [40] has also been a revelation on par with the multiple antenna breakthrough, at least theoretically. And while a general statement of the capacity of a network remains elusive, there are a number of models that give asymptotic bounds on performance. Recent advances in characterizing network capacity were sparked by [30] with its notion of *transport capacity* and a number of works have followed in the same vein including [104], [58], and [73]. These studies focus on the behavior of end-to-end network capacity in the limit as the number of nodes grows large under a variety of models of node interaction and fading conditions. These confirm the basic intuition from [30] that, under traditional technological or physical limitations on node cooperation and signal reception, transmissions require "area" in which to take place and so per node end-to-end throughput decays as $\Theta(\frac{1}{\sqrt{n}})$ for n nodes in the network. The notion of transport capacity, which was the sum rate scaled by the distance traveled, made clear that a traditional wireless network is structurally similar to a planar grid network. Furthermore, this structure is responsible for the end-to-end throughput decay under the assumption of uniformly geographically random traffic (which is highly appealing from the perspective of giving network-wide guarantees). A fundamental change occurs with significant mobility as [29] and [69] show since optimal routing can take on new forms to tradeoff throughput and delay. The tutorial paper [59]

gives a good summary of the many (combinatorially) difficult scheduling problems that arise in large distributed networks even when the network is fairly static.

An alternative characterization of ad hoc network capacity was developed in [92] which defined rate regions for given network configurations and traffic needs. This was extended to the MIMO case in [105] and the notion of "capacity region" was extended in several ways. This versatile approach has the drawback of being prohibitively computationally intensive for analyzing large networks. It also focuses on large network optimization problems that would be difficult to solve in a distributed system at present.

A straightforward way to evaluate a physical layer technique under per node service requirements is to determine the maximum density of concurrent transmissions, or the *optimal contention density*, for which each node's requirements are still met. This leads naturally to the *transmission capacity* metric which is defined in [98] to be the maximum allowable spatial density of successful transmissions multiplied by their data rate given an outage constraint. The transmission capacity is a natural metric for relating individual throughput and interference statistics to those of the network as a whole. Summaries of the results on transmission capacity are available in a number of places as well, including Baccelli and Blaszczyszyn in [3] and [4], Weber and Andrews in [97] and [99], Haenggi and Ganti in [33], and the tutorials [32] and [2].

Computing the transmission capacity is made possible by using a spatial point process to model node positions, as pioneered in the analysis of wireless networks by Kleinrock, *et al.* [70], [53], and [81]. These were inspired by the goal of

quantifying the performance of the ALOHA network [1]. Following [30], Baccelli, *et al.*, [5] led a revival of analysis focusing on the stochastic geometric approach. More recently, Haenggi, *et al.* in [31], [63], and [23] emphasized the importance of network topology by characterizing some of the distinctions in throughput, interference, and outage in regular as well as clustered random networks. This approach was also taken in [96] and [45] which developed bounds on the transmission capacity for general fading models as well as power control and scheduling schemes with only individual channel state information and single antennas. Vaze [93] considered ARQ schemes in the transmission capacity framework.

Several papers, including [80], [47], [48], have studied the effects of co-channel interference on MIMO. However, these studies lack a clear link between point-to-point throughput and network performance gains. It is presently unclear which MIMO technologies yield the highest gains in large random networks. For example, [8] uses a game-theoretic analysis to show that capacity is maximized for mutually interfering sources when each sends only one data stream, while [11] and [106] suggest capacity is improved through spatial multiplexing of transmissions; however, [11] again focuses on asymptotics in the number of nodes and the results of [106] are obscured by the mobility/delay issue. Note that [83] treated adaptive modulation in a Poisson field numerically for specific SISO digital modulation schemes without outage constraints.

In MIMO systems, the need for improved signal quality, generally provided by spatial diversity, and the desire to increase data rate with spatial multiplexing compete for limited degrees of freedom. In a single link setting, this results in a

tradeoff between probability of symbol error and data rate [108], though of course multiplexing maximizes mutual information with sufficient SNR [67, 89]. However, in an interference-limited wireless ad hoc network, a different tradeoff emerges. When outage induced by topology-dependent interference is considered, diversity techniques permit an increase in the density of contending transmitters at a given outage [38]. Spatial multiplexing systems, which increase per transmission data rate at the expense of contention density, will be analyzed in this dissertation. The tradeoff then between multiplexing and diversity becomes a tradeoff between the spectral efficiency of each link and spatial reuse (or increased density). As an analogy, the tradeoff is between having fewer large pipes or many smaller pipes in the network. Unlike the tradeoff in point-to-point throughput, from the perspective of network area spectral efficiency, changes in density and changes in link throughput both directly affect network capacity (not just reliability). Exploring this tradeoff is one objective of the present work, as well as developing optimal strategies for using multiple spatial channels in ad hoc networks.

A similar approach has been taken by Stamatiou, *et al.* [86, 85, 84]. The earlier of these three studied a frequency-hopped system, and using some approximations of the interference moment generating function for a Poisson field of interferers, the optimum number of spatial modes is investigated under fixed power and rate targets. The later work expanded to BLAST architectures (for BLAST see [100]). However, the fast frequency hopping system ignores the need of optimization across the channel of interest for a communication pair. A more detailed physical layer model (taken from the model of [38]) is used for analysis

of spatial multiplexing with zero-forcing receivers in [64] and [66]. This dissertation expands on this to consider more powerful communication techniques and optimization algorithms when the transmitter also has channel state information (CSI).

The most thorough attack on the problem of MIMO in ad hoc networks to date is Govindasamy's thesis [25], which made heavy use of Monte Carlo simulations, but considered a wide variety of multiplexing configurations. Several of the scaling relationships given in Chapter 2 were arrived at in parallel by Govindassamy, *et al.* in [26] and [27]. Govindasamy also investigated spectral efficiency as a function of the ergodic rate treating interference as noise. However, the latter work, particularly [27] focuses on asymptotically large numbers of users and antennas. This thess will distinguish itself in giving exact results for many finite, practical cases, and for arriving at the asymptotics by simple means.

Two lines of work have also sought a general framework for transmission capacity analysis in ad hoc networks. The first is [103] in which the authors developed a framework for analyzing linear MIMO schemes which is similar to that developed in Chapter 2 here. The second is [21] and [22] which developed expansions for general spatial node distributions and fading distributions.

Analyses of spatial interference cancelation systems are made in [26], [44], [36], and [94]. Unlike the present work, these assume CSI is available of all prominent interfering nodes. Under these conditions they determine the spectral efficiency and the optimum number of canceled interferers. Note also that the approach taken in this dissertation is in a sense a more traditional approach

when compared to the recent work in [74] and [75]. That is, throughout we assume nodes communicate point-to-point and relay traffic in a multihop fashion as transmitter-receiver pairs with a random access medium access control (MAC). This is the more practical approach when coordination with and CSI of interfering neighbors is prohibitively costly to the network.

A few studies have approached the difficult problem of medium access control (MAC) analysis in random spatial field of interference including [5], [34], [49], and [20], while at the same time [66], [38], and [37] have considered multi-antenna (MIMO) radios, though they have focused mainly on the Aloha case. As a point of comparison, the study [66] developed a particular coordinated protocol as a comparison point against Aloha. In [51] the Poisson shot noise model was used to study CSMA with channel awareness, and to develop throughput optimizing protocols that also considered fairness. This dissertation develops a new model for the combination of a multiple-antenna physical layer with a tunable CSMA model which includes Aloha as a special case. This allows the interaction of MIMO and CSMA to be studied and provides a framework for determining which MIMO configurations yield the highest gains for carrier-sensing networks as a whole, as well as enabling comparisons against Aloha.

The transmission capacity framework has also been extended in directions beyond the traditional network structure. One example is the space division multiple access (SDMA) work of [56] and [61], which bound the capacity of local transmissions with Poisson interference. The effect of distributed channel-aware scheduling with an underlying Poisson field was also considered in [62]. The limits

of interference alignment were explored in [72].

1.2 Thesis, Contributions, and a Brief Outline

The central goal of the thesis is to develop an analytical framework for quantifying, comparing, and optimizing multi-antenna physical layer techniques in dense ad hoc wireless networks. The framework is applied to a variety of representative techniques and demonstrates the substantial expected benefits of equipping devices in large peer-to-peer networks with multiple antennas.

Chapter 2 discusses the underlying models of stochastic geometry applied to distributed wireless networks. In particular, the transmission capacity framework is developed for standard network model under QoS constraints. Relations are derived for the SINR distribution and the transmission capacity for broad signal and interference classes. Chapter 3 discusses applications of the tools developed to analyze the impact of spatial diversity techniques on transmission capacity. A number of simple scaling relations are derived for the increase in capacity with the number of antennas employed. Chapter 4 extends the analysis to spatial multiplexing systems, expanding of the notion of outage, and tackling for complex optimization scenarios. Chapter 5 describes methods for distributed adaptation in heterogeneous networks. Chapter 6 expands the framework to consider the optimization of multiple antenna techniques with a carrier sensing protocol. Chapter 7 concludes the dissertation. Table 1.2 provides a list of definitions for acronyms that are used in this dissertation.

Table 1.1: Notation and Acronyms

Symbol	Definition
Φ	Poisson point process
λ	Density of point process and/or transmitters
β	SINR threshold
α	Path loss exponent
ϵ	Outage probability/constraint
ρ	Transmit power level
θ_M	Carrier sensing threshold
R	Distance between transmitter and receiver
K_α	Small outage signal factor
C_α	Small outage interference factor
$\mathbf{H}$	Matrix communication channel
$\mathcal{L}_{I_\Phi}$	Laplace transform of the shot noise interference based on the point process Φ
SIR, SINR	Signal-to-noise ratio, signal-to-interference-and-noise ratio
ASE	Area spectral efficiency
CSI	Channel state information
MIMO	Multiple input, multiple output; multi-antenna
SISO	Single-input, single output
MRT/MRC	Maximum ratio transmission/combining
MAC	Medium access control
CSMA	Carrier sense multiple access
QoS	Quality-of-service
OSTBC	Orthogonal space-time block code
ARQ	Automatic repeat request
SVD	Singular value decomposition
MGF	Moment generating function
PDF	Probability density function
CDF, CCDF	Cumulative distribution function, complementary cumulative distribution function

Chapter 2

A Transmission Capacity Framework

This chapter develops the central metrics and analytical tools. The chapter deals exclusively with single-antenna systems to make presentation of the core ideas simple. Section 2.1 introduces the Poisson spatial model for wireless networks. Section 2.2 derives the optimal network contention density in the simplest case as a pattern for later chapters. Section 2.3 states and proves the main result on Poisson shot noise in distributed wireless networks. Section 2.4 describes application of the main theorem to analyze performance in various channel environments, such as Nakagami fading. Section 2.5 gives a simplified form of the main result and describes an accurate approximation method applying the transmission capacity analysis to new problems. Section 2.6 concludes this chapter.

2.1 The Poisson Model of Wireless Ad Hoc Networks

The Poisson spatial model of wireless networks is the starting point for analysis for two main reasons alluded to in the introduction. First, it models completely random spatial processes, that is, processes for which the existence and position of each point is independent of all other points. As a result it is an appropriate model when device placement, mobility, and/or medium access

is random and occurs with little to no coordination with other devices. Second, and however self-serving it may seem to state it, the Poisson process is uniquely tractable at present among all nontrivial point processes, in that no other model has nearly as many fundamental properties which can be stated clearly, concisely, and exactly.

This section defines the network model and presents some results on Laplace functionals of Poisson shot noise processes which will be foundational for later sections. A *shot noise process* is the sum of a function (random or deterministic) evaluated at all the locations of a realization of a spatial point process. The interference power seen by a wireless receiver is such a process, being a stochastic function of the locations of the points and additive over all points. Properties of the Poisson shot noise process are thus keys to understanding the distribution of the SINR of wireless links, and hence their rate, delay, outage, etc. As discussed in [98], the Poisson model matches the collision behavior of distributed random access systems. (while neither addressing nor precluding the issue of routing.) The tractability of the model will also provide a clear relationship between individual link statistics and network performance, between high level metrics, such as area spectral efficiency, and physical layer parameters, such as the number of antennas employed per device.

Let the distribution of transmitting nodes in a network be a stationary marked Poisson point process with intensity λ on $\mathbb{R}^2$; the process is denoted by Φ. This process is the spatial layout of a slotted random access wireless network in a particular time slot. To begin, consider a typical receiver located at the origin.

Conditioning on the event of a node lying at the origin (called a Palm probability) does not affect the statistics of the rest of the Poisson process (see, e.g., Chapter 2 of [87]). Moreover, if the Poisson process is homogeneous, due to stationarity the statistics of signal reception at this receiver are identical to those seen by any receiver.

To model propagation through the wireless channel, let signals be subject to two independent phenomena: (1) the power-law path loss attenuation model $d^{-\alpha}$ for a distance d with exponent $\alpha > 2$, as well as (2) small scale fading for either a Rayleigh or Nakagami-m fading distribution with unit mean. Also, let all nodes have the constraint of a maximum transmit power ρ (and unless otherwise specified, assume all devices use maximum power always). For such a channel, the typical receiver obtains desired signal power $\rho S_0 R^{-\alpha}$ for some fixed transmitter-receiver separation distance R, and with a fading power factor S_0 on the signal from its intended transmitter, labeled 0. From the perspective of this receiver, all other transmitting nodes are interfering nodes, numbered $1, 2, 3, ...$ These constitute the marked process $\Phi = \{(X_i, S_i)\}$, with X_i denoting the location of the ith transmitting node, and with marks S_i that denote fading factors on the power transmitted from the ith node and then received by the typical receiver. Let $F_{S_i}(\cdot)$ and $F^c_{S_i}(\cdot)$ denote the cumulative distribution function (CDF) and the complementary CDF (CCDF) of S_i respectively. Thus the typical receiver receives interference power $\rho S_i |X_i|^{-\alpha}$ from the ith interfering node ($|\cdot|$ denoting magnitude). For single-antenna narrowband systems in Rayleigh fading channels, for example, the power factors S_0 and S_i are distributed exponentially with unit mean

so that the mean interfering power is governed by transmit power ρ and path loss $|X_i|^{-\alpha}$. Note that the simplified attenuation function $|d|^{-\alpha}$ is used here. While this model is inaccurate in the near field, most notably because it explodes at the origin, for systems operating primarily in the far field (e.g., R is many carrier wavelengths), this inaccuracy has negligible effect for the purpose of calculating outage probabilities[1]. One can modify the path loss function to, for example, $\frac{1}{1+|d|^{\alpha}}$ as mentioned in [5] and perform the same analysis. The result is that for R well in the far field, this modification leads to the same transmission capacity conclusions though with more cumbersome expressions. A detailed analysis of this point is given in [39].

Imposing a technological model on the receiver, let successful transmission occur if the inequality

$$\frac{\rho S_0 R^{-\alpha}}{\rho I_\Phi + N_0} \geq \beta \tag{2.1}$$

is satisfied for some target SINR β, aggregate co-channel interference ρI_Φ, and thermal noise power N_0. A further techonological restriction is to treat interference as noise, so that the target link level spectral efficiency b will be taken to be the Shannon rate $\log_2(1+\beta)$. The Shannon rate relation is particularly appropriate when thermal noise is Gaussian, and when signaling of all devices is Gaussian, which would maximize signal information content in the absence of interference. The aggregate interference is a Poisson shot noise process (scaled by ρ), which is

[1]In fact, one might argue that a model for which interference goes to infinity as distance approaches zero is more appropriate when outage probabilites are calculated. This is because the existence of an interferer in the near field may well have effects such as saturating A/D converters, making communication with a distant transmitter impossible.

a sum over the marked point process:

$$I_\Phi = \sum_{X_i \in \Phi} S_i |X_i|^{-\alpha} \tag{2.2}$$

with, again, $|X_i|$ denoting the distance of the interferer X_i from the origin where the receiver under test lies. For now, assume signal reception is statistically interference limited in the sense that $\rho I_\Phi \gg N_0$ so that thermal noise is negligible. Following [5], the probability of successful transmission for the typical receiver is:

$$\begin{aligned} \mathbf{P}(\text{SIR} \geq \beta) &= \mathbf{P}\left(\frac{\rho S_0 R^{-\alpha}}{\rho I_\Phi} \geq \beta\right) \\ &= \mathbf{P}\left(S_0 \geq \beta R^\alpha I_\Phi\right) \\ &= \int_0^\infty \mathbf{P}(S_0 \geq s\beta R^\alpha)\ f_{I_\Phi}(s)\mathrm{d}s \\ &= \int_0^\infty F^c_{S_0}(s\beta R^\alpha) f_{I_\Phi}(s)\mathrm{d}s \end{aligned} \tag{2.3}$$

where the third step is reached by conditioning on s. In the single antenna (SISO) Rayleigh fading case, the received signal power is exponentially distributed with $F^c_{S_0}(s\beta R^\alpha) = e^{-s\beta R^\alpha}$ so that

$$\mathbf{P}(\text{SIR} \geq \beta) = \int_0^\infty e^{-s\beta R^\alpha}\ f_{I_\Phi}(s)\mathrm{d}s\ . \tag{2.4}$$

This integral is now a Laplace transform of the PDF of I_Φ which notationally is $\mathbf{P}(\text{SIR} \geq \beta) = \mathcal{L}_{I_\Phi}(\beta R^\alpha)$. The Laplace transform for a general Poisson shot noise process in $\mathbb{R}^2$ with independent, identically distributed (i.i.d.) marks S_i is given by [52]

$$\mathcal{L}_{I_\Phi}(\zeta) = \exp\left\{-\lambda \int_{\mathbb{R}^2} 1 - E\left[e^{-\zeta S|x|^{-\alpha}}\right] \mathrm{d}x\right\} \tag{2.5}$$

where the expectation, denoted by $E[\cdot]$, is the moment generating function of the random variable S (scaled by $\zeta\|x\|^{-\alpha}$) which has the same distribution as each of the S_i. For Rayleigh fading channels, i.e., $S_0, S_i \sim \text{Exp}(1)$, (2.5) simplifies to

$$\begin{aligned} \mathcal{L}_{I_\Phi}(\zeta) &= \exp\left\{-2\pi\lambda \int_0^\infty \frac{u}{1+|u|^\alpha/\zeta}\mathrm{d}u\right\} \\ &= \exp\left\{-\lambda\frac{2\pi}{\alpha}\Gamma\left(\frac{2}{\alpha}\right)\Gamma\left(1-\frac{2}{\alpha}\right)\zeta^{\frac{2}{\alpha}}\right\} \\ &= e^{-\lambda C\beta^{\frac{2}{\alpha}}R^2} \end{aligned} \tag{2.6}$$

with $\mathcal{L}_{I_\Phi}(\zeta)$ evaluated at $\zeta = \beta R^\alpha$ and $C = \frac{2\pi}{\alpha}\Gamma(\frac{2}{\alpha})\Gamma(1-\frac{2}{\alpha})$, with $\Gamma(t) = \int_0^\infty x^{t-1}e^{-x}\mathrm{d}x$ being the gamma function.

The result (2.6) is the distribution of the SIR as seen from a typical receiver in Rayleigh fading conditions in a Poisson field of interferers. As such it governs the average spatial performance of a wireless node using a single antenna and an Aloha MAC. If it is assumed further that a new random process occurs in each time slot, it also governs the long-run performance of each node in the network. This is the baseline against which more advanced signal reception and network coordination strategies will be measured.

2.2 Network Optimization

Equipped with SIR distribution (2.6), system design, analysis, and optimization can proceed along two lines, which could be called the *micro* perspective, the perspective from a single node, and the *macro* perspective, the perspective from the network as a whole. From the micro perspective, a node finds itself in the

midst of a field of interferers of density λ, with a given path loss exponent, and attempts to communicate over a certain one-hop distance. The long-run throughput which the node can expect is:

$$\begin{aligned} r &= \mathbf{P}(\text{SIR} \geq \beta) \log_2(1+\beta) \\ &= e^{-\lambda C R^2 \beta^{\frac{2}{\alpha}}} \log_2(1+\beta) \, . \end{aligned} \tag{2.7}$$

Given the environment statistics, a node selects its target spectral efficiency and its target outage probability simultaneously by selecting β. The expression (2.7) is log-concave and can easily be optimized numerically for β to maximize the expected throughput, and the results are shown in figure 2.5. As the density increases, the optimal β decreases and the corresponding optimal outage rate increases.

In contrast, from the macro perspective the network as a whole is full of typical receivers, each observing the same interference statistics. A system designer or an *in situ* algorithm can now optimize the network based on some metric, the most natural (but not the only) being total network throughput, or equivalently area spectral efficiency (in bits per second per Hertz per unit area). The two main parameters for the optimization are then the number of attempted transmissions on average, and the target rate for each. Assuming now that every active transmitter-receiver pair self-selects to be about the same distance R apart and that each pair targets a certain desired SIR β, the average density of successful

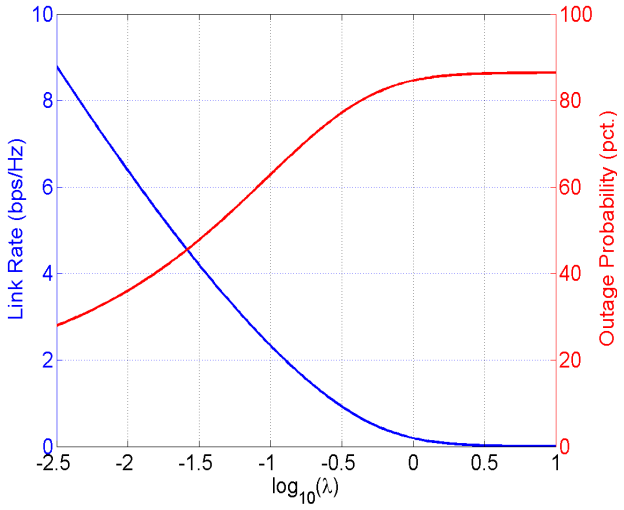

Figure 2.1: Optimal target spectral efficiency (i.e., $\log_2(1+\beta)$) and the corresponding outage probability vs. contention density.

transmissions denoted λ_s is:

$$\begin{aligned} \lambda_s &= \lambda\, \mathbf{P}(\text{SIR} \geq \beta) \\ &= \lambda\, e^{-\lambda C R^2 \beta^{\frac{2}{\alpha}}} \end{aligned} \tag{2.8}$$

and the corresponding area spectral efficiency is:

$$\text{ASE} = \lambda\, e^{-\lambda C R^2 \beta^{\frac{2}{\alpha}}} \log_2(1+\beta)\ . \tag{2.9}$$

Figure 2.2 compares ASE as a function of the contention density for several choices of β.

Maximizing (2.8) over λ, [5] noted that since $\frac{\mathrm{d}}{\mathrm{d}x} cxe^{-x} = ce^{-x}(1-x)$ the maximum occurs whenever $\lambda C \beta^{\frac{2}{\alpha}} R^2 = 1$. For the purpose of optimizing over λ,

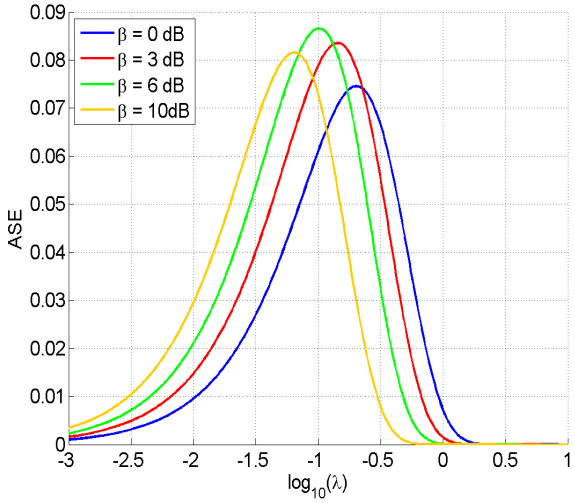

Figure 2.2: Area spectral efficiency vs. contention density for several choices of β. Path loss exponent is 4.

(2.8) and (2.9) are equivalent, and thus the optimization of (2.9) can be simplified:

$$\begin{aligned} \max \text{ASE} &= \max_{\lambda,\beta} \lambda\, e^{-\lambda C R^2 \beta^{\frac{2}{\alpha}}} \log_2(1+\beta) \\ &= (e\, R^2 C)^{-1} \max_{\beta} \beta^{-\frac{2}{\alpha}} \log_2(1+\beta) \end{aligned} \tag{2.10}$$

which is now only an optimization in β. The work in [43] showed that the solution to this particular maximization over β occurs when $\log_2(1+\beta) = b^*$ for

$$b^* = \log_2(e)\left[\frac{\alpha}{2} + W(-\frac{\alpha}{2}e^{-\frac{\alpha}{2}})\right] \tag{2.11}$$

where $W(\cdot)$ is Lambert's W function. For $\alpha = 4$ and R normalized to 1, the optimum target link spectral efficiency $b^* \approx 2.3$ bits/s/Hz and $\lambda \approx 0.1$ nodes/unit area (where unit area is measured relative to the typical transmit distance). Hence, there is a unique static solution to the network throughput maximization problem under SISO Aloha dependent only on R and α.

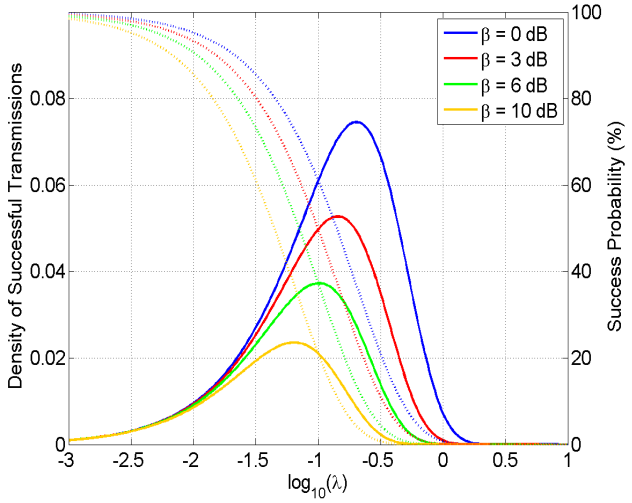

Figure 2.3: Density of successful transmissions (solid lines) and outage probabilities (dashed lines) for fixed SINR targets vs. contention density.

However, there is one unsavory feature of this solution, which is that the probability of successful transmission at this optimal point is e^{-1} or only about 36.8%. A high failure rate can be taxing on practical systems, even if this leads to higher overall throughput, since high failure rates can also be indicative of hardware or software problems, or network congestion or failure. Failures due to high interference also mean more power expended. But more importantly, in a packetized system transmission failure incurs delay. To put this in perspective, a success rate of 36.8% means there is about a 10% chance of five failures in a row, and about a 1% chance of ten failures in a row, and this is only a single hop. Delay-sensitive applications may not be able to tolerate this kind of variability. It so happens that the optimal link level efficiency (i.e., b^*) is a common operating point

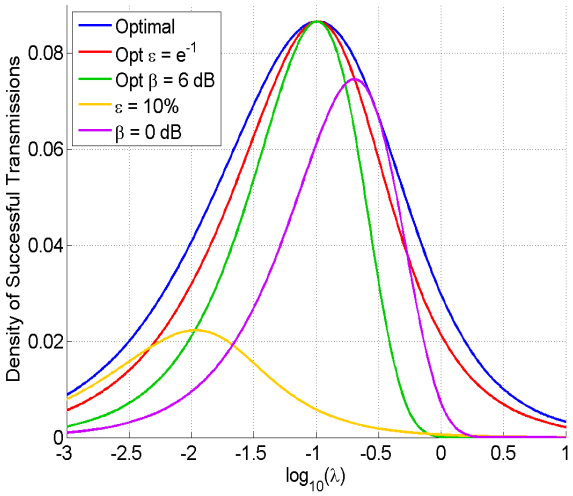

Figure 2.4: Area spectral efficiency vs. contention density for a variety of cases including the optimal operating point for a given density, and two cases each for fixed β and fixed ϵ. For both β and ϵ, one case is the globally optimal value.

for many contemporary systems and thus would not usually be objectionable, though it could just as easily be constrained by factors external to the above optimization.

Applying quality of service (QoS) constraints of both a minimum β and a small outage constraint (e.g., $\epsilon < .1$) to (2.4), the network just meets this constraint when

$$\mathbf{P}(\text{SIR} \geq \beta) = 1 - \epsilon = e^{-\lambda C R^2 \beta^{\frac{2}{\alpha}}} \tag{2.12}$$

and solving for λ yields:

$$\lambda^* = \frac{-\ln(1-\epsilon)}{C R^2 \beta^{\frac{2}{\alpha}}} = \frac{\epsilon}{C R^2 \beta^{\frac{2}{\alpha}}} + \Theta(\epsilon^2)\ . \tag{2.13}$$

The value λ^* is termed the *optimal contention density* given the QoS constraints

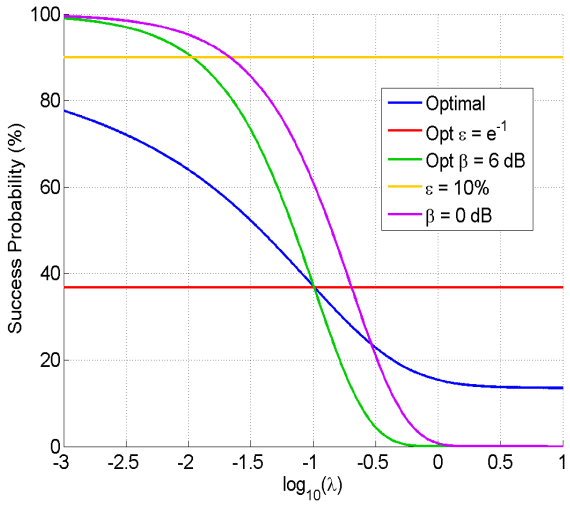

Figure 2.5: Outage vs. contention density for a variety of cases including the optimal operating point for a given density, and two cases each for fixed β and fixed ϵ. For both β and ϵ, one case is the globally optimal value.

and relatedly the *transmission capacity* is the density of successful transmissions

$$\lambda_\epsilon = (1-\epsilon)\lambda^* \, . \tag{2.14}$$

Since the results that follow will focus on the small outage regime, it will be convenient to introduce the notation $\lambda_\epsilon = \bar{\lambda}_\epsilon + O(\epsilon^2)$ allowing equations to be expressed in terms of $\bar{\lambda}_\epsilon$ with the $O(\epsilon^2)$ error terms merely implied.

2.3 The General Small-Outage Relation

The result (2.13), which is also given in [98] and derived from [5], can be generalized and expanded, which this section undertakes to do. For this purpose,

two definitions are in order. First, suppose F_S^c takes the form

$$F_S^c(x) = \sum_n e^{-c_n x} \sum_k a_{nk} x^k \tag{2.15}$$

but with the following limitations. First, the set $c_n \in \mathbb{R}^+$ is finite, and second, k runs over the nonnegative integers, but only a finite set of $a_{nk} > 0$, and lastly, F_S^c is a valid CCDF[1]. The exponential distribution is a simple example for which $c = \{1\}$ and $a_{10} = 1$ with all other $a_{nk} = 0$. This form includes a number of distributions including (finite) phase-type distributions, gamma distributions with integer shape parameter, and exponential distributions, as well as eigenvalue distributions for Wishart matrices. This will be referred to as *standard fading* form in what follows.

Second, let the interfering transmitters form a Poisson process of intensity λ around the typical receiver with the outage probability being $\mathbf{P}(\text{SIR} \leq \beta) = \mathbf{P}(\frac{\rho S_0 R^{-\alpha}}{\rho I_\Phi} \leq \beta)$ with fixed ρ, β, R, ϵ, and α, and with the distribution of the interference fading power identical for all interferers. Similarly, this will be called the *standard network*, one in which all nodes see the same signal and interference power *statistically*.

The following Theorem is a foundational result for this dissertation, generalizing (2.13) and (2.6):

Theorem 2.3.1. *For a standard network, with S_0 having a standard fading dis-*

[1]Note that not all sets lead to valid distributions, e.g., for $c = \{1\}$ let $a_{11} = 1$ and all other $a_{nk} = 0$, $F^c(x) \propto xe^{-x}$ which cannot be a valid CCDF.

tribution, and S_0 independent of the interference shot noise,

$$\mathbf{P}(\text{SIR} \geq \beta) = \sum_n \sum_k \left[a_{nk} \left(-\frac{\zeta}{c_n} \right)^k \frac{d^k}{d\zeta^k} \mathcal{L}_{I_\Phi}(\zeta) \right]_{\zeta = c_n \beta R^\alpha} . \tag{2.16}$$

Furthermore, for $\epsilon \ll 1$, the optimal contention density is:

$$\bar{\lambda_\epsilon} = \frac{K_\alpha}{C_\alpha} \frac{\epsilon}{R^2 \beta^{\frac{2}{\alpha}}} \tag{2.17}$$

where

$$K_\alpha = \left[\sum_n \sum_k a_{nk} c_n^{\frac{2}{\alpha} - k} \prod_{l=0}^{k-1} (l - 2/\alpha) \right]^{-1} \tag{2.18}$$

and

$$C_\alpha \beta^{\frac{2}{\alpha}} R^2 = \int_{\mathbb{R}^2} 1 - E[e^{-\zeta S_i |x|^{-\alpha}}] \mathrm{d}x \, . \tag{2.19}$$

Before embarking on the proof of this Theorem, its significance should be highlighted in several ways. The Theorem's two contributions are (i) that it gives the exact probability of outage for any network density or target SIR but also (ii) that it gives a solution for the optimal contention density in the low outage regime. But the Theorem also establishes several other points as well. First, it confirms the linear dependence of the optimal contention density on the outage constraint for uniformly distributed random access systems for a wide variety of signal and interference distributions. When compared with a regular network topology, ϵ essentially becomes a penalty factor on the area spectral efficiency achievable with random access. Second, it shows that a large class of received signal and fading distributions is amenable to a transmission capacity analysis, which will include a number of MIMO techniques. Third, it demonstrates that derivation of

the transmission capacity consists of two components: (i) determining K_α which is dependent on the received signal distribution, and (ii) determining C_α which is a result of the interfering signal statistics. (Although this holds in general only when the condition of independence between the received signal distribution and the interfering shot noise process is satisfied.) In later chapters these will be referred to as the *signal factor* and the *interference factor*, respectively. In addition, the ratio of the signal factor over the interference factor is termed the *proportionality factor* for transmission capacity.

Proof. The three main objectives in the proof are first to arrive at the general outage probability 2.16, then to establish 2.17 and give 2.18 in the process, and lastly to show the proportionality given in 2.19.

Define the PDF of I_Φ to be $f_{I_\Phi}(t) = \mathrm{d}\mathbf{P}(I_\Phi \leq t)$. Define a transform of $f_{I_\Phi}(t)$ using CCDF $F_S^c(t)$ as

$$\mathcal{G}_{I,S}(s) = \int_0^\infty F_S^c(st) f_{I_\Phi}(t) \mathrm{d}t.$$

The probability of successful transmission can be expressed as

$$\begin{aligned} \mathbf{P}(\mathrm{SIR} \geq \beta) &= \mathbf{P}(S \geq \beta R^\alpha I_\Phi) \\ &= \int_0^\infty F_S^c(st) f_{I_\Phi}(t) \mathrm{d}t \\ &= \mathcal{G}_{I,S}(s)|_{s=\beta R^\alpha} \end{aligned} \tag{2.20}$$

When $S \sim \mathrm{Exp}(1)$, $F_S^c(t) = e^{-t}$ so that the transform of $f_{I_\Phi}(t)$ is

$$\begin{aligned} \mathcal{G}_{I,S}(s) &= \int_0^\infty F_S^c(st) f_{I_\Phi}(t) \mathrm{d}t \\ &= \mathcal{L}\{f_{I_\Phi}(t)\}(s) = \mathcal{L}_{I_\Phi}(s), \end{aligned} \tag{2.21}$$

and the transmission success probability is expressible in terms of the Laplace transform. Next suppose $F_S^c(t)$ has the standard fading form, then the transform of $f_{I_\Phi}(t)$ using CCDF $F_S^c(t)$ is

$$\begin{aligned}
\mathcal{G}_{I,S}(s) &= \int_0^\infty F_S^c(st) f_{I_\Phi}(t)\mathrm{d}t \\
&= \int_0^\infty \left(\sum_n e^{-c_n st}\sum_k a_{nk}(st)^k\right) f_{I_\Phi}(t)\mathrm{d}t \qquad (2.22)\\
&= \sum_n\sum_k a_{nk}s^k\left(\int_0^\infty e^{-c_n t}t^k f_{I_\Phi}(t)\mathrm{d}t\right) \qquad (2.23)\\
&= \sum_n\sum_k a_{nk}s^k\mathcal{L}\{t^k f_{I_\Phi}(t)\}(c_n s) \qquad (2.24)\\
&= \sum_n\sum_k a_{nk}(-s)^k\frac{\mathrm{d}^k}{\mathrm{d}(c_n s)^k}\mathcal{L}_{I_\Phi}(c_n s) \qquad (2.25)\\
&= \sum_n\sum_k \left[a_{nk}\left(-\frac{\zeta}{c_n}\right)^k\frac{\mathrm{d}^k}{\mathrm{d}\zeta^k}\mathcal{L}_{I_\Phi}(\zeta)\right]_{\zeta=c_n\beta R^\alpha} \qquad (2.26)
\end{aligned}$$

where (2.24) uses the Laplace transform property $t^n f(t) \longleftrightarrow (-1)^n\frac{\mathrm{d}^n}{\mathrm{d}s^n}\mathcal{L}[f(t)](s)$. Thus the first destination of 2.16 is reached.

To derive (2.18), the derivatives of $\mathcal{L}_{I_\Phi}$ are needed, which are given by

$$\frac{\mathrm{d}^p}{\mathrm{d}\zeta^p}\mathcal{L}_{I_\Phi}(\zeta) = \frac{e^{-\lambda\zeta^{\frac{2}{\alpha}}C_\alpha}}{(-\zeta)^p}\sum_{k=1}^{p}\left(\lambda\zeta^{\frac{2}{\alpha}}C_\alpha\frac{2}{\alpha}\right)^k(-1)^k\Upsilon_{p,k} \qquad (2.27)$$

where

$$\begin{aligned}
\Upsilon_{p,k} &= \sum_{\delta_j\in\,\mathrm{comb}\binom{p-1}{p-k}}\prod_{l_{ij}\in\delta_j}\left(\frac{2}{\alpha}(l_{ij}-i+1)-l_{ij}\right),\\
&\qquad i=1,2,...,|\delta_j|,\ j=1,2,...,\binom{p-1}{p-k}.
\end{aligned}$$

Here $\mathrm{comb}\binom{a}{b}$ is defined as the set of all subsets of the natural numbers $\{1, 2, ..., a\}$ of cardinality b with distinct elements, i.e., $\mathrm{comb}\binom{a}{b}$ is the set of combinations of $\{1, 2, ..., a\}$ taken b at a time. Thus there are $\binom{a}{b}$ subsets in $\mathrm{comb}\binom{a}{b}$ each with b elements and the δ_j each constitute one such subset[1].

Forming the first order Taylor expansion for the pth derivative around $\kappa = \lambda\beta^{\frac{2}{\alpha}} R^2 C_\alpha = 0$, note that any term with κ^k for $k > 1$ is $o(\kappa)$ and can be discarded so that $\frac{\mathrm{d}^p}{\mathrm{d}\zeta^p}\mathcal{L}_{I_\Phi}(\zeta)\Big|_{\zeta=\beta R^\alpha}$ reduces to

$$\begin{aligned}
\frac{\mathrm{d}^p}{\mathrm{d}\zeta^p}\mathcal{L}_{I_\Phi}(\zeta) &= (-1)^{p+1}\frac{e^{-\lambda\zeta^{\frac{2}{\alpha}}C_\alpha}}{\zeta^p}\lambda\zeta^{\frac{2}{\alpha}}C_\alpha(2/\alpha)\Upsilon_{p,1} + \Theta(\kappa^2) \\
&= (-1)^p e^{-\lambda\zeta^{\frac{2}{\alpha}}C_\alpha}\lambda\zeta^{\frac{2}{\alpha}-p}C_\alpha\prod_{l=0}^{p-1}(l - 2/\alpha) + \Theta(\kappa^2) \\
&= (-1)^p\lambda\zeta^{\frac{2}{\alpha}-p}C_\alpha\prod_{l=0}^{p-1}(l - 2/\alpha) + \Theta(\kappa^2)
\end{aligned} \tag{2.28}$$

where the small error terms are the result of the Taylor expansion. Thus a term from (2.16) becomes:

$$a_{nk}\left(-\frac{\zeta}{c_n}\right)^k\frac{\mathrm{d}^k}{\mathrm{d}\zeta^k}\mathcal{L}_{I_\Phi}(\zeta) = a_{nk}c_n^{\frac{2}{\alpha}-k}\lambda\zeta^{\frac{2}{\alpha}}C_\alpha\prod_{l=0}^{k-1}(l - 2/\alpha) + \Theta(\kappa^2) \tag{2.29}$$

[1]This expression based on sums over subsets is admittedly unwieldy, but for outage constrained systems, it is only necessary as a stepping stone in the proof. The authors in [66] took some pains to derive something simpler under a slightly reduced set of admissible fading distributions. Their results will be used happily in later chapters.

so that the outage probability is given by

$$\begin{aligned}\mathbf{P}(\text{SIR} \leq \beta) &= \lambda \zeta^{\frac{2}{\alpha}} C_\alpha \sum_n \sum_k a_{nk} c_n^{\frac{2}{\alpha}-k} \prod_{l=0}^{k-1} (l - 2/\alpha) + \Theta(\kappa^2) \\ &= \lambda \zeta^{\frac{2}{\alpha}} \frac{C_\alpha}{K_\alpha} + \Theta(\kappa^2) \;=\; \epsilon \end{aligned} \tag{2.30}$$

and with $\zeta = \beta R^\alpha$ and K_α as in (2.18), solving for λ yields the result. Thus the second milestone is reached.

In general C_α depends on S_i, but S_i does not depnd on the relative position of the receiver and interferer. This allows some manipulation of the integral in (2.5), where ζ is evaluated at βR^α. Performing two changes of variable, first the integration over $\mathbb{R}^2$ can be changed to reflect the radial symmetry with $2\pi u \mathrm{d}u = \mathrm{d}x$. Next, letting $v = \zeta u^{-\alpha}$ implies $-\alpha^{-1}\zeta^{\frac{2}{\alpha}} v^{\frac{2}{\alpha}-1} \mathrm{d}v = u \mathrm{d}u$:

$$\begin{aligned}\int_{\mathbb{R}^2} 1 - E\left[e^{-\zeta S_i |x|^{-\alpha}}\right] \mathrm{d}x &= 2\pi \int_0^\infty \left(1 - E\left[e^{-\zeta S_i u^{-\alpha}}\right]\right) u \mathrm{d}u \\ &= \frac{2\pi}{\alpha} \zeta^{\frac{2}{\alpha}} \int_0^\infty v^{\frac{2}{\alpha}-1} \left(E\left[e^{-vS_i}\right] - 1\right) \mathrm{d}v \end{aligned} \tag{2.31}$$

Thus the integral will always be proportional to $(\beta R^\alpha)^{\frac{2}{\alpha}}$. This has the simple sphere packing interpretation that each transmission takes up an "area" proportional to $(\beta^{1/\alpha} R)^2$.

For completeness, the proof concludes with a demonstration of how thermal noise can be included in the analysis. To include noise, I_Φ must be replaced by $I_\Phi + \frac{1}{\rho} N_o$ and so the transform of the distribution $f_{I_\Phi + \frac{1}{\rho}N_o}(x)$, given by $\mathcal{L}_{I_\Phi + \frac{1}{\rho}N_o}(\zeta) = \mathcal{L}_{I_\Phi}(\zeta)\mathcal{L}_{N_o}(\zeta/\rho)$, replaces $\mathcal{L}_{I_\Phi}(\zeta)$ in the above derivations. This follows from the property of Laplace transforms that the transform of the sum of independent

variables is the product of the transforms. Now the transform of the noise is $\mathcal{L}_{N_o}(\zeta/\rho) = e^{\zeta \cdot N_o/\rho}$. Furthermore, since $\frac{\mathrm{d}}{\mathrm{d}\zeta}\mathcal{L}_{N_o}(\zeta) = \frac{N_o}{\rho}\mathcal{L}_{N_o}(\zeta)$, this leads to

$$\frac{\mathrm{d}^p}{\mathrm{d}\zeta^p}\mathcal{L}_{I_\Phi+N}(\zeta) = \mathcal{L}_N(\zeta)\left(\sum_{k=0}^{p}\binom{p}{k}\left(\frac{N_o}{\rho}\right)^{p-k}\frac{\mathrm{d}^k}{\mathrm{d}\zeta^k}\mathcal{L}_{I_\Phi}(\zeta)\right) \tag{2.32}$$

The expression for $\frac{\mathrm{d}^p}{\mathrm{d}\zeta^p}\mathcal{L}_{I_\Phi+\frac{1}{\rho}N_o}(\zeta)$ now replaces $\frac{\mathrm{d}^p}{\mathrm{d}\zeta^p}\mathcal{L}_{I_\Phi}(\zeta)$ in (2.16). Under small outage constraints, the first order Taylor expansion of the probability of outage can be made in a manner analogous to equations (2.28) through (2.30) leading to:

$$K_\alpha = \left[\sum_{\substack{n\in\mathcal{N}\\k\in\mathcal{K}}}\sum_{j=0}^{k}\binom{k}{j}\left(\frac{N_o}{\rho}\right)^{k-j}a_{nk}n^{\frac{2}{\alpha}-j}\prod_{l=0}^{j-1}(l-2/\alpha)\right]^{-1}. \tag{2.33}$$

Note that this expansion is only valid when outage due to the fading of the intended signal and thermal noise is less than ϵ in the absence of any interference. □

2.4 Transmission Capacity in LOS and NLOS Environments

This section presents the first application of Theorem 2.3.1, taking as its subject the comparison of line-of-sight and non line-of-sight channels. The application is itself of minor significance, but the signal and interference factors derived and their behavior will be widely applicable in later chapters.

In [98], the same Poisson network model was used but propagation was modeled with path loss only while [5] incorporated Rayleigh fading in addition to path loss. In order to characterize the effect on network capacity between these extremes, Rayleigh fading and non-fading, let the envelope of the received signal be

Nakagami-m distributed with integer parameter m in addition to being scaled by path loss. The Nakagami distribution includes Rayleigh as a special case ($m = 1$), non-fading as a special case ($m = \infty$), and provides a close parameterized fit for empirical data as well as the Ricean distribution for $m = \frac{(K+1)^2}{(2K+1)}$ for K the Ricean factor [88]. Theorem 2.3.1 is applied as follows:

Proposition 2.4.1. *For a standard network with SISO communnication in Nakagami-m fading for $m \in \mathbb{N}$, the optimal contention density with outage ϵ is given by*

$$\bar{\lambda_\epsilon} = \frac{K_{\alpha,m}\epsilon}{C_{\alpha,m}\beta^{\frac{2}{\alpha}}R^2} \tag{2.34}$$

where $K_{\alpha,1} = 1$ and for $m \geq 2$

$$K_{\alpha,m} = m^{-\frac{2}{\alpha}}\left[1 + \sum_{k=0}^{m-2}\frac{1}{(k+1)!}\prod_{l=0}^{k}(l - 2/\alpha)\right]^{-1} \tag{2.35}$$

and

$$C_{\alpha,m} = m^{-\frac{2}{\alpha}}\frac{\pi\Gamma(n+\frac{2}{\alpha})\Gamma(1-\frac{2}{\alpha})}{\Gamma(n)} \tag{2.36}$$

Further, $K_{\alpha,m}$ and $C_{\alpha,m}$ are monotone and bounded with

$$1 \leq K_{\alpha,m} \leq \Gamma(1 - 2/\alpha) \tag{2.37}$$

and

$$C_{\alpha,1} \leq C_{\alpha,m} \leq \pi\Gamma(1 - 2/\alpha) \tag{2.38}$$

and

$$0 < \frac{K_{\alpha,1}}{C_{\alpha,1}} < \frac{K_{\alpha,m}}{C_{\alpha,m}} < \frac{1}{\pi}. \tag{2.39}$$

Proof. To demonstrate the above let the interfering signals and the desired signal be Nakagami fading with different parameters m_i and m_o respectively. The CCDF of the received power is: $F^c_{S_0}(s) = e^{-m_o s}\sum_{k=0}^{m_o-1}\frac{(m_o s)^k}{k!}$ with $m_o = 1$ being the Rayleigh case. According to Theorem 2.3.1:

$$\mathbf{P}(\text{SIR} \geq \beta) = \sum_{k=0}^{m_o-1}\frac{(-\zeta)^k}{k!}\frac{d^k}{d\zeta^k}\mathcal{L}_{I_\Phi}(\zeta)\bigg|_{\zeta=m_o\beta R^\alpha} \tag{2.40}$$

Note that ζ now includes the fading parameter m_o. To determine the Laplace transform of the shot noise process, with m_i denoting the Nakagami parameter for all interfering transmissions the MGF of each mark is altered to be

$$E\left[e^{-\zeta S_i|x|^{-\alpha}}\right] = \frac{1}{(1+\zeta/m_i|x|^\alpha)^{m_i}} \tag{2.41}$$

and the integral in (2.5) can be evaluated as [28]

$$\begin{aligned}\mathcal{L}_{I_\Phi}(\zeta) &= \exp\left\{-2\pi\lambda\int_0^\infty u\left(1-\frac{1}{(1+u^\alpha/\zeta)^{m_i}}\right)\mathrm{d}u\right\}\\ &= \exp\left\{-2\pi\lambda\int_0^\infty \frac{\sum_{k=1}^{m_i}\binom{m_i}{k}u^{k\alpha+1}(m_i/\zeta)^k}{(1+u^\alpha m_i/\zeta)^{m_i}}\mathrm{d}u\right\}\\ &= \exp\left\{-\lambda C_{\alpha,m_i}\zeta^{\frac{2}{\alpha}}\right\}\end{aligned} \tag{2.42}$$

where $C_{\alpha,m_i} = C_{\alpha,m}$ in (2.36). Note that the equation above leads directly to the formulation

$$C_{\alpha,m} = \frac{2\pi}{\alpha}m^{-\frac{2}{\alpha}}\sum_{k=0}^{m-1}\binom{m}{k}B\left(\frac{2}{\alpha}+k; m-\left(\frac{2}{\alpha}+k\right)\right) \tag{2.43}$$

with $B(a,b) = \frac{\Gamma(a)\Gamma(b)}{\Gamma(a+b)}$ being the Beta function, but this was shown to be equivalent to (2.36) in [66]. By Theorem 2.3.1, the optimal contention density is:

$$\bar{\lambda_\epsilon} = \frac{K_{\alpha,m_o}\epsilon}{C_{\alpha,m_i}\beta^{\frac{2}{\alpha}}R^2} \tag{2.44}$$

where K_{α,m_o} is given by (2.18). If m_o is set to 1 (Rayleigh fading) with $K_{\alpha,1} = 1$, and $m_i \to \infty$, the MGF of the power fading mark on each interferer approaches $e^{-\zeta|x|^{-\alpha}}$. Hence,

$$\begin{aligned} \mathcal{L}_{I_\Phi}(\zeta) &= \exp\left\{-2\pi\lambda \int_0^\infty x(1 - e^{-\zeta|x|^{-\alpha}})dx\right\} \\ &= \exp\left\{-\pi\lambda\zeta^{\frac{2}{\alpha}}\Gamma(1-2/\alpha)\right\} \end{aligned} \tag{2.45}$$

indicating that

$$\lim_{m\to\infty} C_{\alpha,m} = \pi\Gamma(1-2/\alpha). \tag{2.46}$$

If in addition $m_i = \infty$ with $C_{\alpha,\infty} = \pi\Gamma(1-2/\alpha)$ and m_o is allowed to approach infinity, the distribution of S_0 becomes an impulse at $S_0 = 1$. Weber, *et al.* [98], derived bounds on the optimal contention density for path loss only (non-fading):

$$\left(\frac{\alpha-1}{\alpha}\right)\frac{\epsilon}{\pi\beta^{\frac{2}{\alpha}}R^2} \leq \bar{\lambda_\epsilon} \leq \frac{\epsilon}{\pi\beta^{\frac{2}{\alpha}}R^2}.$$

This gives

$$\left(\frac{\alpha-1}{\alpha}\right)\frac{1}{\pi} \leq \lim_{m\to\infty}\frac{K_{\alpha,m}}{C_{\alpha,m}} \leq \frac{1}{\pi} \tag{2.47}$$

which for fixed $C_{\alpha,\infty}$ determines the asymptotic orderwise increase of $K_{\alpha,m}$: $\lim_{m\to\infty} K_{\alpha,m} = c_1$, for some finite, nonzero constant c_1. To fully demonstrate the orderwise behavior of $K_{\alpha,m}$, the bounds

$$1 \leq K_{\alpha,m} \leq c_1 \tag{2.48}$$

hold since $K_{\alpha,m}$ is monotonically increasing but approaches the limit c_1.

Equation (4.17) is more general than (2.34) for which $m_o = m_i = m$, but while the physical significance of modeling this disparity between desired and

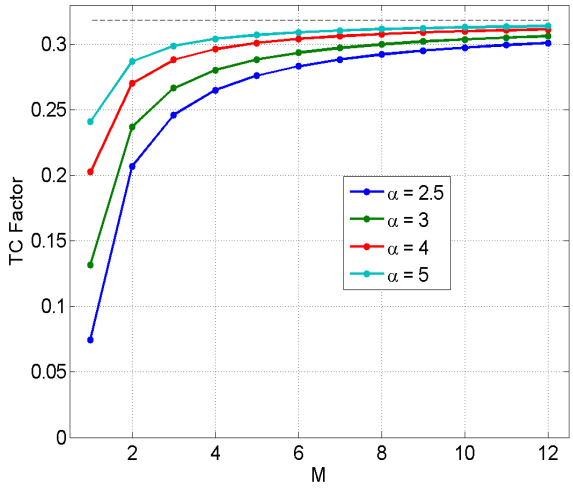

Figure 2.6: $\frac{K_{\alpha,m}}{C_{\alpha,m}} \rightarrow \frac{1}{\pi} \approx .318$ as $m \rightarrow \infty$ for various path loss exponents.

interfering statistics is dubious, it allows the behavior of $K_{\alpha,m}$ and $C_{\alpha,m}$ to be studied. It was shown in [98] that the upper bound is fairly tight which implies that in fact $\lim_{m\rightarrow\infty} \frac{K_{\alpha,m}}{C_{\alpha,m}} \approx \frac{1}{\pi}$. While the upper bound holds, numerically the ratio $\frac{K_{\alpha,m}}{C_{\alpha,m}}$ does in fact approach the upper bound with increasing m. Approximating closely the limit $\frac{K_{\alpha,\infty}}{C_{\alpha,\infty}}$ as $\frac{1}{\pi}$, c_1 can be approximated very closely as $c_1 \approx \Gamma(1 - 2/\alpha)$. □

In [98] the transmission capacity in a non-fading environment is bounded above by $\bar{\lambda_\epsilon} \leq \frac{\epsilon}{\pi\beta^{\frac{2}{\alpha}}R^2}$ and further more this upper bound is fairly tight which implies that in fact $\lim_{m\rightarrow\infty} \frac{K_{\alpha,m}}{C_{\alpha,m}} \approx \frac{1}{\pi}$. Fig. 2.6 shows the ratio $\frac{K_{\alpha,m}}{C_{\alpha,m}}$ for various α versus m. This reinforces the tightness of the upper bound in [98].

Proposition 2.4.1 spans the range of fading and non-fading environments

and demonstrates the potentially significant gain in network capacity for non-fading environments. It also shows that environments with lower path loss suffer more from severe fading (especially for substantial QoS constraints such as $\beta \geq 1$) and improve more with a strong LOS. The distinction is particularly important for dense networks communicating with nearby neighbors which are more likely to have lower path loss *and* a significant LOS. The results also offer a glimpse of the gains to be reaped by diversity techniques that can mitigate fading. The particular results for $K_{\alpha,m}$ and $C_{\alpha,m}$ will also be significant when analyzing MIMO techniques.

2.5 Gamma Approximation for Transmission Capacity Analysis

In [66], a simpler expression for the outage probability was derived when both signal and interference distributions are Gamma distributed with integer shape parameters, which will be reproduced here. Let ϕ denote the link SNR in the abscence of interference, and let the signal fading be distributed as Gamma$[m, \theta]$ and the interference be distributed as Gamma$[n, \Omega]$

$$\begin{aligned} F_S^c(\beta) &= \frac{(-1)^{m-1}}{\Gamma(m)} e^{-\lambda(\frac{\beta\Omega}{\theta})^{\frac{2}{\alpha}} R^2 C_{\alpha,n}} \sum_{l=0}^{m-1} \binom{m-1}{l} \left(-\frac{\beta}{\theta}\right)^l \\ &\quad \times \sum_{i=0}^{m-l-1} s(m-l, i+1) \left(\frac{2}{\alpha}\right)^i \\ &\quad \times \sum_{j=0}^{i} S(i,j) \left(-\lambda \left(\frac{\beta\Omega}{\theta}\right)^{\frac{2}{\alpha}} R^2 C_{\alpha,n}\right)^j \sum_{t=0}^{l} \binom{l}{t} \end{aligned} \tag{2.49}$$

where $s(a,b)$ and $S(a,b)$ are the Stirling numbers of the first and second kind respectively. To clarify the notation, note that all of the summations in 2.50 are nested. When the base thermal noise vanishes, the expression becomes

$$\begin{aligned} F_S^c(\beta) &= \frac{(-1)^{m-1}}{\Gamma(m)} e^{-\lambda(\frac{\beta\Omega}{\theta})^{\frac{2}{\alpha}} R^2 C_{\alpha,n}} \sum_{i=0}^{m-1} s(m,i+1) \left(\frac{2}{\alpha}\right)^i \\ &\quad \times \sum_{j=0}^{i} S(i,j) \left(-\lambda \left(\frac{\beta\Omega}{\theta}\right)^{\frac{2}{\alpha}} R^2 C_{\alpha,n}\right)^j \end{aligned} \tag{2.50}$$

Gamma distributions have long been used as statistical models for unimodal distributions. If a distribution does not fit the standard fading form, but can be well-approximated as a Gamma random variable with integer shape, then (2.50) can be usde to find the distribution of the SINR. Furthermore, the signal and interference factors derived in Sec. 2.4 are the necessary components of the small outage expression (under high SNR):

$$\bar{\lambda_\epsilon} = \left(\frac{\Omega}{\theta}\right)^{\frac{2}{\alpha}} \frac{K_{\alpha,m}\epsilon}{C_{\alpha,n}\beta^{\frac{2}{\alpha}} R^2} \tag{2.51}$$

The maximum likelihood estimation procedure for determining the parameters of a Gamma$[k,\theta]$ distribution fit from a sample set of size N is as follows (see [79]): First, the shape parameter is estimated by the solution to the relation

$$\ln(k) - \psi(k) = \ln\left(\frac{1}{N}\sum_{i=1}^{N} x_i\right) - \frac{1}{N}\sum_{i=1}^{N} \ln(x_i) \tag{2.52}$$

where, $\psi(x) = \frac{\Gamma'(x)}{\Gamma(x)}$ is the digamma function. Given the sample population, this expression can easily be solved numerically for k. Then, the scale parameter is

given by:

$$\hat{\theta} = \frac{1}{kN} \sum_{i=1}^{N} x_i \tag{2.53}$$

since the mean of a Gamma random variable equals the product $k\theta$. If one then desires to restrict k to be an integer, rounding k and adjusting θ to maintain the appropriate mean value yields good results for large k or whenever k is close to an integer.

A prime example of the usefulness of this technique is with the distribution of the eigenvalues of complex Wishart matrices. These eigenvalues describe the channel strengths of orthogonal MIMO channels in Rayleigh fading (which will be discussed more in Chapter 3. Expressions for the distribution of these eigenvalues have been known for at least since [50] in the form of sums of determinants, but it is also known that they can be expressed in standard fading form. Attempts to provide an explicit term-by-term formula have failed so far, though symbolic manipulation software like MATHEMATICA® can give the form for small Wishart matrices. On the other hand, approximation by a Gamma distribution is highly accurate for these distributions, and then immediately amenable to transmission capacity analysis. This Gamma approximation and integer parameter restriction will be termed for convenience *restricted standard fading form*.

2.6 Conclusion

In summary, this chapter presented the concept of transmission capacity in the Poisson power-law shot noise model of ad hoc networks and presented some general expressions for evaluating and optimizing network performance. In

particular, the distribution of the SINR for a large class of signal and fading distributions was derived, as well as a method generating a standard fading form solution. Furthermore, given this standard form solution, a simple expression can be derived relating network spatial traffic to QoS constraints and to environmental and signal processing parameters. Chapter 3, which follows, gives a number of applications of the main Theorem given above, with special attention paid to multi-antenna spatial diversity techniques employed at the physical layer.

Chapter 3

Applications I: Spatial Diversity

This chapter presents a variety of applications of the central Theorem 2.3.1 given in Chapter 2 to a variety of MIMO physical layer configurations. The focus here is on single-data stream techniques, with the framework and examples of multi-data stream scenarios worked out in Chapter 4. Section 3.1 describes an application to a simple model for sectorized antennas. Section 3.2 describes the multi-antenna Rayleigh channel, and its optimal decomposition for point-to-point communication. Section 3.3 analyzes the performance of eigenmode beamforming techniques. Section 3.4 analyzes the performance of orthogonal space-time block coding (OSTBC) techniques. Section 3.5 analyzes the performance of antenna selection techniques. Section 3.6 gives a brief comparison of the applications covered in the chapter and concludes.

3.1 Sectorized Antennas

Consider the standard network model but with transmitters and receivers that are each equipped with M sectorized antennas. Let each antenna cover an angle of $\frac{2\pi}{M}$ radians with an aperture gain of M for both transmitting and receiving in its sector and (potentially) with some small input/output gain outside its sector.

Table 3.1: Radiated Power Densities

–	In sector	Out of sector	Combined
Power emitted:	$\frac{\rho}{1+\gamma(M-1)}$	$\frac{\rho\gamma(M-1)}{1+\gamma(M-1)}$	Sum: ρ
Sector size (rad):	$2\pi\frac{1}{M}$	$2\pi\frac{M-1}{M}$	Sum: 2π
Power density:	$\frac{M/2\pi}{1+\gamma(M-1)}$	$\frac{\gamma M/2\pi}{1+\gamma(M-1)}$	Ratio: γ

Assume each transmitter picks a receiver in a uniformly random direction, and for each transmitter/receiver pair both know the sector in which to communicate with their intended partner. The model can include a constant sidelobe level γ, where the ratio of the sidelobe level to the main lobe is $0 \leq \gamma \leq 1$, for out-of-sector power which is both transmitted and received by the sectorized antenna. Fig. 3.1 depicts the model. The Table 3.1 conveys the power emitted by a transmitter in and out-of sector subject to constant total power ρ. Under this model, the following Proposition holds:

Proposition 3.1.1. *For a random access wireless network in which nodes have M sectorized directional antennas in Nakagami-m fading with a constant (fractional) sidelobe level $\gamma \in [0,1]$ for out of sector power transmitted and received, the optimal contention density with outage ϵ is given by:*

$$\bar{\lambda_\epsilon} = \left(\frac{M}{1+\gamma^{\frac{2}{\alpha}}(M-1)}\right)^2 \frac{K_{\alpha,m}\epsilon}{C_{\alpha,m}\beta^{\frac{2}{\alpha}}R^2} \tag{3.1}$$

where $K_{\alpha,m}$ is given by (2.35) and $C_{\alpha,m}$ by (2.36). Thus $\gamma^{-\frac{4}{\alpha}}$ is an upper bound on the transmission capacity increase due to antenna sectorization.

Proof. The fading statistics of the received signal are assumed to be unchanged by

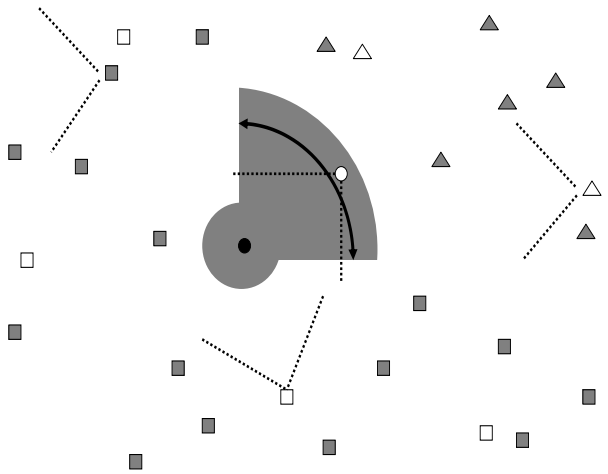

Figure 3.1: Sectorized antenna model with a 90° sector main beam and constant sidelobe level for the receiver of interest (black dot), its intended transmitter (white dot), and the four sets of interferers: Φ_1 the interferers in the active sector transmitting toward the receiver (white triangles), Φ_2 the interferers in the active sector transmitting away from the receiver (shaded triangles), Φ_3 the interferers out of the active sector transmitting toward the receiver (white squares), and Φ_4 the interferers out of the active sector transmitting away from the receiver (shaded squares).

the sectorized antennas, but rather are merely scaled by the emitted and received power density. That the fading statistics are unchanged is reasonable for a small to moderate number of sectors, while for very directional antennas, the scattering seen by any given sector will be reduced and no longer have the typical isotropic properties. As a result of sectorization, four interference terms surface as follows: Let Φ_1 be the set of interferers which are in the active sector of the receiver of interest and are transmitting toward the receiver. Let Φ_2 be the set of interferers in the receiver's active sector which are not transmitting toward the receiver. Let Φ_3

Table 3.2: Interference Shot Noise Processes

–	λ_i	θ_i	ψ_i
I_{Φ_1}	$\lambda\frac{1}{M}$	$2\pi\frac{1}{M}$	$\left(\frac{M}{1+\gamma(M-1)}\right)^2$
I_{Φ_2}	$\lambda\frac{M-1}{M}$	$2\pi\frac{1}{M}$	$\gamma\left(\frac{M}{1+\gamma(M-1)}\right)^2$
I_{Φ_3}	$\lambda\frac{1}{M}$	$2\pi\frac{M-1}{M}$	$\gamma\left(\frac{M}{1+\gamma(M-1)}\right)^2$
I_{Φ_4}	$\lambda\frac{M-1}{M}$	$2\pi\frac{M-1}{M}$	$\gamma^2\left(\frac{M}{1+\gamma(M-1)}\right)^2$

be the set of interferers outside the receiver's sector which are transmitting toward the receiver. And let Φ_4 consist of those interferers transmitting away from the receiver and which are not in the receiver's sector. The independence property of the Poisson process implies these four shot noise processes are independent as well. Furthermore, the I_{Φ_i} are each related to I_Φ since they occur over disjoint subsets of the plane (i.e., a certain sector), are scaled by the combined antenna gains, and the point process of interferers is thinned according to the direction the interferers transmit. The table summarizes the interference contributions from each of these processes with λ_i the effective node density of the process, θ_i the sector size over which the process occurs from the perspective of the typical receiver, and ψ_i the combined antenna gains.

The transforms of the shot noise processes of the I_{Φ_i} are given by

$$\mathcal{L}_{\Phi_i}(\zeta) = \exp\left\{-\lambda_i\theta_i\int_0^\infty 1 - E\left[e^{-\zeta\psi_i S|x|^{-\alpha}}\right]\mathrm{d}x\right\} \tag{3.2}$$

for $\zeta = \psi_0^{-1}\beta R^\alpha$ with ψ_0 being the combined antenna gain between the typical receiver and its intended transmitter, and $\psi_0 = \psi_1$. Consider the Rayleigh fading

case. The outage probability at a typical receiver is

$$\begin{aligned}
\mathbf{P}(\text{SIR} \geq \beta) &= \mathbf{P}\left(\frac{\psi_0 \rho S_0 R^{-\alpha}}{\rho \sum_{i=1}^{4} I_{\Phi_i}} \geq \beta\right) \\
&= \int_0^\infty F_{S_0}^c(\psi_0^{-1}\beta R^\alpha s) f_{[I_{\Phi_1}+I_{\Phi_2}+I_{\Phi_3}+I_{\Phi_4}]}(s) \\
&= \prod_{i=1}^{4} \mathcal{L}_{\Phi_i}(\zeta)|_{\zeta=\psi_0^{-1}\beta R^\alpha} \\
&= \exp\left\{-\lambda \beta^{\frac{2}{\alpha}} R^2 C_\alpha \left(\frac{1+\gamma^{\frac{2}{\alpha}}(M-1)}{M}\right)^2\right\}
\end{aligned} \tag{3.3}$$

and solving for λ gives

$$\bar{\lambda_\epsilon} = \left(\frac{M}{1+\gamma^{\frac{2}{\alpha}}(M-1)}\right)^2 \frac{\epsilon}{C_\alpha \beta^{\frac{2}{\alpha}} R^2}. \tag{3.4}$$

Next note that

$$\frac{M}{1+\gamma^{\frac{2}{\alpha}}(M-1)} \leq \frac{1}{\gamma^{\frac{2}{\alpha}}} \tag{3.5}$$

and as M becomes large, it approaches the limit

$$\lim_{M\to\infty} \left(\frac{M}{1+\gamma^{\frac{2}{\alpha}}(M-1)}\right)^2 = \frac{1}{\gamma^{\frac{4}{\alpha}}}. \tag{3.6}$$

This results in an upper bound of $\gamma^{-\frac{4}{\alpha}}$ on the improvement (over (2.34)) in optimal contention density from sectorized antennas. If signals are Nakagami-m distributed instead, since the desired and interfering signals are independent, $C_{\alpha,m}$ replaces C_α and $K_{\alpha,m}$ appears in the numerator of (3.4). □

These results firstly indicate that directional antennas increase transmission capacity by nearly a factor of M^2 for low sidelobe levels. This indicates

that MIMO techniques that avoid or reduce interference in an ad hoc network are highly beneficial at the physical layer. In addition there are advantages at higher network layers such as increased ability to learn the topology of the network, perform directional routing, etc; see [77] and [13] and references therein for more details. This section has characterized the potential increase in area spectral efficiency due to antenna sectorization which by itself provides greater potential and flexibility for routing and network management, but the full relationship between directional antennas and these higher layer functions is still an area of ongoing research.

However, this analysis also indicates that if for practical reasons, sidelobe levels cannot be reduced, then the sidelobes limit the potential gains even for very directional antennas. This model also suffers from very idealistic assumptions about the real propagation environment, especially since dense multipath can result in signal angle of arrival being quite different from the geographic angle to the transmitter. As pointed out in [77], real antenna patterns are far from "pie slices" and in multipath environments, static antennas are much less robust to fluctuating channels.

3.2 Decomposing the MIMO Channel

In order to study multi-antenna techniques, a model of the MIMO channel is needed. When each transmitter has M_t antennas and each receiver has M_r antennas, and $m = \min\{M_t, M_r\}$ data streams are transmitted, each with a separate packet, in Rayleigh fading the channel is $R^{-\frac{\alpha}{2}}\mathbf{H}_{00}$ which is an $M_t \times M_r$

matrix of i.i.d. complex Gaussian entries with unit variance. This channel can be decomposed into spatial modes by means of its singular value decomposition (SVD):

$$\mathbf{H}_{00} = \mathbf{U}_{00}\mathbf{\Sigma}_{00}\mathbf{V}_{00}^{H} , \tag{3.7}$$

where $(\cdot)^H$ denotes a conjugate transpose, $\mathbf{V}_{00}$ and $\mathbf{U}_{00}$ are the unitary matrices of input and output singular vectors respectively and $\mathbf{\Sigma}_{00}$ is the diagonal matrix of singular values, which are the square roots of the eigenvalues of $\mathbf{H}_{00}\mathbf{H}_{00}^{H}$. The ith interferer has the channel

$$R^{-\frac{\alpha}{2}}\mathbf{H}_{ii} = R^{-\frac{\alpha}{2}}\mathbf{U}_{ii}\mathbf{\Sigma}_{ii}\mathbf{V}_{ii}^{H} \tag{3.8}$$

between itself and its intended receiver with $|X_i|$ denoting the distance between it and the receiver of interest; and $|X_i|^{-\frac{\alpha}{2}}\mathbf{H}_{0i}$ is the channel between the ith interferer and the receiver of interest. The M spatial modes can be accessed by pre-coding the vector of symbols $\mathbf{s}_0$ by $\mathbf{V}_{00}$ and post-coding by $\mathbf{U}_{00}^{H}$ and the receiver of interest sees interference according to:

$$\begin{aligned}
\mathbf{y} &= R^{-\frac{\alpha}{2}}\mathbf{H}_{00}\mathbf{V}_{00}\mathbf{s}_0 + \sum_i |X_i|^{-\frac{\alpha}{2}}\mathbf{H}_{0i}\mathbf{V}_{ii}\mathbf{s}_i + \mathbf{n} \\
\mathbf{z} &= \mathbf{U}_{00}^{H}\mathbf{y} \\
&= R^{-\frac{\alpha}{2}}\mathbf{U}_{00}^{H}\mathbf{H}_{00}\mathbf{V}_{00}\mathbf{s}_0 + \sum_i |X_i|^{-\frac{\alpha}{2}}\mathbf{U}_{00}^{H}\mathbf{H}_{0i}\mathbf{V}_i\mathbf{s}_i + \mathbf{U}_{00}^{H}\mathbf{n} \\
&= R^{-\frac{\alpha}{2}}\mathbf{\Sigma}_0\mathbf{s}_0 + \sum_i |X_i|^{-\frac{\alpha}{2}}\mathbf{H}_{\text{eff},i}\mathbf{s}_i + \tilde{\mathbf{n}}
\end{aligned} \tag{3.9}$$

where the SINR is calculated on the statistic $\mathbf{z}$. In a Rayleigh fading environment, $\mathbf{H}_{\text{eff},i}$ is a standard random Gaussian matrix. It is assumed in the above that $\mathbf{s}_0$ and $\mathbf{s}_i$ have norm ρ with power allocated among their respective entries. In

point-to-point MIMO links, SVD pre- and post-coding is optimal and achieves the maximum received SNR on each of the spatial modes, but other coding strategies could be used. For instance, in the absence of CSI at the transmitter, an identity matrix could be substituted for the pre-coding matrices $\mathbf{V}_{00}$ and the receiver could substitute the pseudo-inverse of $\mathbf{H}_{00}$ for $\mathbf{U}_{00}^{H}$ for a zero-forcing detection strategy.

3.3 Eigen-Beamforming

Dynamic beamforming is one of the most prominent multiple antenna techniques, having been employed for decades in electromagnetic detection and imaging applications. The complexity is manageable and it can be performed on any number of antennas in any configuration ([7], ch. 6). However, to be explicit since "beamforming" has become quite an overloaded term, this section uses the term to mean the following: At the receiver it refers to a coherent linear combination of the antenna outputs, while at the transmitter it refers to sending linearly weighted versions of the same signal on each antenna. Thus, unlike the previous section, no attention is paid to the specific physical pattern of energy propagation. In each case for this analysis, the weights are determined by the dominant singular vectors or eigenvectors (hence, "eigen-beamforming") of the channel. Throughout this section it is assumed that both the transmitter and receiver have perfect channel knowledge of their own channel, but not of interfering channels. Hence, signaling strategies would maximize SNR over a specific channel without knowledge of the interference structure. The focus falls first on the vector (SIMO or MISO) channel for which eigen-beamforming is equivalent

to maximal ratio transmission or combining. Attention then turns to the general matrix (MIMO) channel for which a single data stream is sent over the dominant eigenmode.

3.3.1 Transmit-Only and Receive-Only Eigen-Beamforming

Consider first a wireless system in which all transmitters transmit with power ρ using only one antenna and receivers beamform on M antennas by coherently combining the received signals. Again, this is beamforming along the dominant (and only) eigenmode of the $1 \times M$ channel. As shown in [47], this is equivalent to an $M \times 1$ vector channel for which maximal ratio transmission is performed at the transmitter and one receive antenna is used. The channel model for the desired signal in a Rayleigh fading environment is a vector of i.i.d. unit variance, complex Gaussian entries scaled by the power law path loss function: $\mathbf{h}_0\sqrt{|R|^{-\alpha}}$ for the kth entry of $\mathbf{h}_0$ independently $[\mathbf{h}_0]_k \sim \mathcal{CN}(0,1)$, and similarly the channel between a receiver and the ith interferer is $\mathbf{h}_i\sqrt{|X_i|^{-\alpha}}$ with $[\mathbf{h}_i]_k \sim \mathcal{CN}(0,1)$. Under this model, the following Proposition holds. As before the Proposition will be given in two parts: the first is an expression for the exact optimal contention density for small outage constraints and the second is a set of bounds that help interpret the exact results.

Proposition 3.3.1. *For a random access wireless network in which nodes transmit on a single antenna and perform maximal ratio combining with M antennas; or equivalently perform maximal ratio transmission with M antennas and receive on a single antenna; the optimal contention density under Rayleigh fading with*

outage constraint ϵ is given by:

$$\bar{\lambda_\epsilon} = \frac{K_{\alpha,M}\epsilon}{C_\alpha \beta^{\frac{2}{\alpha}} R^2} \tag{3.10}$$

where $K_{\alpha,M}$ is given by (2.35) and $C_\alpha = C_{\alpha,1}$ in (2.36). Further, $\bar{\lambda_\epsilon}$ is $\Theta(M^{\frac{2}{\alpha}})$ and bounded by:

$$\frac{M^{\frac{2}{\alpha}}\epsilon}{C_\alpha \beta^{\frac{2}{\alpha}} R^2} \leq \bar{\lambda_\epsilon} \leq \frac{\Gamma(1-\frac{2}{\alpha})M^{\frac{2}{\alpha}}\epsilon}{C_\alpha \beta^{\frac{2}{\alpha}} R^2}. \tag{3.11}$$

Proof. To characterize the interference seen by an M-antenna receiver that ignores interfering signals, beamforming simply to maximize its own received signal power (again thermal noise is assumed negligible), the SIR expression is:

$$\begin{aligned} \text{SIR} &= \frac{\frac{\rho}{M}|\mathbf{h}_0^H \mathbf{h}_0|^2 R^{-\alpha}}{\frac{\rho}{M}\sum_{X_i \in \Phi} |\mathbf{h}_0^H \mathbf{h}_i|^2 |X_i|^{-\alpha}} \\ &= \frac{\|\mathbf{h}_0\|^2 R^{-\alpha}}{\sum_{X_i \in \Phi} \left| \frac{\mathbf{h}_0^H}{\|\mathbf{h}_0\|} \mathbf{h}_i \right|^2 |X_i|^{-\alpha}}. \end{aligned} \tag{3.12}$$

As shown in [80], since a linear combination of Gaussian variables is again Gaussian, the product $\frac{\mathbf{h}_0^H}{\|\mathbf{h}_0\|}\mathbf{h}_i$ is distributed as a single complex Gaussian random variable with zero mean and unit variance. Letting $S_i = \left| \frac{\mathbf{h}_0^H}{\|\mathbf{h}_0\|} \mathbf{h}_i \right|^2$, which is exponentially distributed, the SIR expression is

$$\text{SIR} = \frac{\|\mathbf{h}_0\|^2 R^{-\alpha}}{\sum_{X_i \in \Phi} S_i |X_i|^{-\alpha}} = \frac{\|\mathbf{h}_0\|^2 R^{-\alpha}}{I_\Phi}. \tag{3.13}$$

Setting $S_0 = \|\mathbf{h}_0\|^2$ and considering a standard network but with beamforming receivers with M antennas, the distribution of the received signal is now χ^2 with $2M$ degrees of freedom. The CCDF of S_0 is $F_{S_0}^c(x) = e^{-x}\sum_{k=0}^{M-1} \frac{x^k}{k!}$. However, the interference has the same form as the shot noise process for the

single-antenna case. Applying now a small outage constraint and Theorem 2.3.1, it can be stated simply that $K_{\alpha,M}$ is given by (2.35) and $C_\alpha = C_{\alpha,1}$ in (2.36). As shown in (2.38),

$$1 \leq \frac{K_{\alpha,M}}{M^{\frac{2}{\alpha}}} \leq \Gamma(1-2/\alpha)$$

which indicates that

$$\frac{M^{\frac{2}{\alpha}}\epsilon}{C_\alpha \beta^{\frac{2}{\alpha}} R^2} \leq \frac{K_{\alpha,M}\epsilon}{C_\alpha \beta^{\frac{2}{\alpha}} R^2} \leq \frac{\Gamma(1-\frac{2}{\alpha})M^{\frac{2}{\alpha}}\epsilon}{C_\alpha \beta^{\frac{2}{\alpha}} R^2} \tag{3.14}$$

with equality to the lower bound at $M = 1$ and approaching the upper bound with increasing M since C_α is constant while $K_{\alpha,M}$ is increasing in M. The term in the middle is now equal to $\bar{\lambda}_\epsilon$. □

Proposition 3.3.1 gives a general scaling[1] of the optimal contention density with the number of antennas, target SIR, path loss, the transmitter-receiver separation, and the outage constraint. Fig. 3.2 gives the transmission capacity versus M for four different path loss exponents. Fig. 3.3 gives the $K_{\alpha,M}$ factor versus M for the same path loss exponents. As evident from the figures, as path loss reduces and interference becomes less attenuated by distance, the gain of the MIMO technique over the SISO case increases. However, higher path loss results in higher transmission capacity for smaller numbers of antennas since path loss helps to spatially separate transmissions. Fig. 3.4 demonstrates the relationship of the exact $K_{\alpha,M}$ factor to the upper and lower bounds. The upper bound is both asymptotically tight and a good approximation for higher path loss.

[1]Under somewhat different assumptions, this scaling with the number of antennas was shown earlier by [26].

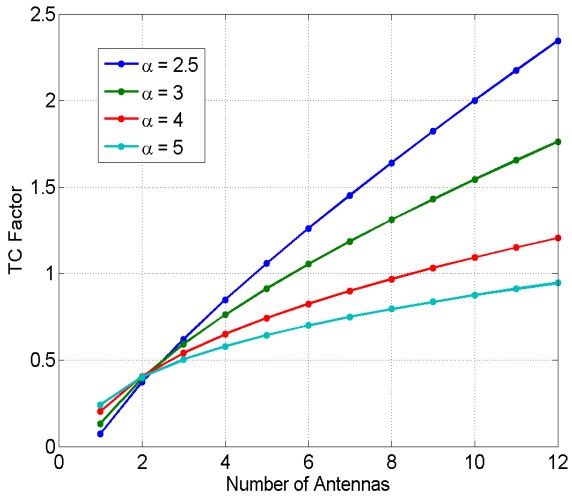

Figure 3.2: Transmission capacity proportionality constant (i.e., ratio of signal factor over interference factor) versus M for four path loss exponents, $2.5, 3, 4$, and 5, for $1 \times M$ MRC. Higher path loss separates transmissions spatially and is the dominant effect for smaller numbers of antennas. But with a larger number of antennas, ultimately network performance is improved more through interference robustness than spatial separation.

3.3.2 Dominant Eigenmode Beamforming

Now consider the same network but with nodes each equipped with M_t transmit and M_r receive antennas to perform dynamic eigen-beamforming at both transmitter and receiver ends. This extension of MRC has significant advantages even over $1 \times M$ MRC since the diversity order increases as $M_t M_r$. The Rayleigh fading MIMO channel is modeled as a matrix of i.i.d. zero-mean, unit-variance complex Gaussian entries scaled by path loss. The channel of the desired signal for the transmitter-receiver pair of interest is denoted $\mathbf{H}_{00}$. The transmitter and receiver beamform using the input and output singular vectors $\mathbf{v}_0$ and $\mathbf{u}_0$, respec-

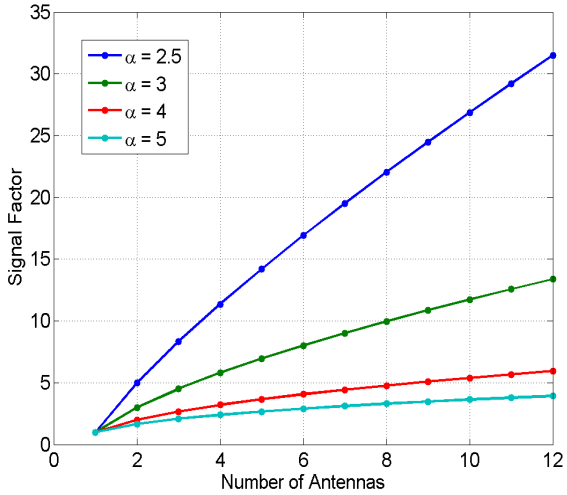

Figure 3.3: The $K_{\alpha,M}$ factor versus M for four path loss exponents, $2.5, 3, 4$, and 5, for $1 \times M$ MRC. Lower path loss results in much greater gains over the SISO case ($M = 1$).

tively, corresponding to the maximum singular value of $\mathbf{H}_{00}$. This results in the received power being equal to the square of the maximum singular value $\phi^2_{\max}$ scaled by path loss and the transmit power. Each interfering transmitter, on the other hand, beamforms to maximize received power across some other Rayleigh channel $\mathbf{H}_{ii}$ using beamforming vector $\mathbf{v}_i$, and interferes at the receiver of interest through channel $\mathbf{H}_{0i}$. For such a network, the following bounds hold:

Proposition 3.3.2. *For a random access wireless network in which nodes perform maximal ratio transmission and combining on M_t and M_r antennas respectively, for small outages the optimal contention density is bounded by:*

$$\frac{\max\{M_t, M_r\}^{\frac{2}{\alpha}}\epsilon}{C_\alpha R^2 \beta^{\frac{2}{\alpha}}} \leq \bar{\lambda_\epsilon} \leq \frac{\Gamma(1-\frac{2}{\alpha})(M_t M_r)^{\frac{2}{\alpha}}\epsilon}{C_\alpha R^2 \beta^{\frac{2}{\alpha}}} \tag{3.15}$$

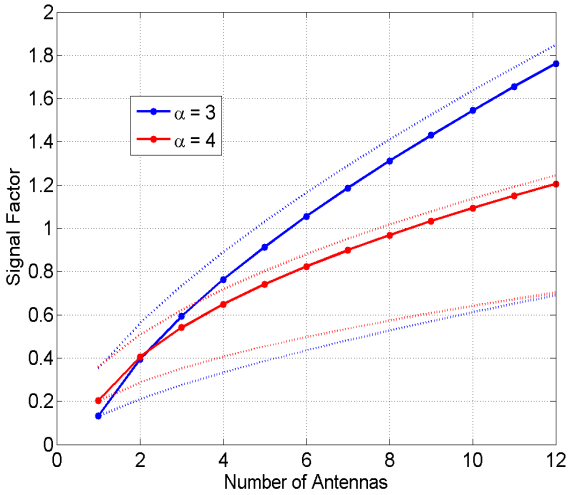

Figure 3.4: Demonstration of the bounds on transmission capacity for $1 \times M$ or equivalently $M \times 1$ MRC. The upper bound is asymptotically tight and a good approximation for higher path loss.

for $C_\alpha = C_{\alpha,1}$ *given in (2.36).*

Proof. To begin, the SIR expression for this model is

$$\text{SIR} = \frac{\rho \phi_{\max}^2 R^{-\alpha}}{\rho \sum_{X_i \in \Phi} |X_i|^{-\alpha} |\mathbf{u}_0^H \mathbf{H}_{0i} \mathbf{v}_i|^2} \cdot \tag{3.16}$$

Note that $\mathbf{u}_0$, $\mathbf{H}_{0i}$, and $\mathbf{v}_i$ are all independent. As discussed in [48], the full product $\mathbf{u}_0^H \mathbf{H}_{0i} \mathbf{v}_i$ is distributed as a single zero-mean, unit-variance, complex Gaussian variable since the inner product of a vector i.i.d. complex Gaussian variables with an arbitrary unit vector is a single complex Gaussian variable. This simplifies the SIR expression to $\text{SIR} = \frac{\phi_{\max}^2 R^{-\alpha}}{I_\Phi}$. with the distribution of the interference unchanged from the single antenna Rayleigh fading case. Again neglecting thermal

noise, the received and interfering signals are independent and $C_\alpha = C_{\alpha,1}$ in (2.36) by equivalence of the shot noise processes.

As for the received signal, note that the CCDF of the square of the maximum singular value of the desired channel (or equivalently the largest eigenvalue of a complex Wishart matrix), has been reported by Kang and Alouini [47] (originally given by Khatri [50]):

$$F^c_{\phi^2_{\max}}(x) = 1 - \frac{|\Psi(x)|}{\Pi_{k=1}^{q}\Gamma(q-k+1)\Gamma(s-k+1)}$$

where $|\cdot|$ denotes a determinant, $q = \min\{M_t, M_r\}$, $s = \max\{M_t, M_r\}$, and the entries of the $q \times q$ matrix $\Psi(x)$ are given by

$$\{\Psi(x)\}_{i,j} = \gamma(s-q+i+j-1, x)\ ,\ i,j = 1,\ \ldots\ , q \tag{3.17}$$

where $\gamma(\cdot,\cdot)$ is the lower incomplete gamma function. Recall

$$\gamma(n,x) = (n-1)!\left(1 - e^{-x}\sum_{k=0}^{n-1}\frac{x^k}{k!}\right), \tag{3.18}$$

for $n \in \mathbb{N}$, which clearly facilitates the application of Theorem 2.3.1 yielding the outage probability and the optimal contention density, which will again have the form:

$$\bar{\lambda_\epsilon} = \frac{K^{mrt}_{\alpha,M_t,M_r}\epsilon}{C_\alpha R^2 \beta^{\frac{2}{\alpha}}}\ .$$

A general expression for K^{mrt}_{α,M_t,M_r} is unavailable since the explicit sum-of-exponentials-and-polynomials form for $F^c_{\phi^2_{\max}}$ is not known. However, the largest squared singular value is bounded by [35]:

$$\|\mathbf{H}_{00}\|_F^2 \geq \phi^2_{\max} \geq \frac{\|\mathbf{H}_{00}\|_F^2}{\min\{M_t, M_r\}}.$$

Since $\|\mathbf{H}_{00}\|_F^2$ is χ^2 with $2M_tM_r$ degrees of freedom this is equivalent to a particular MRC case in (3.10) and (3.11) indicating that

$$K^{mrt}_{\alpha,M_t,M_r} \leq K_{\alpha,(M_tM_r)} \leq \Gamma(1-2/\alpha)(M_tM_r)^{\frac{2}{\alpha}} \tag{3.19}$$

so that

$$\bar{\lambda_\epsilon} \leq \frac{\Gamma(1-\frac{2}{\alpha})(M_tM_r)^{\frac{2}{\alpha}}\epsilon}{C_\alpha R^2 \beta^{\frac{2}{\alpha}}}. \tag{3.20}$$

Furthermore, a lower bound can be obtained from (3.11) as

$$\begin{aligned} K^{mrt}_{\alpha,M_t,M_r} &\geq \frac{K_{\alpha,(M_tM_r)}}{\min\{M_t,M_r\}^{\frac{2}{\alpha}}} \\ &\geq \frac{(M_tM_r)^{\frac{2}{\alpha}}}{\min\{M_t,M_r\}^{\frac{2}{\alpha}}} \\ &= \max\{M_t,M_r\}^{\frac{2}{\alpha}} \end{aligned} \tag{3.21}$$

so that

$$\bar{\lambda_\epsilon} \geq \frac{\max\{M_t,M_r\}^{\frac{2}{\alpha}}\epsilon}{C_\alpha R^2 \beta^{\frac{2}{\alpha}}}\,. \tag{3.22}$$

□

Since K^{mrt}_{α,M_t,M_r} cannot be given explicitly for arbitrary M_t and M_r at present, consider as an example the case $M_t = M_r = 2$ for which

$$F^c_{\phi^2_{\max}}(x) = 2e^{-x} - e^{-2x} + x^2e^{-x}.$$

Applying Theorem 2.3.1 for small outages:

$$\mathbf{P}(\text{SIR} < \beta) \approx \lambda C_\alpha R^2 \beta^{\frac{2}{\alpha}} \left(2 - 2^{\frac{2}{\alpha}} - \frac{2}{\alpha}\left(1 - \frac{2}{\alpha}\right)\right). \tag{3.23}$$

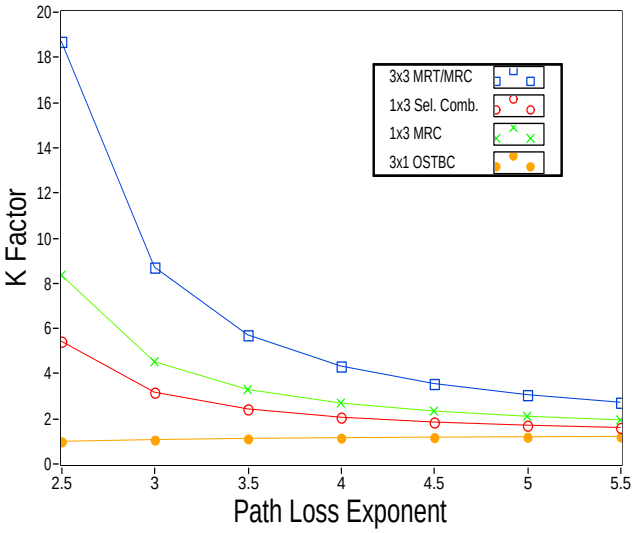

Figure 3.5: $K_{\alpha,3}^{mrt}$ (3×3 MRT/MRC), $K_{\alpha,3}$ (1×3 MRC), $K_{\alpha,M}^{sc}$ (1×3 selection combining), and $\frac{K_{\alpha,M_t}}{C_{\alpha,M_t}} C_{\alpha,1}$ (3×1 OSTBC) versus α for various M. The factor for OSTBCs is the only which increases (slightly) with increasing path loss since interference reduces. (The factor $C_{\alpha,1}$ is a normalizing factor for fair comparison with other techniques and the SISO case for which $K = 1$.)

For $M_t = M_r$ and both large, $\phi_{\max}^2$ of the channel matrix approaches $4M_t$ [16]. This leads to the conjecture that for moderately large numbers of antennas (e.g., $M_t, M_r > 3$), the lower bound reflects the orderwise behavior in a rich scattering environment. However, the upper bound should be more appropriate in a LOS channel. Fig. 3.5 depicts both $K_{\alpha,M}$ and for the square channel case $M = M_t = M_r$, $K_{\alpha,M}^{mrt}$ for various M, α. Again $K_{\alpha,M}^{mrt} \to 1$ with increasing α. This implies that as α becomes large, nodes are already spatially separated through path loss, and spatial diversity yields less improvement over the single antenna case.

3.4 Orthogonal Space-Time Block Coding

Orthogonal space-time block coding has been one of the more quickly accepted transmit diversity techniques for several good reasons. First, OSTBCs achieve full diversity in point-to-point links without requiring channel state information at the transmitter. Second, an optimum receiver design is simply a matched filter without any need for joint decoding of multiple symbols (error correction codes notwithstanding). Furthermore, space-time coding results in far less variability in the effective channel, greatly reducing the frequency and duration of deep fades. However, there is another source of effective channel instability, particularly in decentralized networks, which is cochannel interference. In light of the results on reduced fading as well as MRT/MRC earlier in this paper, for which the latter results in much greater network improvement, it is unclear how OSTBCs compare in a decentralized, interference-limited environment and warrants further investigation.

Specific codes are characterized by the number of transmit antennas used (M_t), the number of time slots used (N), and the number of independent data symbols sent (N_s) [57]. Again M_r denotes the number of receive antennas but this has no effect on the code structure. However, it will also be necessary to characterize OSTBCs the degrees of freedom of the resulting interference[1], which is the number of symbols transmitted per time slot (N_r). The familiar Alamouti

[1]Originally, in [38] the degrees of freedom of the interference were given as the number of time slots each symbol was transmitted. It was shown in [66] that a better approximation is the number of symbols transmitted each time slot. These are equal for some codes, such as Alamouti's, but simulations bear out the superiority of the latter approximation in other cases.

code has $M_t = N = N_s = N_r = 2$.

Proposition 3.4.1. *For a random access wireless network in which transmitting nodes use orthogonal space-time block codes with M_t transmit antennas and code parameter N_r and receiving nodes perform maximal ratio combining with M_r antennas in Rayleigh fading, the optimal contention density under the outage constraint ϵ is given by:*

$$\bar{\lambda_\epsilon} = \frac{K_{\alpha,M_tM_r}\epsilon}{C_{\alpha,N_r}\beta^{\frac{2}{\alpha}}R^2} \tag{3.24}$$

where K_{α,M_tM_r} is given by (2.35) and C_{α,N_r} in (2.36). Further, $\bar{\lambda_\epsilon}$ is $\Theta(M_r^{\frac{2}{\alpha}})$:

$$\frac{M_r^{\frac{2}{\alpha}}\epsilon}{C_{\alpha,1}\beta^{\frac{2}{\alpha}}R^2} \leq \bar{\lambda_\epsilon} \leq \frac{M_r^{\frac{2}{\alpha}}\epsilon}{\pi\beta^{\frac{2}{\alpha}}R^2}. \tag{3.25}$$

Proof. For the received signal, since detection decouples for OSTBCs [76] over the N_r time slots as well as M_r antennas, the received amplitude is $\|\mathbf{H}_0\|_F^2$ for each symbol [76], where $\mathbf{H}_0$ is the $M_r \times M_t$ complex Gaussian channel. The distribution of $\|\mathbf{H}_0\|_F^2$ is χ^2, just as with MRC, but with $2M_tM_r$ degrees of freedom. So applying Theorem 2.3.1, the K factor is $K_{\alpha,M}$ in (2.35) for $M = M_tM_r$.

The interference seen by an OSTBC processing system is more complicated, however. To determine the distribution of S_i, consider the expression for the interference term from a single interferer:

$$|X_i|^{-\alpha}S_i = |X_i|^{-\alpha}\sum_{k=1}^{N_r}\frac{\mathbf{h}_0^H}{\|\mathbf{h}_0\|}\mathbf{h}_i^{(k)}s_i^{(k)} = |X_i|^{-\alpha}\sum_{k=1}^{N_r}S_i^{(k)} \tag{3.26}$$

where $\mathbf{h}_0 = \text{vec}(\mathbf{H}_0)$ and $\mathbf{h}_i^{(k)}$ is a permutation of the entries in $\text{vec}(\mathbf{H}_i)$ depending on the block coding structure. Since desired symbols are repeated N_r times, each

S_i is a sum N_r terms $S_i^{(k)}$ each of which is exponentially distributed though not independent. In a strict sense, this violates the independence of S_0 and S_i required by Theorem 2.3.1. However, rough independence of received and interfering signal statistics is assumed, with the statistics of the sum of $S_i^{(k)}$ nearly indistinguishable from a Gamma distribution independent of S_0. The nature of the post-processing interference here was also reported in [12]. Note that this assumption removes some inherent structure in the interference so that the analysis becomes worst case.

Since the Gamma distribution is the same mark distribution encountered for Nakagami-m fading interferers, C_{α,N_r} is given by (2.36). As shown before, the factor increases with $N_r^{\frac{2}{\alpha}}$ indicating that repeating the symbols introduces more cochannel interference. Applying Theorem 2.3.1 for small outages

$$\bar{\lambda_\epsilon} = \frac{K_{\alpha,M_tM_r}\epsilon}{C_{\alpha,N_r}R^2\beta^{\frac{2}{\alpha}}} \leq \frac{(M_tM_r)^{\frac{2}{\alpha}}\epsilon}{\pi N_r^{\frac{2}{\alpha}}R^2\beta^{\frac{2}{\alpha}}} = \frac{M_r^{\frac{2}{\alpha}}\epsilon}{\pi R^2\beta^{\frac{2}{\alpha}}} \tag{3.27}$$

for most practical block codes since $M_t = N_r$, which is the best case. For the lower bound, one can simply ignore the change in the constant C_{α,N_r} substituting $C_{\alpha,1}$ which is greater than π. (That is, let $K_{\alpha,M}$ increase but not C_{α,N_r}). □

The primary insight from the analysis of OSTBCs is that in an environment of significant cochannel interference, they accomplish little. As is evident from the bounds, the number of receive antennas is the primary factor in network performance. While block codes harden the channel resulting in a network performance gain equivalent to that gained from reducing fading, they also tend to amplify interference since symbols are repeated. When symbols are repeated

multiple times from the same antenna, as in some orthogonal designs, this effect is worsened so that $N_r = M_t$ is the best case. Furthermore, even though power is split between simultaneously transmitted symbols, the transmit antennas become multiple independent interference sources for other nodes in the network. Furthermore, OSTBCs take a hit in the data rate for any code beside Alamouti's. So for a larger number of antennas, OSTBCs are typically inferior to other schemes and are likely not worth even the slight added complexity.

Fig. 3.6 compares the optimal contention density for $M \times 1$ OSTBCs for which the receiver receives on only one antenna, $M \times M$ OSTBCs for which the receiver performs MRC on M antennas in addition to the transmit block coding, as well as $1 \times M$ MRC without block coding. The figure shows the optimal contention density for $\alpha = 3$, target SINR 4.77dB, and transmitter-receiver separation 10m. First, there is little gain over simply performing MRC in contention density. But what is not shown is that for the number of antennas larger than two, the transmission capacity for $M \times M$ OSTBCs actually falls below the MRC curve since it must use a reduced rate code. If only one receive antenna is used, then for any number of transmit antennas beyond two, there is essentially no gain when code rate is taken into account. This confirms that the primary source of gain is at the receiver and that for any system beyond 2×2, it would be better to simply select one antenna and operate in the $1 \times M$ MRC mode.

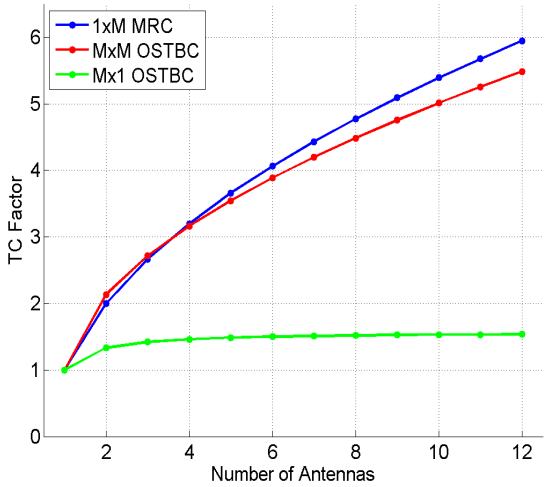

Figure 3.6: Comparison of the transmission capacity proportionality factor for $M \times M$ OSTBC/MRC, $1 \times M$ MRC, and $M \times 1$ OSTBC respectively. Full OSTBC yields optimal contention density similar to receiver MRC only but is actually worse (due to self-interference) for a large antenna array.

3.5 Selection Diversity and Combining

A fundamental characteristic of MIMO fading channels is that due to polarization, pattern diversity, or spatial separation, one or more antenna elements may be receiving above average signal strength. Simply selecting the best often has the practical advantage over more sophisticated combining schemes of simpler implementation, or less expensive hardware. There are a variety of ways to perform antenna selection, and antenna selection can be used in conjunction with other diversity techniques. As an example let the transmitter operate one antenna and the receiver select one of M which has the best instantaneous channel with

i.i.d. Rayleigh fading between all antennas. In this case,

$$F_{S_0}^c(x) = 1 - (1 - e^{-x})^M = \sum_{k=1}^{M} \binom{M}{k} (-1)^{k+1} e^{-kx} \tag{3.28}$$

and the interference fading channels S_i remain exponentially distributed. This can be extended by considering a system that selects the best pair of antennas (one transmit and one receive) from among M_t transmit and M_r receive antennas. The parameter M in (3.28) is simply replaced by $M_t M_r$. Here the full matrix channel is $\mathbf{H}_{00}$ as in Sec. 3.2 from which the element with the largest magnitude is selected. The following Proposition characterizes the gain from selection diversity:

Proposition 3.5.1. *For a random access wireless network in which nodes perform selection diversity/combining by selecting the best pair among M_t transmit and M_r receive antennas in Rayleigh fading, the optimal contention density under the outage constraint ϵ is given by:*

$$\bar{\lambda_\epsilon} = \frac{K_{\alpha,M^2}^{sc}}{C_\alpha} \frac{\epsilon}{\beta^{\frac{2}{\alpha}} R^2} \tag{3.29}$$

for $M^2 = M_t M_r$, $C_\alpha = C_{\alpha,1}$ in (2.36), and

$$K_{\alpha,M^2}^{sc} = \left[\sum_{k=1}^{M^2} \binom{M^2}{k} (-1)^{k+1} k^{\frac{2}{\alpha}} \right]^{-1}. \tag{3.30}$$

Proof. This is given by simply substituting the coefficients in (3.28) into Theorem 2.3.1 and noting that the statistics of the interference are identical to the SISO case for any pair of antennas. □

There are a number of other distributions resulting from antenna selection that can be considered. For example, in an $M_r \times M_t$ system performing MRC at the

receiver, one transmit antenna may be selected which has the largest magnitude vector channel to the intended receiver. The distribution of the interference after MRC processing will remain the same but S_0 will have

$$\begin{aligned} F^c_{S_0}(x) &= 1 - \left(1 - e^{-x} \sum_{k=0}^{M_r-1} \frac{x^k}{k!}\right)^{M_t} \\ &= \sum_{m=1}^{M_t} e^{-mx} \sum_{k=0}^{M_t(M_r-1)} a_{mk} x^k \end{aligned} \tag{3.31}$$

for

$$a_{mk} = (-1)^{M_t+m} \binom{M_t}{m} \sum_{\substack{n_1,n_2,\ldots n_m \leq M_r-1 \\ n_1+n_2\ldots+n_m=k}} \prod_{i=1}^{m} (n_i!)^{-1} \tag{3.32}$$

with the sum running over all (ordered) m-tuples of positive integers less than $M_r - 1$ which add to k. From Theorem 2.3.1 the K factor can now be determined which specifies the optimal contention density as well. Fig. 3.7 compares the gain in transmission capacity for a number of systems versus the number of antennas, including MRT/MRC, OSTBCs, as well as two kinds of selection diversity/combining: one in which the transmitter transmits on one antenna and the receiver selects the best of its own antennas, and the second in which the receiver and transmitter jointly select the best pair of single antennas. Clearly antenna selection can significantly enhance network performance since it improves the typical channel without amplifying interference. Of course, as the number of antennas becomes large, obtaining M^2 statistically independent pairs is difficult, and array gain quickly becomes superior in terms of network performance. Still, Proposition 3.5.1 implies that antenna selection may be a desirable tradeoff in terms of performance and complexity.

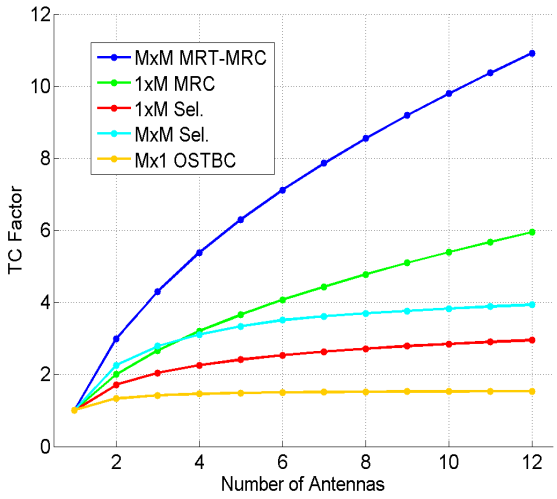

Figure 3.7: Comparison of the transmission capacity for MRT, MRC, OSTBC, and selection combining (relative to the SISO case). Note that $M \times M$ OSTBC/MRC is nearly identical to the $1 \times M$ MRC case. Also note that $M \times M$ selection combining means selecting the best pair of transmitting and receiving antennas.

3.6 Summary Comparison and Conclusion

Figure 3.7 compares the gain in transmission capacity in the low outage regime as a function of the number of antennas for the major diversity techniques covered here. A result of particular note is the poor performance of standard spatial block coding. In general diversity techniques are shown to perform according to how they improve signal quality, except in the case of channel-independent block coding in which increases interference roughly in the same proportion that it enhances signal quality. There is also significant gain to be reaped from providing CSI at the transmitter, when possible.

While Fig. 3.7 considers low outage, Fig. 3.7 shows transmission capacity

versus network density for a few physical layer configurations. With the proper physical layer techniques, maximum total throughput increases with the number of antennas, but with similar behavior in terms of optimum operating points.

Thus the chapter has covered a variety of representative multi-antenna diversity techniques as the first set of applications of the standard form solution derived in Chapter 2. Simple scaling relationships were derived for several of them. All cases considered were single-data stream techniques, but the following chapter will analyze and optimize multiplexing systems.

Chapter 4

Applications II: Spatial Multiplexing

The analysis of spatial multiplexing systems in a Poisson field of interferers begins here by analyzing systems with static constraints on power allocation, target data rates, and outage. Throughout this and the following chapters, the constraints will be successively relaxed leading to richer optimization problems and better overall network performance.

Section 4.1 expands the notion of transmission capacity to the multi-stream or multi-channel scenario. Section 4.2 is a parenthetical note on the gamma approximation from Chapter 2 applied to the eigenvalue distributions of Wishart matrices. Section 4.3 applies the small outage Theorem to open-loop and SVD pre-coding systems with uniform power and outage. Section 4.4 discusses methods for optimal (static) power allocation for multiplexing systems in ad hoc networks. Section 4.5 gives some asymptotic results for many antenna systems. Section 4.6 discusses the nature of the tradeoff between diversity and multiplexing in interference-limited ad hoc networks, which is analogous to, but different from, the classic result of Zheng and Tse [108]. Section 4.7 concludes.

4.1 Transmission Capacity with Multiple Channels

When a device has multiple channels available, the complexity of QoS constraints increases and a number of resource allocation problems arise. For each channel there is now a choice whether to use the channel, how much power to allocate, what rate to expect, and what outage probability to tolerate. The constraints could be independent for each channel or could be an average or total over all channels used. With fixed individual constraints

$$\mathbf{P}(\text{SIR} \leq \beta_i) \leq \epsilon_i \, \forall i, \tag{4.1}$$

on both β_i and ϵ_i, the optimal contention density is constrained by the worst-case channel

$$\bar{\lambda_\epsilon} = \min_i \{\max \lambda \mid \mathbf{P}(\text{SIR} \leq \beta_i) \leq \epsilon_i\} \tag{4.2}$$

since the SIR statistics are a function of the density of interfering transmitters λ. If outage is a total constraint on M channels,

$$\bar{\lambda_\epsilon} = \max \lambda \left| \frac{1}{M} \sum_i \mathbf{P}(\text{SIR} \leq \beta_i) \leq \epsilon_i. \right. \tag{4.3}$$

These formulations have the distinct advantage that even if channels or outage are correlated, channel statistics can be investigated independently for evaluating long-run performance. However, joint constraints could be given such as

$$\bar{\lambda_\epsilon} = \max \lambda \left| \mathbf{P}\left[\sum_i \mathbf{P}(\text{SIR} \leq \beta_i) \cdot \log_2(1+\beta_i) \leq b_t\right] \leq \epsilon \right. \tag{4.4}$$

that is, the probability that the total successful rate exceeds some target b_t at least $(1-\epsilon)$ fraction of the time, or even sum mutual information constraints.

In any case, the transmission capacity is the density of successful transmissions under the performance constraints, and the ASE is

$$\text{ASE} = \bar{\lambda_\epsilon}\, E\left[\sum_i \log_2(1+\beta_i)\right]. \tag{4.5}$$

Note that in a slotted packet network, the SIR statistics apply both at the symbol level and the packet slot level, but if multiple data streams are sent, each with a separate packet[1], different SIR statistics will be seen on the different data streams. Unless otherwise stated, it will be assumed here that a separate packet is sent on each channel, and that while packet failures are correlated, outage constraints are long-run averages, while target SIR objectives and power allocations are instantaneous.

4.2 The Gamma Approximation for Wishart Distributions

To make the analysis of spatial multiplexing concrete, it is necessary to have *standard fading* form expressions for the strengths of the respective channels. As noted before, channel strengths for Rayleigh fading are distributed as the eigenvalues of complex Wishart matrices, many of whose distributions are known to be in standard fading form, but are notoriously difficult to express in general. Some are known, however, and some can be derived by simple means. For those that remain, the Gamma approximation of Sec. 2.5 yields highly accurate results and will suffice as a substitute. This section presents the known results and

[1]This assumption, while not standard, and not completely necessary, makes the definition of outage and application of Theorem 2.3.1 clear.

approximations fitting the standard fading form for a number of important cases, as well as simple rules for combining them.

As noted in Chapter 3 vector channel strengths are already Gamma distributed. Another distribution which can be given explicitly in standard fading form is that of an unordered (i.e., randomly selected) eigenvalue. Equivalently, for a typical (randomly chosen) spatial mode, the channel gain of the received signal has the distribution of an unordered eigenvalue of the complex Wishart matrix $\mathbf{H}_{00}\mathbf{H}_{00}^H$. If all spatial modes are used, the marginal pdf is:

$$f_\phi(\phi) = \frac{1}{M}\sum_{k=0}^{M-1}[L_k(\phi)]^2 e^{-\phi} \tag{4.6}$$

where $L_k(x)$ is the Laguerre polynomial of order k

$$L_k(x) = \sum_{i=0}^{k}\binom{k}{k-i}\frac{(-x)^i}{i!}. \tag{4.7}$$

Writing $F_{S_0}^c$ in terms of $f_\phi(\phi)$ and integrating term by term,

$$F_{S_0}^c(x) = 1 - \int_0^x f_\phi(\phi)d\phi = e^{-x}\sum_{j=0}^{2(M-1)} a_M^{(j)}x^j \tag{4.8}$$

where the coefficients $a_M^{(j)}$ are given by the formula

$$a_M^{(j)} = \frac{1}{j!M}\sum_{m=0}^{M-1}\frac{1}{2^{2m}}\sum_{k=0}^{m}\frac{(2k)!}{(k!)^2}\binom{2m-2k}{m-k}\sum_{i=j}^{2k}\frac{(-2)^i}{i!}\binom{2k}{2k-i} \tag{4.9}$$

It is also known that the smallest eigenvalue has an exponential distribution with mean $\frac{1}{M}$, though this is the least important for communication purposes. In [47], the CCDF of the square of the maximum singular value of the desired channel

(which is the largest eigenvalue of a complex Wishart matrix), has been reported (originally given by [50]):

$$F^c_{\phi^2_{\max}}(x) = 1 - \frac{\det|\Psi(x)|}{\Pi_{k=1}^{q}\Gamma(q-k+1)\Gamma(s-k+1)}$$

where $q = \min\{N_t, N_r\}$, $s = \max\{N_t, N_r\}$, and the entries of the $q \times q$ matrix $\Psi(x)$ are

$$\{\Psi(x)\}_{i,j} = \gamma(s-q+i+j-1, x)\ ,\ i,j = 1,\ \ldots, q$$

where $\gamma(\cdot,\cdot)$ is the lower incomplete gamma function. Recall the identity for the lower incomplete gamma function [28]:

$$\gamma(n,x) = (n-1)!\left(1 - e^{-x}\sum_{k=0}^{n-1}\frac{x^k}{k!}\right). \tag{4.10}$$

For the $2 \times N$ channel when only the top spatial mode is used,

$$F^c_{S_0} = \frac{\gamma(N-1,x)\gamma(N+1,x) - \gamma^2(N,x)}{\Pi_{k=1}^{2}\Gamma(N-k+1)} \tag{4.11}$$

and when both are used,

$$F^c_{S_0} = 1 - \int_0^x \frac{1}{2}\sum_{k=1}^{2}[L_k^{N-2}(t)]^2 t^2 e^{-t}\mathrm{d}t. \tag{4.12}$$

While the full sum of exponentials and polynomials expressions are somewhat complicated and yield little intuition (and are hence omitted), they lend themselves to numerical evaluation and to the application of Theorem 2.3.1.

For many other individual ordered eigenvalue distributions, including the maximum given above for certain numbers of antennas, the Gamma approximation was applied to Monte Carlo simulations of complex Wishart matrices. The

Table 4.1: Gamma Approximation Shape Parameters

(M_t,M_r)	σ_1^2	σ_2^2	σ_3^2	σ_4^2	σ_5^2	σ_6^2	σ_7^2	σ_8^2	σ_9^2	σ_{10}^2	σ_{11}^2	σ_{12}^2
$(1,1)$	1	-	-	-	-	-	-	-	-	-		
$(1,2)$	2	-	-	-	-	-	-	-	-	-	-	-
$(1,3)$	3	-	-	-	-	-	-	-	-	-	-	-
$(1,4)$	4	-	-	-	-	-	-	-	-	-	-	-
$(2,2)$	4	1	-	-	-	-	-	-	-	-	-	-
$(2,3)$	6	2	-	-	-	-	-	-	-	-	-	-
$(2,4)$	7	3	-	-	-	-	-	-	-	-	-	-
$(3,3)$	8	4	1	-	-	-	-	-	-	-	-	-
$(3,4)$	10	6	2	-	-	-	-	-	-	-	-	-
$(4,4)$	13	9	4	1	-	-	-	-	-	-	-	-
$(2,6)$	10	5	-	-	-	-	-	-	-	-	-	-
$(2,8)$	14	8	-	-	-	-	-	-	-	-	-	-
$(2,12)$	20	13	-	-	-	-	-	-	-	-	-	-
$(4,6)$	18	14	8	3	-	-	-	-	-	-	-	-
$(4,8)$	23	19	12	6	-	-	-	-	-	-	-	-
$(4,12)$	32	29	21	11	-	-	-	-	-	-	-	-
$(6,6)$	25	22	15	9	4	1	-	-	-	-	-	-
$(6,8)$	31	29	22	15	8	3	-	-	-	-	-	-
$(6,12)$	42	43	36	27	17	8	-	-	-	-	-	-
$(8,8)$	38	38	31	24	16	9	4	1	-	-	-	-
$(8,12)$	52	55	49	40	31	21	13	6	-	-	-	-
$(12,12)$	70	78	75	66	56	45	34	25	16	9	4	1

shape parameters were rounded to the nearest integer, and the scale parameters were adjusted to maintain the mean values. The results for a few interesting cases are given in Table 4.1.

The cases given in the table are for individual eigenvalue distributions in order of their magnitude. But as with the unordered eigenvalue distribution,

sometimes the appropriate distribution is from an *a priori* unknown one from among a set of the eigenvalues, such as the top two, or all but the least. Given a set of independent random variables $Z_i, i = 1, 2, ..., N$ with individual (or marginal) probability densities $f_i(x)$, let Y be the random variable defined as selecting a randomly from among the Z_i with equal probability. The probability density of Y is then $f_Y(x) = \frac{1}{N}\sum_i f_i(x)$. Hence, whenever certain eigenmodes are discarded, it is trivial to obtain the distribution of an unordered eigenmode from among the rest.

4.3 Analysis of Spatial Multiplexing Systems

The interference is modeled as a sum over the marked point process defined by (2.2). When multiplexing across M modes, the interfering power mark has the form:

$$S_i = \sum_{k=1}^{M} \left| \mathbf{u}^H \mathbf{H}_{0i} \mathbf{v}_i^{(k)} s_i^{(k)} \right|^2 . \tag{4.13}$$

Here $\mathbf{H}_{0i}$ is the Rayleigh fading channel between the receiver and the ith interferer, $\mathbf{u}^H$ is the combining vector applied at the receiver for the packet of interest, $\mathbf{v}_i^{(k)}$ is the kth column of the pre-coding matrix applied by the interferer to transmit the symbol $s_i^{(k)}$. All $\mathbf{u}^H$, $\mathbf{v}_i^{(k)}$, $\mathbf{H}_{0i}$, and $s_i^{(k)}$ are independent of one another. The interfering power is the sum of the interference from the M independent data symbols transmitted by the interferer. Each factor $\left|\mathbf{u}^H \mathbf{H}_{0i} \mathbf{v}_{ik} \mathbf{s}'\right|^2$ is an exponential random variable and all M factors are independent. Thus the factor S_i for spatial multiplexing systems is a Gamma distributed variate with scale parameter one

and shape parameter M. The mean of S_i is M and its MGF is

$$E\left[e^{-\zeta S_i|x|^{-\alpha}}\right] = \frac{1}{(1+\zeta|x|^{-\alpha})^M}. \tag{4.14}$$

Carrying out the integral in (2.5)

$$\mathcal{L}_{I_\Phi}(\zeta) = e^{-\lambda\zeta^{\frac{2}{\alpha}}C_{\alpha,M}} \tag{4.15}$$

for $C_{\alpha,M}$ given in (2.36) and $B(a;b) = \Gamma(a)\Gamma(b)/\Gamma(a+b)$ being the beta function, and $\zeta = \beta R^\alpha$. Note that while the terms and factors in (4.13) were all independent, the interference powers seen by different simultaneous data streams across the link of interest are not independent at all. The reason is that they depend heavily on $|X_i|^{-\alpha}$, the distance-dependent attenuation of the signal from the ith interferer. When an interferer happens to be nearby, it will likely cause high interference to all data streams at the same time, while if no interferers are nearby, it is likely that all data streams will experience light interference. This is the motivation for an ergodic analysis, i.e., of determining the statistics of a random symbol (or packet) through the reference link.

For a typical (i.e., randomly selected) spatial mode, the channel gain of the received signal has the distribution of an unordered eigenvalue of $\mathbf{H}_{00}\mathbf{H}_{00}^H$ from among the spatial modes used. Its distribution was given in Sec. 4.2. If instead the weakest spatial mode is not used and the power is split among the other modes, then the CCDF of an unordered eigenvalue from among the top $M-1$ is

$$F_{S_0}^c(x) = e^{-x}\sum_{j=0}^{2(M-1)} \frac{M-1}{M} a_M^{(j)} x^j - \frac{1}{M}e^{-Mx}. \tag{4.16}$$

Via Theorem 2.3.1, this permits the transmission capacity to be computed: For small outage constraints ϵ, the optimal contention density is given by

$$\bar{\lambda_\epsilon} = \frac{K_{\alpha,M}^{sm}\epsilon}{\beta^{2/\alpha}R^2 C_{\alpha,M}}. \tag{4.17}$$

with the signal factors computed according to Theorem 2.3.1.

4.3.1 Open-Loop Multiplexing

As mentioned in Sec. 2.5, the authors in [66] followed the Laplace transform approach to consider open-loop spatial multiplexing, i.e., without CSI at the transmitter. The work considers two types of linear receivers, zero-forcing and MRC. For an open-loop system, no power, rate, or phase adaptation is possible, the system is easier to implement, and so it provides a baseline for spatial multiplexing systems. An exact expression for the SIR distribution is given [66] as:

$$\begin{aligned}\mathbf{P}(\beta \geq \text{SIR}) &= \frac{(-1)^{m-1}e^{-\lambda(\frac{\beta\Omega}{\theta})^{\frac{2}{\alpha}}R^2}\eta(n)}{\Gamma(m)}\sum_{i=0}^{m-1} s(m,i+1)\left(\frac{2}{\alpha}\right)^i \\ &\quad \times \sum_{j=0}^{i} S(i,j)\left(-\lambda\left(\frac{\beta\Omega}{\theta}\right)^{\frac{2}{\alpha}}R^2\eta(n)\right)^j \end{aligned} \tag{4.18}$$

where $\theta = \frac{1}{N}$ and $\Omega = \frac{1}{M}$ with zero-forcing receivers. As a baseline for comparison, the following Proposition applies the small outage principle to the result given in [65], for the particular case in which nodes operating without CSI at the transmitter use zero-forcing receivers:

Proposition 4.3.1. *For a random access wireless network in which nodes perform zero-forcing detection of spatial multiplexing on M_t transmit and M_r antennas*

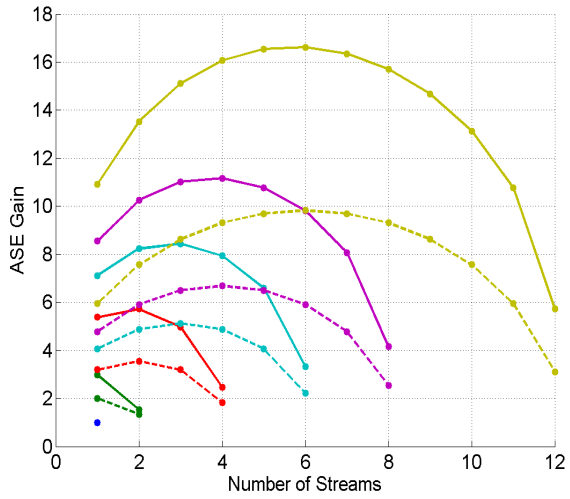

Figure 4.1: Area spectral efficiency for square ($M_t = M_r$) closed-loop and open-loop spatial multiplexing systems (i.e., with and without CSI), but equal power allocation. Lines connect points based on number of antennas with $1, 2, 4, 6, 8$, and 12 shown for both open- and closed-loop systems. Solid lines are closed-loop, dashed lines are open-loop.

without transmitter CSI, let $M_t \leq M_r$ *and* $m = M_r - M_t$*, for small outages the signal factor is given by:*

$$K_{\alpha,m}^{\mathrm{zf}} = \left[1 + \sum_{k=0}^{m-2} \frac{1}{(k+1)!} \prod_{l=0}^{k} (l - 2/\alpha)\right]^{-1} \tag{4.19}$$

and the interference factor C_{α,M_t} *is given by (2.36).*

Figure 4.1 compares equal power multiplexing with CSI with zero-forcing open-loop multiplexing for square systems ($M_t = M_r$) when the path loss exponent is 4. For both open- and closed-loop systems, the optimal (static) number of spatial modes is roughly half the number of antennas available. Though transmit

CSI can be difficult to obtain in some scenarios, the potential for network throughput gain is between 50 and 100%. Or from another perspective, compared to an open-loop $M \times M$ system, a closed-loop $\frac{M}{2} \times \frac{M}{2}$ system will perform similarly.

4.3.2 Fixed Rate SVD Multiplexing

Without a power or rate adaptation strategy (that is, with equal power and rate on each subchannel), the distributions of the various modes of an $M_t \times M_r$ MIMO channel using all spatial modes is all that is necessary to reach transmission capacity conclusions. Note that power and rate adaptation are separate from instantaneous phase adaptation based on CSI. Adaptation in this sense is necessary achieve maximal orthogonal channels, but since power and rate adaptation have effects on network interference and QoS, they will be handled separately later. For clarity of presentation the symmetric case with equal numbers of antennas on each end is stated, though the more general result is obtained in an analogous fashion. Specifically, the system performs as follows:

Proposition 4.3.2. *For a random access wireless network in which nodes perform SVD based spatial multiplexing on $M_t = M_r = M$ antennas with equal power, equal target rate, and equal outage constraint on each subchannel, and for small outages the optimal contention density is:*

$$\bar{\lambda_\epsilon} = \frac{K_{\alpha,M}^{\mathrm{sm}} \epsilon}{C_{\alpha,M} R^2 \beta^{\frac{2}{\alpha}}} \tag{4.20}$$

for

$$K_{\alpha,M}^{\mathrm{sm}} = M^{-\frac{2}{\alpha}} \left[1 + \sum_{k=1}^{2(M-1)} a_M^{(k)} \prod_{l=0}^{k} (l - 2/\alpha) \right]^{-1} \tag{4.21}$$

and with $C_{\alpha,M}$ given in (2.36) and $a_M^{(k)}$ coefficients of the CCDF of an unordered eigenvalue of a complex Wishart matrix.

Proof. This is a straightforward application of Theorem 2.3.1 with the coefficients $a_M^{(k)}$ given above. □

Because of the outage constraint, clearly the weakest spatial channels become the limiting cause of outage, hence transmission capacity can usually be improved by eliminating the weakest spatial mode. The network performance achieved is then:

Proposition 4.3.3. *For a random access wireless network in which nodes perform SVD based spatial multiplexing on $M_t = M_r = M$ (and $M > 1$) antennas on only $M - 1$ subchannels, for small outages the optimal contention density is as in Proposition 1 with:*

$$K_{\alpha,M}^{\mathrm{sm}'} = \left[1 + \sum_{k=1}^{2(M-1)} \frac{M-1}{M} a_M^{(k)} \prod_{l=0}^{k} (l - 2/\alpha) - \frac{2}{\alpha} M^{\frac{2}{\alpha}-1}\right]^{-1}. \tag{4.22}$$

and $C_{\alpha,M} = C_{\alpha,M-1}$ in (2.36).

Proof. In the zero-forcing receiver case, the interference has the same structure as the cases above, but as noted in [76] the received signal on a typical detected data stream is distributed as a χ^2 random variable with $2(M_r - M_t + 1)$ degrees of freedom whose distribution falls under the class covered by Theorem 2.3.1 as shown in Chapter 3. □

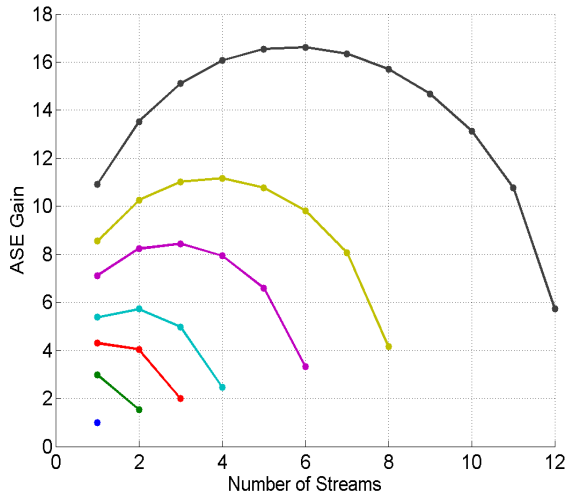

Figure 4.2: Area spectral efficiency for square ($M_t = M_r$) spatial multiplexing systems with CSI and equal power allocation. Lines connect points based on number of antennas (with $1, 2, 3, 4, 6, 8$, and 12 shown).

A variety of related results could be obtained, such as also removing the second weakest spatial mode, but will not be pursued here, as they lend little insight directly into the optimum use of spatial multiplexing in ad hoc networks. Figure 4.3 gives a number of cases graphically, and includes the two Propositions presented in this section. It indicates that eliminating the worst spatial mode is uniformly superior for equal power and rate allocation. The following section begins to loosen these constraints and explore the results.

4.4 Optimization of Spatial Multiplexing

When CSI is available, equal power and rate across the available spatial modes is not optimal in point-to-point channels, and as this section shows, is also

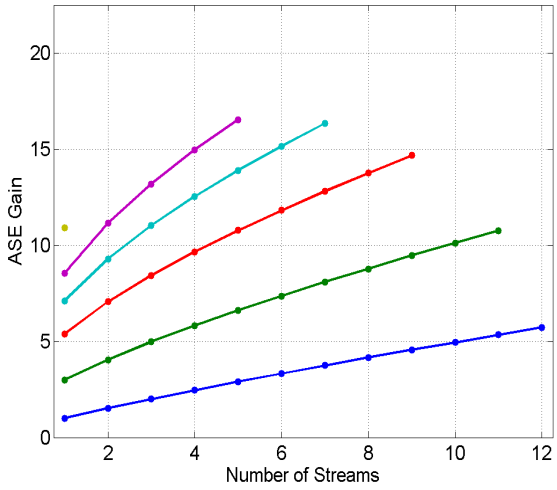

Figure 4.3: Area spectral efficiency for square ($M_t = M_r$) spatial multiplexing systems with CSI and equal power allocation. Lines connect points based on number of modes ignored, e.g., the bottom blue line is for all spatial modes included. Shown are $0, 1, 3, 5, 7$, and 11 modes ignored.

not optimal in a Poisson field of interferers. However, the freedom to optimize comes with the need to relax the constraints.

4.4.1 Power Allocation for Fixed Rate Multiplexing

First, for each communicating pair of nodes in the network, each with a statistically identical set of spatial subchannels to select from whose signal distributions meet the requirements of Theorem 2.3.1. (The emphasis on *spatial* indicates the subchannels overlap in time and frequency.) Next, let $\rho_i \geq 0$ be the fraction of power allocated to the ith subchannel with the constraint $\sum_i \rho_i \leq 1$, and let ϵ_i and β_i be the outage and target SINR constraints respectively. Further,

let these constraints hold for every communicating pair in the network. Lastly, let m denote the number of subchannels for which ρ_i is nonzero. Then in a network of given density, for each subchannel a relation

$$\bar{\lambda_\epsilon} = \frac{K_i \rho_i^{\frac{2}{\alpha}} \epsilon_i}{C'_\alpha R^2 \beta_i{}^{\frac{2}{\alpha}}}. \tag{4.23}$$

holds. Note that C'_α is not necessarily given by (2.36) and will depend on the power allocation set, both the number of spatial modes in use and the relative power levels. However, as shown in the Appendix at the end of this chapter, setting $C'_\alpha \approx C_{\alpha,m}$ in (2.36) is typically an appropriate (and conservative) approximation and will be used for clarity of presentation. Furthermore, $C_{\alpha,m} \to \frac{2\pi}{\alpha}\Gamma(\frac{2}{\alpha})$ as m grows large. These approximations are equivalent to assuming equal power allocation which is both worst-case and limiting as m and/or M grow large.

Remark 4.4.1. Given fixed constraints ρ_i, β_i, ϵ_i, with subchannels characterized by K_i, the optimum contention density is:

$$\lambda_\epsilon = \min_i \left\{ \frac{K_i \rho_i^{\frac{2}{\alpha}} \epsilon_i}{C_{\alpha,m} R^2 \beta_i{}^{\frac{2}{\alpha}}} \right\}. \tag{4.24}$$

A relaxation of the constraints is to permit instead an average outage across the available channels, rather than prescribed, per-channel constraints. Note that typically, for random access systems very high outage (greater than fifty percent) maximizes throughput [5]. The difficulties are caused by this level of outage are part of the motivation for small outage constraints. So relaxing this constraint must be done with some care, both since there is a natural tendency to prefer

high outage when maximizing only throughput, and since the low outage limits break down if channels are permitted to be in outage too often. To maintain a total outage constraint on the typical packet which may be sent on any of m channels, the relation $\frac{1}{m}\sum_i \epsilon_i \leq \epsilon$ must hold. For simplicity in analyzing the effect of optimizing power allocation and channel outage, consider a fixed rate multiplexing system where the addition of each channel adds linearly to the target data rate.

Proposition 4.4.1. *Given the fixed constraint β for all m spatial channels, an average outage constraint ϵ, and a total power constraint $\sum_i \rho_i \leq 1$ with subchannels characterized by K_i, the optimum contention density is:*

$$\bar{\lambda_\epsilon} = \frac{K^{'}\epsilon}{C_{\alpha,m}R^2\beta^{\frac{2}{\alpha}}} \tag{4.25}$$

for

$$K^{'} = m\left(\sum_{i=1}^{m} K_i^{-\delta}\right)^{-\delta}. \tag{4.26}$$

with $\delta = \frac{2}{\alpha} + 1$.

Proof. Solving for ϵ_i in terms of the rest of the parameters above,

$$m\epsilon = \lambda C_{\alpha,m}R^2\beta^{\frac{2}{\alpha}}\sum_{i=1}^{m}\frac{1}{K_i\rho_i^{\frac{2}{\alpha}}} \tag{4.27}$$

The transmission capacity is maximized when $\sum_{i=1}^{m} K_i^{-1}\rho_i^{-\frac{2}{\alpha}}$ is minimized since λ is then maximized. To solve for the optimal power allocation ρ_i, the Lagrangian is:

$$\mathcal{L}(\rho_i;\mu) = \sum_{i=1}^{m} K_i^{-1}\rho_i^{-\frac{2}{\alpha}} + \mu(\sum_i \rho_i - 1) \tag{4.28}$$

for which the solution can easily be found to be

$$\rho_i = \frac{K_i^{-1/\delta}}{\sum_j K_j^{-1/\delta}} \tag{4.29}$$

and substituting the ρ_i into (4.27) yields the result. □

Note that the solution for the optimal power allocation is dependent only on the relative channel gains and the path loss exponent. The optimal contention density can then be found by solving for λ in (4.27). Since an outage constraint is applied, more power is allocated to the weaker modes to make them more robust to interference, thus allowing a higher density of interferers.

On the other hand, allocating more power to weaker modes is an inefficient use of the channel. Unfortunately, improving the power allocation also turns out not to be terribly valuable. The greatest improvements arise when all or most of the spatial modes are used and the weaker modes, being the primary source of outage, are shored up, resulting in best-case gains of around 20%. Improving the power allocation has little effect when only a few strong spatial modes are used. This is explained by the semi-circle law for eigenvalues of random matrices (which will come up again in Sec. 4.5) which indicates that the largest few eigenvalues converge to the same value. Hence, the power allocation has virtually no effect on the rankings of the cases given in the Figs. 4.3 through 4.2, though it does improve the highest link rate cases some.

4.4.2 Joint Power and Rate Optimization

Now consider a transmitter-receiver pair with full CSI in a standard network for which:

$$\bar{\lambda_\epsilon} = \frac{K_i \rho_i^{\frac{2}{\alpha}} \epsilon_i}{C'_\alpha \beta_i^{\frac{2}{\alpha}} R^2} \tag{4.30}$$

for the ith channel available to the communicating pair where ρ_i is the fraction of the total power assigned to channel i and channel specific outage levels ϵ_i are given. Note also that the C'_α factor depends on the number of channels and potentially on power allocation strategies as well. Again the approximation $C'_\alpha = \frac{2\pi}{\alpha}\Gamma(\frac{2}{\alpha})$ is made, which is equivalent to $C_{\alpha,\infty}$ for a large number of interfering streams, with the details left to the Appendix at the end of the chapter.

Proposition 4.4.2. *In a random access network with fixed outage constraints, a total power limit, and in which nodes have current CSI of their own subchannels, area spectral efficiency is maximized by the channel-aware algorithm*

$$\beta_i = \frac{\epsilon_i}{\sum_i \epsilon_i} \frac{1 + \sum_i \gamma_i}{\gamma_i} - 1 \tag{4.31}$$

employed by each mode, with $\gamma_i = \left(\frac{\lambda R^2 C'_\alpha}{K_i \epsilon}\right)^{\frac{\alpha}{2}}$.

Proof. To determine the optimum rate and power for each channel the algorithm maximizes the expression $\sum_i \log_2(1+\beta_i)$ subject to the constraints $\rho_i = \gamma_i \beta_i$ and $\sum_i \rho_i = 1$. Applying Lagrange multipliers, the optimum target SINR for the ith channel is found as above. If a β_i is found to be negative, the channel is abandoned and the algorithm is run again with a smaller set of channels. □

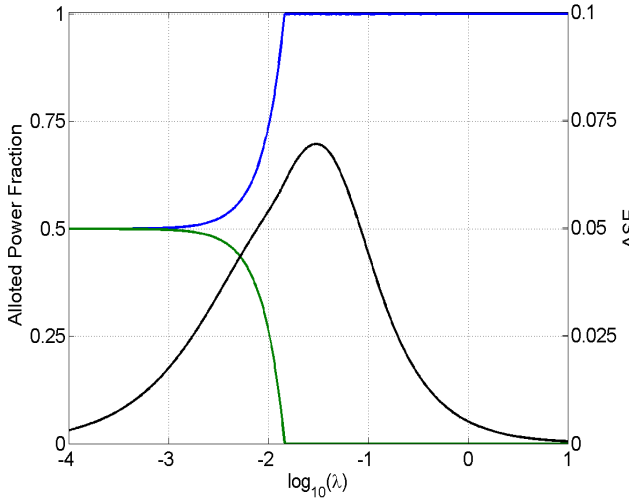

Figure 4.4: Power allocation and resulting ASE vs. contention density for a 2×2 system with $\alpha = 4$ and $\epsilon = 0.1$. Black line is ASE, colored lines are power fraction by spatial mode (with the smaller modes falling to zero earlier).

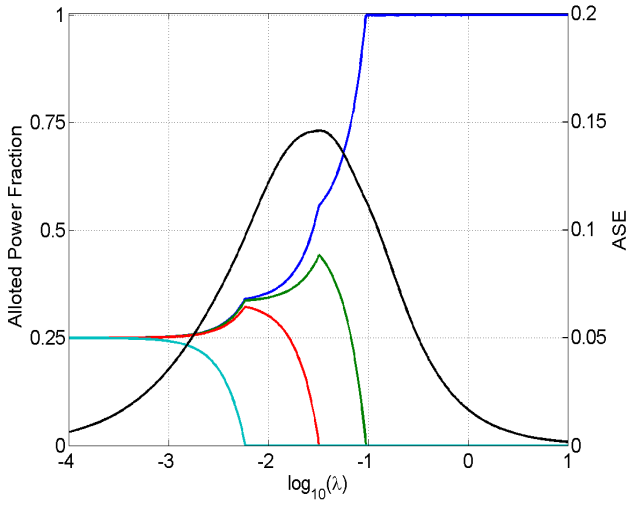

Figure 4.5: Power allocation and resulting ASE vs. contention density for a 4×4 system with $\alpha = 4$ and $\epsilon = 0.1$.

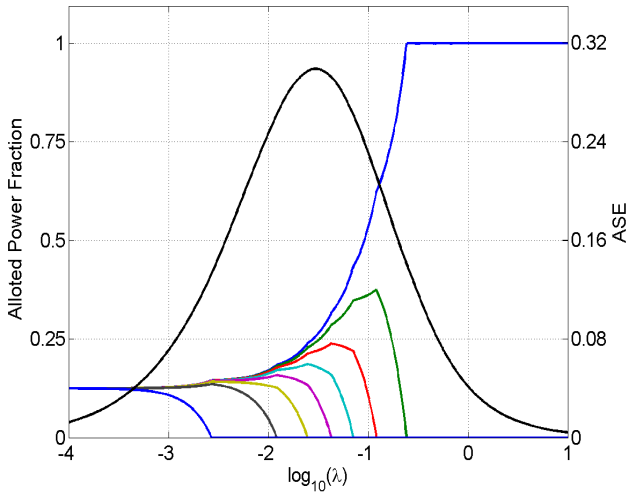

Figure 4.6: Power allocation and resulting ASE vs. contention density for an 8×8 system with $\alpha = 4$ and $\epsilon = 0.1$. Black line is ASE, colored lines are power fraction by spatial mode (with the smaller modes falling to zero earlier).

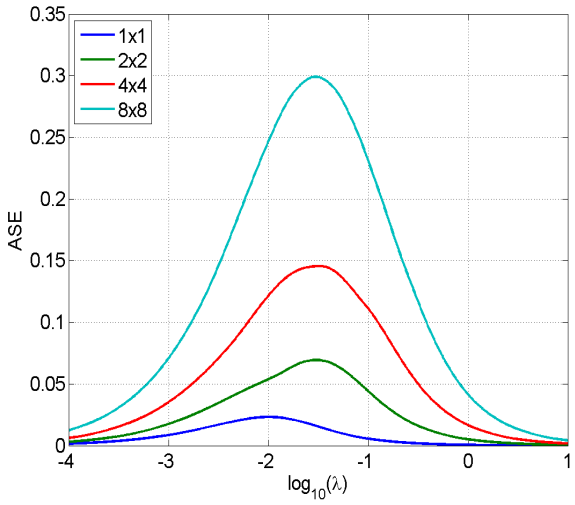

Figure 4.7: ASE vs. contention density comparison for several square configurations with $\alpha = 4$ and $\epsilon = 0.1$.

Figures 4.4 through 4.6 give examples of the result of the power allocation algorithm and its corresponding ASE, while Fig. 4.7 provides a direct comparison of the ASE of the various configurations. In all cases, the outage constraint was set to be $\epsilon = 0.1$.

4.5 A Note on Large MIMO Channels

While there remain many technical difficulties with implementing large MIMO arrays and using a large number of spatial modes, the large array regime helps to bring out some principles behind the tradeoff between diversity and multiplexing.

Remark 4.5.1. In a standard network of nodes with a large number of antennas $M \gg 1$, using M antennas for pre-coding but sending only $m \ll M$ data streams, the product of successful data streams and optimum contention density is bounded by:

$$1 \leq \frac{C_{\alpha}^{'} R^2 (m\beta)^{\frac{2}{\alpha}}}{(4M)^{\frac{2}{\alpha}} \epsilon} \cdot \lambda_{\epsilon} \leq \Gamma(1 - 2/\alpha) \tag{4.32}$$

The best case increase in ASE would come from a set of (statistically) equally good channels for which the gain would be $M^{1-\frac{2}{\alpha}}$ over any single channel. Since $K_i = K \ \forall i$, then $K^{'} = m^{-\frac{2}{\alpha}} K$ indicating that multiplexing reduces the optimal contention density, while it linearly increases the per transmission data rate. This provides an upper bound on the potential improvement in transmission capacity of spatial multiplexing, even with the optimal power allocation, since the

eigenmodes of the channel have a strict ordering (i.e., they are not equal): Using m modes must achieve less than an $m^{1-\frac{2}{\alpha}}$ gain over using only a single eigenmode.

However, according to the semi-circle law of large symmetric (say $M \times M$) random matrices [68], the largest few (say $m \ll M$) ordered eigenvalues converge in the same way as the largest eigenvalue. In particular, for a $M \times M$ complex Wishart matrix, the largest few eigenvalues converge to $4M$. That is, for m sufficiently smaller than M, as M grows large, the eigenvalues $\sigma_1^2, \sigma_m^2 \rightarrow 4M + o(M)$ and $\sigma_1^2 - \sigma_m^2 \rightarrow o(M)$. Note that the coefficient of variation of the distribution of these eigenvalues also continually shrinks with increasing M so that this approximation has less and less proportional error.

4.6 The Tradeoff between Multiplexing and Diversity

Classically, in a point-to-point link the tradeoff between diversity and multiplexing is one of choosing error exponents over degrees of freedom or vice versa, i.e., of choosing the rate at which bits errors vanish with increasing SNR over the number of orthogonal information bearing channels available. In ad hoc network framework developed here, there is an analogous tradeoff, though the tradeoff has different design implications. The small outage proportionalities $\lambda \propto \beta^{-\frac{2}{\alpha}}$ and $\lambda \propto \epsilon$ quantify the conflict between spatial reuse and link reliability or individual data rates for single channel systems. Given β and ϵ as *constraints*, naturally additional spatial reuse will fill the void until the constraints are active, but the ratio of signal to interference factors ($\frac{K}{C}$) determine the rate at which density is sacrificed for individual rate (or reliability). Clearly if S_0 corresponds to the square of

the largest singular value of the channel, this stochastically dominates any other effective channel gain [76] and so results in the largest possible contention density. Devoting any power to lesser channels reduces contention. On the other hand, the maximum individual rate is achieved by using all spatial degrees of freedom. Thus the tradeoff between diversity and multiplexing techniques in standard network is the multichannel expansion of the tradeoff between individual rate and the number of users. Given the large channel bounds, the end points of the tradeoff can be stated:

Remark 4.6.1. The maximum achievable increase in contention density is on the order $(4M)^{\frac{2}{\alpha}}$ which achieves multiplexing gain 1, while the maximum achievable increase in rate is on the order M which achieves contention scaling of $M^{-\frac{2}{\alpha}}$.

As mentioned in the opening section, no single metric is appropriate in all cases. However, it should be noted that neither end points of the tradeoff tell the whole story, because another important metric is ASE, which is a product of these. It turns out that for larger numbers of antennas and/or higher path loss, ASE is not optimized at either end point.

4.7 Conclusion

This chapter covered the second set of applications of the general framework, which were spatial multiplexing systems. The concepts of the QoS constraints were expanded and this led to a number of optimization problems over rate and power locally, as well as network density. The tradeoff between link

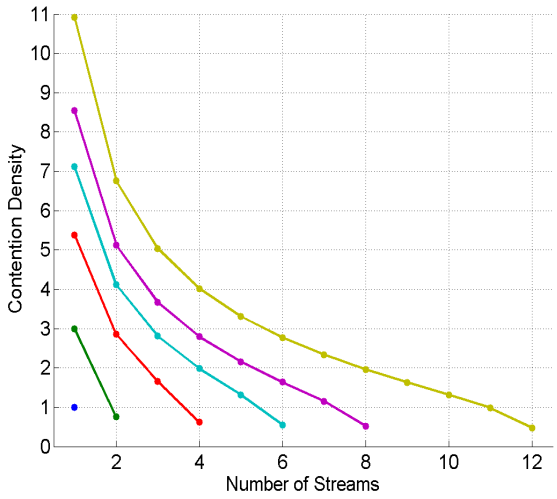

Figure 4.8: Maximum contention density with $\alpha = 4$ and $\epsilon = 0.1$ for a variety of antenna configurations (all possible equal power modes for $1, 2, 4, 6, 8, 12$ antennas).

rate and network density was investigated as an analogue of the classic diversity-multiplexing tradeoff in point-to-point links. However, all of the solutions presented in this chapter were effectively static, network-wide solutions. Taking a statistical perspective, the various spatial channels were treated as identical across the network, with SVD pre-coding serving merely to orthogonalize channels in a maximal way. The next chapter considers the opportunity for further adaptation given this channel awareness.

Appendix: The Fixed Point Problem of the Interference Factor

For a node to setup an optimization problem to allocate power, rate, or outage, some statistical information about the interference is needed in the framework used. Primarily, the node should know the contention density λ, the interference factor C'_α, and the path loss exponent. The factor C'_α depends on the interaction between the interference and the processing at the receiver of interest who is assumed to know only this factor, and nothing more about the instantaneous interference. In the formulation in Appendix I, it was assumed that each node allocates constant power to each mode, resulting in the closed form expression for C'_α. However, if the kth interferer independently applies a fraction $\rho_{k,i}$ to its ith subchannel, and $\rho_{k,i} \in [0,1] : \forall k, \sum_i \rho_{k,i} = 1$ follows some distribution then a modification of C'_α is necessary. In turn the distribution of the power allocation process is dependent upon this factor. It now becomes necessary to find this fixed point numerically.

However, two cases form bounds on the resulting C'_α. First, if all power is always allocated to one subchannel, $C'_\alpha = C_{\alpha,1}$ which forms a lower bound. Secondly, if the power is split evenly among N modes, $C'_\alpha = C_{\alpha,N}$ which approaches $\frac{2\pi}{\alpha}\Gamma(\frac{2}{\alpha})$ as N grows large. This forms an upper bound on the factor. Since for large α these two bounds do not differ by much, practically, an algorithm could easily select an appropriate approximation of the true C'_α.

To demonstrate these bounds, begin at the point of applying the allocation algorithm, considering just one subchannel with magnitude η. Using a limiting

expansion from [38]:

$$\mathbf{P}(\mathrm{SIR}_i \geq \beta_i) = \sum_{k=0}^{\infty} \frac{(-\zeta)^k}{k!} \frac{d^k}{d\zeta^k} \mathcal{L}_{I_\Phi}(\zeta) \Big|_{\zeta=\rho_i \beta R^\alpha/\eta} \tag{4.33}$$

Note that ζ includes the the current channel strength η. For interfering nodes using m_i spatial modes with equal power allocation, the Laplace transform of the shot noise process can be evaluated as [87]

$$\begin{aligned} \mathcal{L}_{I_\Phi}(\zeta) &= \exp\left\{-2\pi\lambda \int_0^\infty u \left(1 - \frac{1}{(1+u^\alpha/\zeta)^{m_i}}\right) \mathrm{d}u\right\} \\ &= \exp\left\{-\lambda C_{\alpha,m_i} \left(\frac{\zeta}{m_i}\right)^{\frac{2}{\alpha}}\right\} \end{aligned} \tag{4.34}$$

where $C_{\alpha,m_i} = C_{\alpha,m}$ in (2.36). To take into account the fact that interfering nodes are also allocating power unequally across spatial modes, let $\mathbf{p} = [\rho_i]$ be the vector of powers allocated by an interferer over its subchannels with $\sum_i \rho_i = 1$. Also let $\mathcal{U}^{m_i}$ denote the region over which the elements of $\mathbf{p}$ are in the unit interval and meet the sum constraint. The Laplace transform can be written as:

$$\mathcal{L}_{I_\Phi}(\zeta) = \exp\left\{-2\pi\lambda \int_{\mathcal{U}^{m_i}} \int_0^\infty u \left(1 - \prod_i \frac{1}{1+\rho_i u^\alpha/\zeta}\right) \mathrm{d}u \mathrm{d}\mathbf{p}\right\} \tag{4.35}$$

This is difficult to find in closed form in general, however, it does show that since $C_{\alpha,m}$ is monotonic in m, $C_{\alpha,1}$ and $C_{\alpha,\infty}$ are extreme points of this integral, yielding bounds.

For higher path loss exponents in particular, the gap between these bounds is small ($\approx 13\%$ for $\alpha = 4$). Thus selecting *any* value in this range results in limited error. As an example suppose a target outage of 1% were in place and the maximum density was being estimated, and that the interference factor was in

error 2% low. The bias in the estimation of the contention density would not then result in an outage of $\approx 3\%$, but only about 1.02%. Thus an approximation to the interference factor is unlikely to be the dominant source of uncertainty about the environment and network. When necessary another close approximation can be obtained by taking

$$\begin{aligned} C_{\alpha,\rho} &= \frac{2\pi}{\alpha} \sum_{k=0}^{M-1} \binom{M}{k} \rho_k^{'} B\left(\frac{2}{\alpha}+k; M-\left(\frac{2}{\alpha}+k\right)\right) \\ &= \sum_{k=0}^{M-1} \rho_k^{'} C_{\alpha,k} \end{aligned} \tag{4.36}$$

where the $\rho^{'}$ are the power allocation values sorted in ascending order. In other words, this approximation takes the total interference factor to be a weighted average of the interference factors resulting from using various numbers of modes. Note that if instead of different power settings, the interference contributions of a node took on a random distribution of degrees of freedom, the average weighted by the probability of the number of degrees of freedom would be exact.

Chapter 5

Adaptation for Transmission Capacity

Many of the multiple antenna techniques utilized in Chapters 3, and 4 required either full or partial CSI at the transmitter. While intuitive relations were developed for the tradeoffs in terms of per user throughput, contention density, and ASE, the resource allocation decisions were static and network-wide, with nodes adapting only to create multiple and/or maximal channels. When CSI is available, the network can perform better, not surprisingly, if each communicating pair is able to adapt to its particular channel conditions.

This chapter begins by developing an algorithm for such adaptation and examining its effect on network performance. The algorithm is carried out by each communicating pair separately, opening the door for further relaxations of network-wide decision making and the analysis of heterogeneous systems. Before analyzing the adaptive algorithm, Section 5.1 derives expressions for ergodic rate over standard fading channels with a Gamma approximation. Section 5.2 then introduces adaptive rate control in a Poisson field of interferers which is extended and optimized for multiple channels in Section 5.3. Section 5.4 then considers the performance of ideal hybrid-ARQ mechanisms and Section 5.5 extends the analysis to MIMO configurations. Lastly, Section 5.6 considers the application

of the small outage framework to heterogeneous networks, i.e., networks whose nodes have a variety of PHY layer configurations.

5.1 Ergodic Rate over Standard Fading Channels

In the simplest sense, the *ergodic* rate achieved by a communication system [24] in a (slowly) time-varying channel is $E_\phi[\log_2(1+\phi)]$ where ϕ is the effective SNR, which may vary due to, among other things, fading, CSI quality, or target rate control decisions. When ϕ is Rayleigh fading,

$$\begin{aligned} E[\log_2(1+\phi)] &= \int_0^\infty \log_2(1+\phi) f_\phi(\phi) \mathrm{d}\phi \\ &= \int_0^\infty \log_2(1+\phi) \gamma e^{-\gamma\phi} \mathrm{d}\beta \\ &= \frac{1}{\ln(2)} e^\gamma \mathrm{Ei}(\gamma) \end{aligned} \tag{5.1}$$

where $\mathrm{Ei}(x) = \int_x^\infty \frac{e^{-t}}{t}\mathrm{d}t$ is a particular exponential integral and this last step is from [28]. The integral

$$\int_1^\infty t^{\nu-1} e^{-at} (\ln t)^m \mathrm{d}t = \frac{\partial^m}{\partial \nu^m} a^{-\nu} \Gamma(\nu, a) \tag{5.2}$$

is also known [28]. This enables the expression to be generalized when ϕ takes on a Gamma distribution with integer shape parameter:

$$\begin{aligned} E[\log_2(1+\phi)] &= \int_0^\infty \log_2(1+\phi') \frac{\gamma}{\Gamma(n)} \phi'^{n-1} e^{-\gamma\phi'} \mathrm{d}\phi' \\ &= \int_1^\infty \log_2(\phi) \frac{\gamma}{\Gamma(n)} (\phi-1)^{n-1} e^{-\gamma(\phi-1)} \mathrm{d}\phi \\ &= \int_1^\infty \log_2(\phi) \frac{-\gamma}{\Gamma(n)} e^{-\gamma\phi} e^{-\gamma} \sum_{k=0}^{n-1} \binom{n-1}{k} \phi^k (-1)^{n-k} \mathrm{d}\phi \end{aligned}$$

$$= \frac{-\gamma e^{-\gamma}}{\ln(2)\Gamma(n)} \sum_{k=0}^{n-1} \binom{n-1}{k} (-1)^{n-k} \left[\frac{\partial}{\partial \nu} \gamma^{-\nu} \Gamma(\nu, \gamma) \right]_{\nu=k+1} \quad (5.3)$$

where the second step is a simple change of variable $\phi = \phi' + 1$ and the third step is the familiar binomial expansion. The remaining derivative can be simplified further with

$$\frac{\partial}{\partial \nu} \gamma^{-\nu} \Gamma(\nu, \gamma) = -\nu \gamma^{-\nu-1} \Gamma(\nu, \gamma) + \gamma^{-\nu} \frac{\partial}{\partial \nu} \Gamma(\nu, \gamma). \quad (5.4)$$

The derivatives $\frac{\partial}{\partial \nu} \Gamma(\nu, \gamma)$ are known in a form involving a case of the Meijer-G function, but are well-behaved and also easy to compute directly with numerical methods. The ergodic capacity of in a Poisson field of interferers was also considered in [6] and [25].

5.2 Adaptive Rate Control over a Single Channel

Consider a SISO transmitter-receiver pair with full CSI and a single channel over which to communicate with fixed power and a current channel (power) fade level η, in the midst of a *standard network*. The following relates the probability of outage to the current propagation and interference environment:

$$\bar{\lambda_\epsilon} = \frac{\Gamma(1 - \frac{2}{\alpha}) \eta^{\frac{2}{\alpha}} \epsilon}{C_\alpha \beta^{\frac{2}{\alpha}} R^2}. \quad (5.5)$$

and in particular in this section it will be assumed that $\log_2(1+\beta)$ is the achievable spectral efficiency for a given target β. Note that the signal factor is taken to be the limiting value $K_{\alpha,\infty}$ for a fixed power channel whose coefficient of variation around the mean vanishes. Given a sequence of channel state realizations, this

relation suggests an algorithm for adapting β to present conditions given a (lone) QoS constraint ϵ. By maintaining the relation, success probability is always ϵ though the target rate varies with the channel strength. Note also that since the channel is known, outage is due strictly to interference, and not channel fading.

Proposition 5.2.1. *In a standard network and a fixed outage, a power limit, in which SISO nodes have current CSI, area spectral efficiency is maximized by the contention density:*

$$\bar{\lambda_\epsilon^*} = \arg\max_{\lambda} \ \lambda \exp\left\{(\lambda C_\alpha R^2 \epsilon^{-1})^{\frac{\alpha}{2}}\right\} \mathrm{Ei}\left((\lambda C_\alpha R^2 \epsilon^{-1})^{\frac{\alpha}{2}}\right) \tag{5.6}$$

for $\mathrm{Ei}(x) = \int_x^\infty \frac{e^{-t}}{t}\mathrm{d}t$ *with the channel-aware algorithm*

$$\beta' = \frac{\eta}{R^\alpha}\left(\frac{\epsilon}{\lambda C_\alpha}\right)^{\frac{\alpha}{2}} \tag{5.7}$$

employed by each mode.

Proof. The optimality of the algorithm is demonstrated simply by solving the governing channel equation (5.5) for β given instantaneous CSI. Note that $\frac{\eta}{R^\alpha}$ is the actual path loss, and hence is easily measured at the receiver. To determine the optimal area spectral efficiency, note that the link at all times retains a $(1-\epsilon)$ probability of success and so achieves throughput:

$$(1-\epsilon)E[\log_2(1+\beta)] = (1-\epsilon)\int_0^\infty \log_2(1+\beta) f_\beta(\beta)\mathrm{d}\beta \tag{5.8}$$

For a SISO Rayleigh fading link, letting $\gamma = (\lambda C_\alpha R^2 \epsilon^{-1})^{\frac{\alpha}{2}}$, it was established in Section 5.1 that

$$E[\log_2(1+\beta)] = \frac{1}{\ln(2)} e^\gamma \mathrm{Ei}(\gamma). \tag{5.9}$$

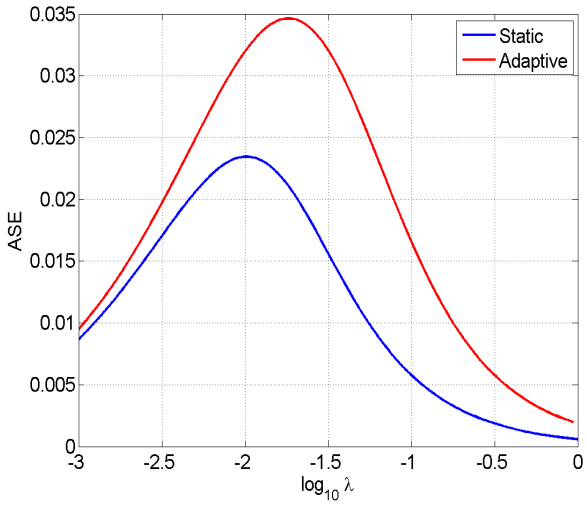

Figure 5.1: Adaptive vs. static rate control for SISO Rayleigh channels in a Poisson field of interferers for a path loss exponent of $\alpha = 4$ and and an outage constraint of $\epsilon = 0.1$.

This is the expression for the ergodic rate of a single link in the network. It assumes that the field of interferers changes over time, and for simplicity will be taken to be independent from one time slot to the next. To maximize transmission capacity and/or area spectral efficiency, there is the average area spectral efficiency:

$$\text{ASE} = (1 - \epsilon)\, \lambda\, E[\log_2(1 + \beta)]. \tag{5.10}$$

Maximizing this expression over λ is equivalent to maximizing (5.6) and has a nontrivial solution, but can be readily found numerically. □

Figure 5.1 gives a comparison of optimal static, network-wide rate control versus the channel-aware algorithm employed by each communicating pair, with

each case held to the same outage constraint. Here "optimal static" rate control picks a single β constant for each λ for a Rayleigh fading channel.

5.3 Adaptive Rate Control over Multiple Channels

Now consider a transmitter-receiver pair with full CSI in a standard network for which:

$$\bar{\lambda_\epsilon} = \frac{\eta_i \rho_i^{\frac{2}{\alpha}} \epsilon_i}{C'_\alpha \beta_i^{\frac{2}{\alpha}} R^2} \tag{5.11}$$

for the ith channel available to the communicating pair, where ρ_i is the fraction of the total power assigned to channel i and channel specific outage levels ϵ_i are given. Note also that the C'_α factor depends potentially on the number of channels and on power allocation strategies as well. For the purpose of the present development with a view toward MIMO channels, the approximation $C'_\alpha = \frac{2\pi}{\alpha}\Gamma(\frac{2}{\alpha})$ will be used, which is equivalent to $C_{\alpha,\infty}$ for a large number of interfering streams. Given the channel set (5.11), the algorithm becomes nearly identical to Proposition 4.4.2.

Proposition 5.3.1. *In a random access network with fixed outage constraints, a total power limit, and in which nodes have current CSI of their own subchannels, area spectral efficiency is maximized by the channel-aware algorithm*

$$\beta_i = \frac{\epsilon_i}{\sum_i \epsilon_i} \frac{1 + \sum_i \gamma_i}{\gamma_i} - 1 \tag{5.12}$$

employed by each mode, with $\gamma_i = \left(\frac{\lambda R^2 C'_\alpha}{\Gamma(1-\frac{2}{\alpha})\eta_i \epsilon}\right)^{\frac{\alpha}{2}}$.

Proof. To determine the optimum rate and power for each channel the algorithm maximizes the expression $\sum_i \log_2(1+\beta_i)$ subject to the constraints $\rho_i = \gamma_i \beta_i$ and

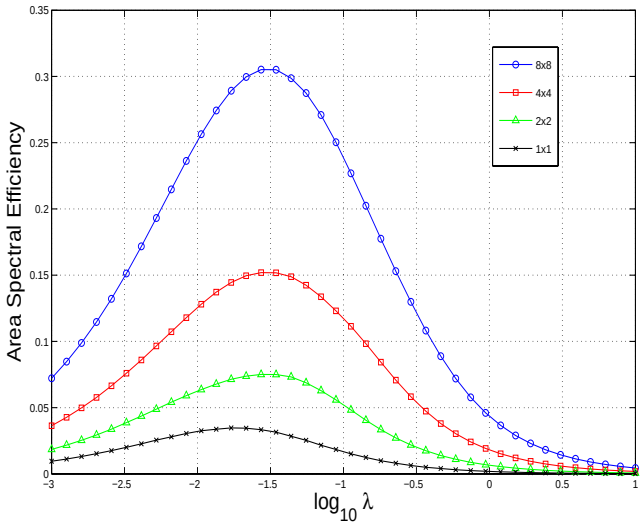

Figure 5.2: Area spectral efficiency versus contention density for one, two, four, and eight antennas with optimal adaptive rate control.

$\sum_i \rho_i = 1$. Applying Lagrange multipliers, the optimum target SINR for the ith channel is found as above. If a β_i is found to be negative, the channel is abandoned and the algorithm is run again with a smaller set of channels. Since the channel values η_i are known and fixed for a given transmission, they are equivalent to perfectly hardened channels with the effective signal factor being $\eta_i \Gamma(1 - \frac{2}{\alpha})$. $\square$

This is quite similar to the water-filling solution for the point-to-point MIMO channel in which better spatial modes are assigned more power and carry greater information content. Finally, the ASE of a network composed of many

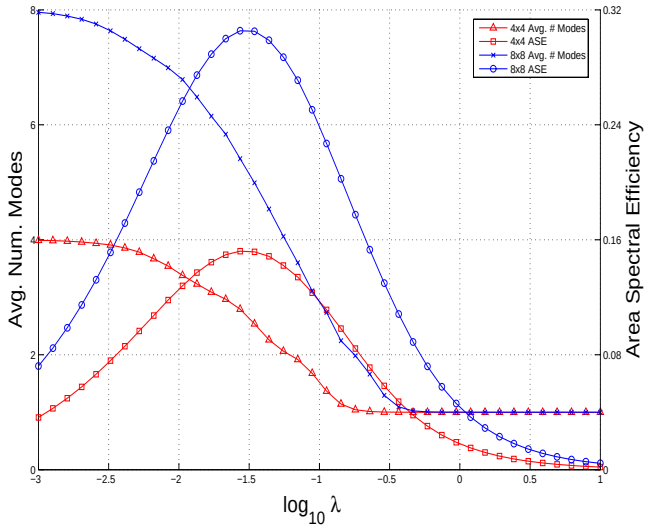

Figure 5.3: Area spectral efficiency and mean number of spatial modes used with adaptive rate control. As density increases, the optimal rate control abandons spatial modes in favor of increased power (diversity) on the remaining modes.

such communicating pairs of density λ employing this algorithm would be:

$$\begin{aligned} \text{ASE} &= \lambda E\left[\sum_i (1-\epsilon_i)\log_2(1+\beta_i(\lambda))\right] \\ &= \lambda \int_{[0,\infty]^N} \sum_i (1-\epsilon_i)\log_2(1+\beta_i(\lambda))\mathrm{d}F_{\beta_i}(\beta_i) \end{aligned} \tag{5.13}$$

where, as shown, the expectation is over all realizations of the β_i (each in $\mathbb{R}^+$) which are functions of the channel strength and power allocation on channel i. In general this expectation depends on the distribution of channel strengths (e.g., eigenvalues of Wishart matrices), the outcome of the water-filling-like power allocation algorithm, and the value of the "interference" constant C'_α whose derivation was discussed in the Appendix of the previous chapter. Hence, we do not have a simple rule for the distribution of the optimum number of spatial modes which

should be used and must analyze this numerically as in Fig. 5.3.

5.4 Adaptation with Hybrid-ARQ

The previous sections studied simple mechanisms for adapting to current channel conditions, but a superior adaptation mechanism already exists in many modern wireless systems, namely hybrid-ARQ with incremental redundancy. This mechanism adapts not just to the current channel but to the observed SINR. At a high level an H-ARQ scheme retransmits a packet whenever failure is detected at the receiver, but in such a way that new parity bits are sent so that a packet can be decoded when the accumulated mutual information at the receiver matches that of the original packet. ARQ and H-ARQ have been analyzed in point-to-point SISO settings in [82], [14], [9], and [101] and MIMO settings in [19] and [107]. Vaze [93] considered basic ARQ in the transmission capacity framework, in part using similar methods to Sec. 2.3, but focused on multi-hop performance estimation, where this section focuses on the throughput for a single link with near mutual information accumulation. As an upper bound, an ideal SINR accumulator will be assumed here with the property that the average throughput r is given by:

$$r = E\left[\log_2(1 + \mathrm{SINR})\right] \tag{5.14}$$

This kind of mechanism suggests removing the concept of outage altogether, and with it, the target SINR. Instead, the density of interferers drives the distribution of the SINR and hence the average rate. Now ignoring thermal noise, the PDF of

the SIR is given by (letting $\phi = \text{SIR}$):

$$\begin{aligned} f_\phi(x) &= \mathrm{d}\mathbf{P}(\phi \leq x) \\ &= \frac{\mathrm{d}}{\mathrm{d}x} 1 - e^{-\lambda C_\alpha R^2 x^{\frac{2}{\alpha}}} \\ &= \left(\lambda C_\alpha R^2 \frac{2}{\alpha}\right) x^{\frac{2}{\alpha}-1} e^{-\lambda C_\alpha R^2 x^{\frac{2}{\alpha}}} \end{aligned} \tag{5.15}$$

In the SISO case, taking $\gamma = \lambda C_\alpha R^2$,

$$\begin{aligned} r &= E_\phi \left[\log_2(1+\phi)\right] \\ &= \int_0^\infty \log_2(1+x) f_\phi(x) \\ &= \gamma \frac{2}{\alpha} \int_0^\infty \log_2(1+x) x^{\frac{2}{\alpha}-1} e^{-\gamma x^{\frac{2}{\alpha}}} \mathrm{d}x \end{aligned} \tag{5.16}$$

There is not a known closed-form solution to the integral in (5.16), but it will be denoted

$$\Delta(a,b,c) = \int_0^\infty \log_2(1+x) x^{c-1} e^{-bx^a} \mathrm{d}x \tag{5.17}$$

for $a, b, c > 0$, since it will form the kernel of a number of calculations in the following section. This integral can be computed numerically, though some care must be taken for $b \ll 1$.

Figures 5.4 and 5.5 compare SISO H-ARQ to the optimal fixed point solution of Sec. 2.2. Recall the optimal fixed point solution was the optimum operating point for β and ϵ given λ, which resulted in the best possible area spectral efficiency in a standard network with no outage or rate constraint. These figures demonstrate that a mutual information accumulation design achieves more than twice the throughput at the peak.

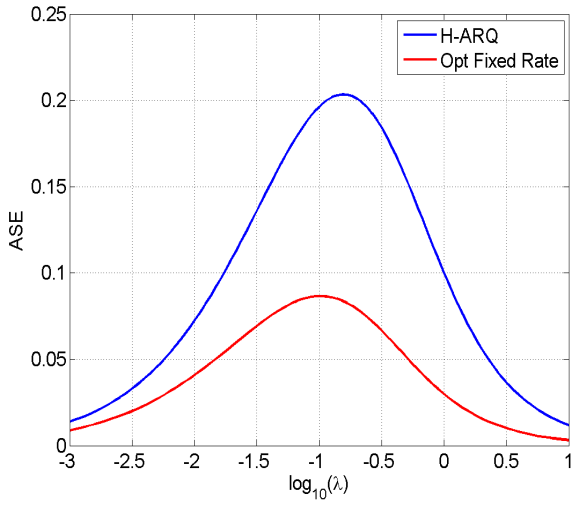

Figure 5.4: Comparison the area spectral efficiency of SISO HARQ and the optimal fixed rate vs. contention density.

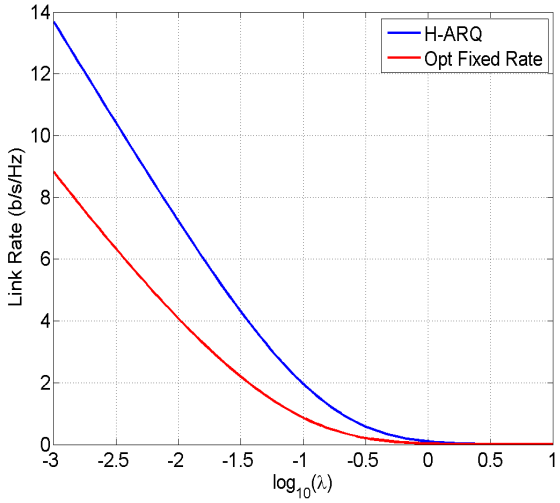

Figure 5.5: Comparison of maximum link efficiency for SISO HARQ and the optimal fixed rate vs. contention density. Path loss exponent is 4.

5.5 H-ARQ with Multiple Streams

The MIMO architecture considered here is one for which an independent H-ARQ stream is sent over each spatial mode that is used. No outage constraints or rate constraints apply, but when channel information is available, the allocation of power across spatial modes must be decided. As always, increasing the number of modes increases the effective interference level.

Given a channel with a signal distribution according to *restricted* standard fading form, to compute the average throughput of the channel with ideal H-ARQ according to (5.1) the PDF of the SINR ϕ is necessary. For restricted standard fading form, the PDF can be obtained by (letting $\gamma = \lambda R^2 C_{\alpha,n}(\Omega/\theta)^{\frac{2}{\alpha}}$):

$$\begin{aligned}
f_\phi(x) &= \frac{\mathrm{d}}{\mathrm{d}x}\left\{\frac{(-1)^m}{\Gamma(m)}e^{-\gamma x^{\frac{2}{\alpha}}}\sum_{i=0}^{m-1}s(m,i+1)\left(\frac{2}{\alpha}\right)^i\sum_{j=0}^{i}S(i,j)\left(-\gamma x^{\frac{2}{\alpha}}\right)^j\right\} \\
&= \frac{(-1)^m}{\Gamma(m)}\sum_{i=0}^{m-1}s(m,i+1)\left(\frac{2}{\alpha}\right)^i\sum_{j=0}^{i}S(i,j)\frac{\mathrm{d}}{\mathrm{d}x}\left\{e^{-\gamma x^{\frac{2}{\alpha}}}\left(-\gamma x^{\frac{2}{\alpha}}\right)^j\right\} \\
&= \frac{(-1)^m}{\Gamma(m)}\sum_{i=0}^{m-1}s(m,i+1)\left(\frac{2}{\alpha}\right)^i\sum_{j=0}^{i}S(i,j)(-\gamma)^j \\
&\quad\times e^{-\gamma x^{\frac{2}{\alpha}}}\left[\left(\frac{2}{\alpha}\right)(-\gamma)x^{\frac{2}{\alpha}(j+1)-1}+\left(\frac{2}{\alpha}j\right)x^{\frac{2}{\alpha}j-1}\right] \\
&= \frac{(-1)^m}{\Gamma(m)}e^{-\gamma x^{\frac{2}{\alpha}}}\sum_{i=0}^{m-1}s(m,i+1)\left(\frac{2}{\alpha}\right)^{i+1}\sum_{j=0}^{i}S(i,j)(-\gamma)^j \\
&\quad\times\left[jx^{\frac{2}{\alpha}j-1}-\gamma x^{\frac{2}{\alpha}(j+1)-1}\right] \qquad (5.18)
\end{aligned}$$

As a result the throughput of this channel can be given as

$$E_\phi(\gamma) = \frac{(-1)^m}{\Gamma(m)}\sum_{i=0}^{m-1}s(m,i+1)\left(\frac{2}{\alpha}\right)^{i+1}\sum_{j=0}^{i}S(i,j)(-\gamma)^j$$

$$\times \left[j\Delta\left(\frac{2}{\alpha}, \gamma, \frac{2}{\alpha} j\right) - \gamma\Delta\left(\frac{2}{\alpha}, \gamma, \frac{2}{\alpha}(j+1)\right)\right]. \qquad (5.19)$$

5.6 Heterogeneous Networks

The standard network definition included the assumption that all nodes behaved identically in a statistical sense. However, the algorithms developed in the previous sections were carried out by individual communicating pairs, without regard to the behavior of other nodes, *given that the interference factor and contention density are known.* First, the algorithm causes β to be no longer a network-wide constraint. In the multi-channel case, the number of spatial modes and the power allocation are no longer identical. There is then no reason that target outage need be identical, or even that all nodes have an identical antenna configuration. What is necessary for the algorithm to work is simply that, whatever the behavior of each node, the net statistical effect is known to all. For example, suppose each node has two antennas, but half of the nodes always transmit a single spatial mode, and the other half always transmit two, and the two classes of nodes are randomly intermixed. In this case, an effective $C'_\alpha = (C_{\alpha,1} + C_{\alpha,2})/2$ and the total contention density λ is all a node requires to carry out the algorithm.

5.7 Conclusion

This chapter considered channel adaptive strategies for MIMO, with and without constraints. The ultimate channel adaptive strategy, H-ARQ with IR,

was shown to perform best, but with little effect on the relative performance of various MIMO configurations.

Chapter 6

Transmission Capacity Optimization of CSMA and MIMO

The work up to this point has developed relations assuming a homogeneous Poisson field of interferers. This assumption is best suited to an Aloha MAC protocol and has several analytical consequences, such as the perennial linear relationship of ϵ and λ for small outage constraints. On the other hand, variants of CSMA have been the most common multiple access protocols in both wireless and wireline networks for many years. Performance analysis of CSMA began with Kleinrock, *et al.* [54, 90, 91], which discussed many of the features that are still grappled with today including the exposed and hidden node problems, and reservation strategies. CSMA has been considered in countless papers since, but was brought under the analysis of stochastic geometry models in [5]. Both CSMA and Aloha have known drawbacks. Aloha is relatively inefficient, especially when compared to an all-knowing central scheduler. CSMA is often a practical design which ensures some level of QoS, but to be done properly with a full request-to-send/clear-to-send (RTS/CTS) mechanism can be costly [78]. However, recent advances have suggested that fully distributed channel-aware and queue-length-aware CSMA policies could approach maximal scheduling arbitrarily well [71, 41, 42], in the sense that queues can be held stable, delay held low, and utility

maximized, for nearly all achievable points in the network capacity region. While Aloha provide a good mechanism for investigating the impact of multiple antennas on network performance, CSMA is arguably a more important use case, and since it changes the distribution of interference, it is worth investigating how much this changes the optimal use of multiple antennas.

This chapter is laid out as follows: Section 6.1 describes a particular inhomogeneous Poisson model for CSMA. Section 6.2 takes a detour to consider effects of multiple antennas on the sensing mechanism itself. Section 6.3 develops SINR distributions under CSMA for multi-antenna systems in a manner applicable to the Gamma approximation method of Chapter 2. Section 6.4 explores the resulting optimization problems and Section 6.6 concludes.

6.1 "Soft" Carrier Sensing

The CSMA mechanism is difficult to analyze in general and many models have been advanced. Baccelli, *et al.* [5], introduced Matern's hard-core point process as a model for CSMA, and later developed an inhomogeneous Poisson approximation to it [3]. In the interest of tractability, a Poisson approximation will be made here, which will be called a "soft" CSMA model for reasons that should become clear. The model will be considered which can be broken down into two main parts:

1. Large-scale density λ_t of transmitters.

2. Shot range inhibition.

Large-scale density : A Matern model similar to that in [5] is used for obtaining the final average density of transmitters. In this model each node is associated with a set $\hat{\mathcal{N}}$ consisting of transmitters which individually cause an interference greater than θ_{M}. A node is finally selected to transmit if its timer (a uniform random variable in $[0,1]$) is the smallest. Given an initial density λ_i of nodes attempting to access the channel, after carrier sensing the resulting large-scale density λ_t is [5]

$$\lambda_t = \lambda_i \cdot \frac{1-\exp(-\mathcal{N})}{\mathcal{N}}, \tag{6.1}$$

where $\mathcal{N}$ is the average number of nodes in a typical contention set $\hat{\mathcal{N}}$ and equals

$$\begin{aligned} \mathcal{N} &= \int_{\mathbb{R}^2} \lambda_i \cdot e^{-\theta_{\mathrm{M}}|x|^{\alpha}} \mathrm{d}x, \\ &= \pi\Gamma(1+2/\alpha)\theta_{\mathrm{M}}^{-\frac{2}{\alpha}}\lambda_i. \end{aligned} \tag{6.2}$$

Shot range inhibition: A further approximation is made that from the perspective of a typical receiver, the set of interferers is distributed around it as a radially symmetric inhomogeneous Poisson process with density $(1-e^{-\theta_{\mathrm{M}}|X|^{\alpha}})\lambda_t$, where λ_t is the average density of the set of currently transmitting nodes. The factor $e^{-\theta_{\mathrm{M}}|X|^{\alpha}}$ is the probability that an exponentially distributed power fade will exceed a threshold θ_{M} at that distance. The average density is all that is necessary to model the interference contribution from nodes at long distances, while at close ranges the presence of the communicating node has the dominant effect on the distribution of interferers. Furthermore, the model treats the channel through which carrier sensing decisions were made as independent of the Poisson shot noise interference process of data transmission. In this sense the carrier sensing

is "soft," being neither an exact geographic disk, nor exactly representative of mutually interfering nodes during data communication.

Final model: Hence, from the perspective of a typical receiver the interferers form a non-homogeneous Poisson point process of density $(1 - e^{-\theta_{\mathrm{M}}|X|^{\alpha}})\lambda_t$. This model has several advantages over the hard-core model: First, it brings fading into play when modeling carrier sensing. Second, it allows for modeling imperfect carrier sensing. Third, it enables modeling of a behavior specific to multi-antenna systems in which network interference differs between the control/carrier sensing modes and high data rate modes. Lastly, it provides more tractable results that give simpler functional relationships between the carrier sensing parameters and other environmental and system parameters. In addition, a model in which the probability of inhibition rises at least as fast as the power-law path loss function results in the interference power from the nearest interferer having finite mean. This removes problems related to the behavior of the path loss model near the origin (a feature shared by the Matern hard-core model).

6.2 CSMA Sensing with Multiple Antennas

Another way a CSMA ad hoc network can take advantage of multiple antennas is in the carrier sensing itself. When the carrier sensing mechanism is subject to fading, more conservative thresholds must be met to guarantee outage requirements. One approach which is readily tractable in the current model is to use selection or combining diversity on multiple receive antennas for carrier sensing and to impose a threshold on the selected or combined output (the former

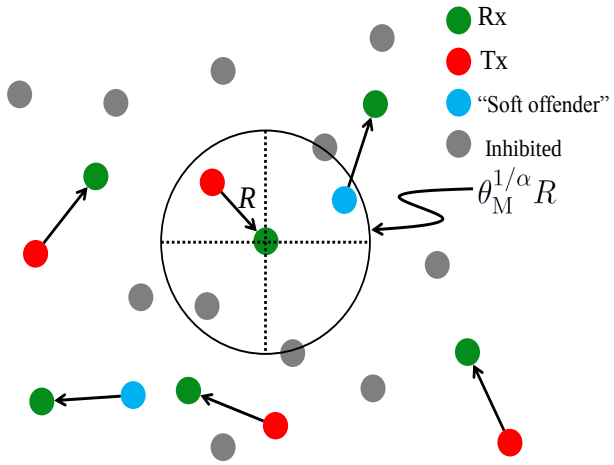

Figure 6.1: Contention around the typical receiver. Fading and channel sensing errors lead to a "soft" CSMA model unlike the corresponding hard care boundary marked here.

approach being appropriate when CSI over the control channel is difficult to obtain). As an example, suppose a node with M_c multiple receive antennas performs carrier sensing on each antenna, but averages the result across antennas before applying the threshold. In this case

$$\begin{aligned} \mathcal{N} &= \int_{\mathbb{R}2} \lambda_i \cdot e^{-\theta_{\mathrm{M}} M_c |x|^\alpha} \sum_{k=0}^{M_c-1} \frac{(\theta_{\mathrm{M}} M_c |x|^\alpha)^k}{k!} \mathrm{d}x \\ &= \frac{2\pi}{\alpha} \theta_{\mathrm{M}}^{-\frac{2}{\alpha}} \lambda_i \sum_{k=0}^{M_c-1} \frac{\Gamma(\frac{2}{\alpha}+k)}{M_c^{\frac{2}{\alpha}} \Gamma(k+1)}. \end{aligned} \tag{6.3}$$

Note that in the limit of a large number of antennas, the carrier sensing behavior approaches that of a hard-core process as the influence of small scale fading on sensing decisions disappears. While channel hardening techniques make

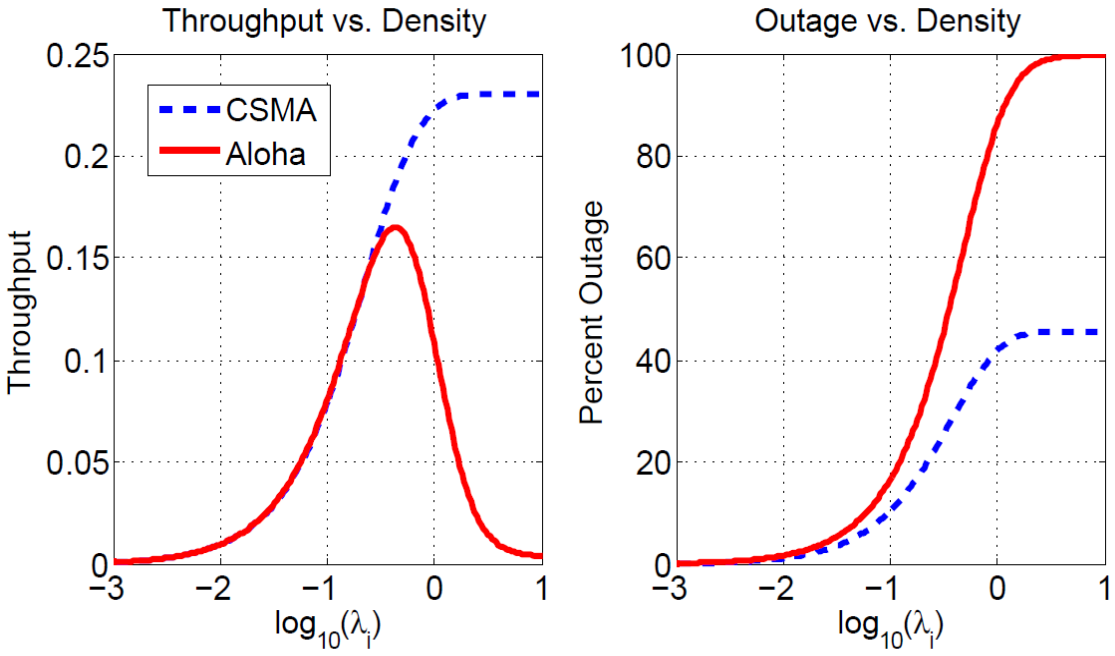

Figure 6.2: Comparison of throughput and outage for CSMA and Aloha, for SISO system. Density is *initial* density, i.e., before thinning via carrier sensing. Outage is counted among active transmitters (i.e., those not thinned by CSMA). Parameters were $R = 1, \alpha = 4, \theta_{\mathrm{S}} = 0\mathrm{dB}$.

the carrier sensing mechanism more efficient, primarily by reducing errors due to deep fades, the net benefit turns out to be small (particularly compared to the benefit of CSMA over Aloha). Therefore, for the main analysis of multiplexing systems, a SISO carrier sensing channel is assumed.

6.3 Spatial Multiplexing with CSMA

This section gives the central result of the chapter which gives the probability of success or equivalently the SINR distribution for *restricted* standard fading form, with a particular development for open-loop spatial multiplexing.

Proposition 6.3.1. *Given a network of nodes performing CSMA, open-loop spatial multiplexing, and with per-stream decoding success defined in (1),*

$$\mathbf{P}_{\mathrm{S}}(\theta_{\mathrm{S}}) = \sum_{k=0}^{N_r-1} \left[\frac{(-s)^k}{k!} \frac{\mathrm{d}^k}{\mathrm{d}s^k} \mathcal{L}_{I_\Phi}(s) e^{-\frac{1}{\mathrm{SNR}}}(s) \right]_{s=N_t \theta_{\mathrm{S}} R^\alpha},$$

where

$$\begin{aligned}
\mathcal{L}_{I_\Phi}(s) &= \exp\left\{ -\frac{2\pi}{\alpha} (s/N_t)^{\frac{2}{\alpha}} \lambda_t [C_{\alpha,N_t} - T_{\mathrm{M}}(s)] \right\} \\
C_{\alpha,N_t} &= \sum_{i=1}^{N_t} \binom{N_t}{i} B(N_t - i_\alpha, i_\alpha) \\
T_{\mathrm{M}}(s) &= \sum_{i=1}^{N_t} \binom{N_t}{i} \Gamma(N_t - i_\alpha) U\left(N_t - i_\alpha, -i_\alpha - 1, \frac{\theta_{\mathrm{M}}}{N_t} s \right)
\end{aligned}$$

with $i_\alpha = i - \frac{}{\alpha}$ *for notational convenience and* $B(x,y) = \frac{\Gamma(x)\Gamma(y)}{\Gamma(x+y)}$ *being the beta function, and where* $U(a,b,x) = \frac{1}{\Gamma(a)} \int_0^\infty e^{-xt} t^{a-1} (1+t)^{b-a+1} \mathrm{d}t$ *is Kummer's confluent hypergeometric U-function.*

Proof. These expressions are developed using techniques similar to those of Sec. 2.3 (as well as[5], [38], and [66]). For a given stream at the receiver using the ZF solution $S_o \sim \mathrm{Gamma}[N_r, 1/N_t]$ with $F^c_{S_o}(x) = e^{-N_t x} \sum_{k=0}^{N_r-1} \frac{(N_t x)^k}{k!}$ so that

$$\mathbf{P}_{\mathrm{S}}(\theta_{\mathrm{S}}) = \mathbf{P}\left(\frac{S_o R^{-\alpha}}{\sum_{i \in \Phi} S_i d_i^{-\alpha} + \frac{1}{\mathrm{SNR}}} > \theta_{\mathrm{S}} \right)$$

$$= \int_0^\infty F_{S_o}^c(\theta_{\mathrm{S}} R^\alpha t) f_{I_\Phi + \frac{1}{\mathrm{SNR}}}(t)\mathrm{d}t$$
$$= \sum_{k=0}^{N_r-1} \frac{1}{k!} \int_0^\infty (st)^k e^{-s\cdot t} f_{I_\Phi + \frac{1}{\mathrm{SNR}}}(t)\mathrm{d}t$$
$$= \sum_{k=0}^{N_r-1} \left[\frac{(-s)^k}{k!} \frac{\mathrm{d}^k}{\mathrm{d}s^k} \mathcal{L}_{I_\Phi}(s) \mathcal{L}_{\frac{1}{\mathrm{SNR}}}(s) \right]_{s=N_t\theta_{\mathrm{S}}R^\alpha},$$

where the Laplace transform of the sum of the random variables is the product of the transforms. Now $\mathcal{L}_{\frac{1}{\mathrm{SNR}}}(s) = e^{-s/\mathrm{SNR}}$ and if in addition $S_i \sim \mathrm{Gamma}[N_t, 1/N_t]$ as in open-loop multiplexing across the network, the Laplace transform of the Poisson shot noise is

$$\mathcal{L}_{I_\Phi}(s) = \exp\left\{ \int_{\mathbb{R}^2} \left(\mathrm{E}_{S_i}\left[e^{-S_i|x|^{-\alpha}s} \right] - 1 \right) \mathrm{d}\Phi \right\} \tag{6.4}$$
$$= \exp\left\{ -2\pi\lambda_t \int_0^\infty u \left(1 - \frac{1}{(1+s/N_t u^\alpha)^{N_t}} \right) \times (1 - e^{-\theta_{\mathrm{M}} u^\alpha}) \mathrm{d}u \right\} \tag{6.5}$$
$$= \exp\left\{ -\frac{2\pi}{\alpha} \theta_{\mathrm{S}}^{\frac{2}{\alpha}} R^2 \lambda_t \sum_{i=1}^{N_t} \binom{N_t}{i} [B(N_t - i_\alpha, i_\alpha) - \Gamma(N_t - i_\alpha) U(N_t - i_\alpha, -i_\alpha - 1, \theta_{\mathrm{M}}\theta_{\mathrm{S}} R^\alpha)] \right\} \tag{6.6}$$
$$= \exp\left\{ -\frac{2\pi}{\alpha} \theta_{\mathrm{S}}^{\frac{2}{\alpha}} R^2 \lambda_t [C_{\alpha,N_t} - T_{\mathrm{M}}] \right\}. \tag{6.7}$$

Our last task is to find an explicit and efficient method of calculating derivatives of these Laplace transforms. For this, Faà di Bruno's formula for derivatives of composite functions $\frac{\mathrm{d}^k}{\mathrm{d}s^k} f(g(s))$ is necessary, which can be represented as a determinant [46]:

$$\frac{\mathrm{d}^k}{\mathrm{d}s^k} f(g(s)) = \det \mathbf{M}\, f(g(s))$$

for the $k \times k$ matrix

$$\mathbf{M} = \begin{pmatrix} g^{(1)}D & -1 & 0 & 0 & \dots \\ g^{(2)}D & g^{(1)}D & -1 & 0 & \dots \\ g^{(3)}D & 2g^{(2)}D & g^{(1)}D & -1 & \dots \\ g^{(4)}D & 3g^{(3)}D & 3g^{(2)}D & g^{(1)}D & \dots \\ \vdots & \vdots & \vdots & \vdots & \end{pmatrix},$$

where $D^k f(g(s)) = f^{(k)}(g(s))$, and where the coefficients applied to each row are rows of Pascal's triangle. To apply Faà di Bruno's formula to the derivatives of $\mathcal{L}_{I_\Phi}(s)\mathcal{L}_{\frac{1}{\mathrm{SNR}}}(s)$, one can write $\mathcal{L}_{I_\Phi}(s)\mathcal{L}_{\frac{1}{\mathrm{SNR}}}(s) = f(g(s))$, where $f(s) = e^s$ and

$$g(s) = \log\left(\mathcal{L}_{I_\Phi}(s)\mathcal{L}_{\frac{1}{\mathrm{SNR}}}(s)\right)$$

whose derivatives are (for $k > 1$):

$$\begin{aligned} g^{(k)}(s) &= -\frac{2\pi}{\alpha}\lambda_t (s/N_t)^{\frac{2}{\alpha}-k}\left[C_{N_t}^{\alpha}\prod_{j=0}^{k-1}\left(\frac{2}{\alpha}-j\right) - \right. \\ &\left. \sum_{i=1}^{N_t}\sum_{j=0}^{k} K_{ijk} s^j U\left(\begin{bmatrix} N_t - i_\alpha + j \\ -i_\alpha - 1 + j \end{bmatrix}, \frac{\theta_{\mathrm{M}}}{N_t}s\right)\right], \end{aligned} \tag{6.8}$$

where

$$\begin{aligned} K_{ijk} &= (-\theta_{\mathrm{M}}/N_t)^j \binom{N_t}{i}\Gamma(N_t - i_\alpha)\binom{k}{j} \\ &\quad \times (N_t - i_\alpha + j)_j \prod_{n=0}^{k-j-1}\left(\frac{2}{\alpha} - n\right). \end{aligned} \tag{6.9}$$

It is necessary to add a term $-1/\mathrm{SNR}$ to $g^{(1)}$, which subsequently vanishes. This relied on the relation for the nth derivative of $U(a,b,x)$ which is expressible as

$$\frac{\mathrm{d}^n}{\mathrm{d}x^n}U(a,b,x) = (-1)^n (a)_n U(a+n, b+n, x) \tag{6.10}$$

where $(\cdot)_n$ is the Pochhammer symbol for the rising factorial [88]. □

Again note that as $s \to \infty$, $U(a,b,s) \to 0$ and thus $T_{\mathrm{M}} \to 0$ which corresponds to the Aloha case. As $s \to 0$, $\Gamma(a)U(a,b,s) \to B(a,b)$, which implies that $T_{\mathrm{M}} \to C_{\alpha,N_t}$ as the threshold $\theta_{\mathrm{M}} \to 0$. In this case the probability of success approaches 1 among active transmitters, at the expense of λ_t vanishing.

6.4 Optimal CSMA threshold

Specializing Theorem 2.3.1 to the case $N_r = N_t = 1$, the success probability in a SISO system becomes

$$\mathbf{P}_{\mathrm{S}}(\theta_{\mathrm{S}}) = \exp\left\{-\theta_{\mathrm{S}}^{2/\alpha} R^2 \lambda_t \left[C_\alpha - T_{\mathrm{M}}\right]\right\} e^{-\theta_{\mathrm{S}} R^\alpha/\mathrm{SNR}},$$

where $C_\alpha = \pi\Gamma(1+\frac{2}{\alpha})\Gamma(1-\frac{2}{\alpha})$ is the familiar Aloha constant and T_{M} reduces to

$$T_{\mathrm{M}} = \frac{2\pi}{\alpha} e^{\theta_{\mathrm{M}}\theta_{\mathrm{S}}R^\alpha} \Gamma\left(1-\frac{2}{\alpha}, \theta_{\mathrm{M}}\theta_{\mathrm{S}}R^\alpha\right) \tag{6.11}$$

the two-parameter gamma function being the upper incomplete gamma function. Note that T_{M} is a factor related to the carrier sensing threshold, but also that λ_t is dependent on this threshold. This expression holds for any outage level or transmitter density. As the inhibition threshold rises so that very few nodes are inhibited, $\lambda_t \to \lambda_i$ and $T_{\mathrm{M}} \to 0$ recovering the Aloha result [5]. Note also that with a fixed threshold

$$\lim_{\lambda_i \to \infty} \lambda_{t,\infty} = \left(\pi\Gamma\left(1+\frac{2}{\alpha}\right)\theta_{\mathrm{M}}^{-\frac{2}{\alpha}}\right)^{-1}, \tag{6.12}$$

which indicates that regardless of the number of users requesting access, the carrier sensing process limits the set of active transmitters to a limiting density, as it should.

A natural question then is to find the optimal carrier sensing threshold. The optimum threshold is then the unique maximum to:

$$\theta_{\mathrm{M}}^{*} = \arg\max_{\theta_{\mathrm{M}}} \lambda_t \cdot \exp\left\{-\theta_{\mathrm{S}}^{2/\alpha} R^2 \lambda_t \left[C_\alpha - T_{\mathrm{M}}\right]\right\}. \tag{6.13}$$

This expression is log-concave in θ_{M} and hence is relatively easy to optimize numerically. At this point there are a few observations that can be made to assist further analysis: First, as $\lambda_i \to \infty$ the optimum threshold approaches a limit which is the unique solution to (6.13) at $\lambda_{t,\infty}$. Second, as λ_i becomes small, for a fixed threshold, very little inhibition takes place and the sum throughput performance of Aloha and CSMA are nearly identical[1] so that there is very little difference in an optimum versus a non-optimum threshold. Hence, a useful approximation is to consider the optimum threshold for any initial density to be roughly equal to that of the limiting density $\lambda_{t,\infty}$.

Lastly, as $\lambda_i \to 0$, the network is sparse enough that very little inhibition takes place and $\lambda_t \to \lambda_i$, and the spatial density of transmissions can be related to the outage probability:

$$\lambda_t = \frac{\epsilon}{\theta_{\mathrm{S}}^{2/\alpha} R^2} \cdot \frac{1}{\left[C_\alpha - T_{\mathrm{M}}\right]} + o(\epsilon^2). \tag{6.14}$$

Since $T_{\mathrm{M}} \leq C_\alpha$, carrier sensing with an appropriate threshold performs at least as well as Aloha. For the multiple antenna case, the optimum θ_{M} can be found

[1] This is very different from saying that the transmission capacity at a fixed outage is nearly the same for both. At a fixed λ_i, if Aloha experiences 1% outage, then CSMA can increase throughput at the same λ_i by no more than 1% at best. On the other hand, for a fixed 1% outage constraint, CSMA can maintain a substantially greater λ_t than Aloha can.

numerically. As in the single-antenna case, the optimum threshold reaches a limit as λ_i grows large, which is a relatively good selection at all λ_i.

6.5 Examples and Discussion

Fig. 6.2 compares throughput and outage of CSMA and Aloha for the base SISO case. Here the CSMA is not fully optimized, but rather has a fixed threshold for all initial contention densities. Note that the figures plot throughput and outage versus the initial contention density, prior to thinning via carrier sensing, in order to fairly compare with Aloha. This convention was used for all plots versus density. Fig. 6.3 compares 4-antenna MIMO configurations at a high base SNR (with fully optimized CSMA). Fig. 6.4 compares 4-antenna MIMO configurations with a relatively small outage constraint applied. These curves demonstrate several distinctions between the performance of CSMA networks versus Aloha networks. The first is simply that as the initial contention density increases, CSMA throughput overtakes Aloha substantially and reaches a non-zero plateau. Furthermore, comparing throughput levels for Fig. 6.2 and Fig. 6.4, it becomes clear that CSMA MIMO systems achieve a higher throughput at substantially lower outage among transmitting nodes. This can substantially reduce the burden on PHY layer decoding implementations and conserve energy. In particular, a 1×3 antenna configuration with an optimized threshold can achieve a network throughput equivalent to the best Aloha configuration but with a fourfold reduction in the outage probability.

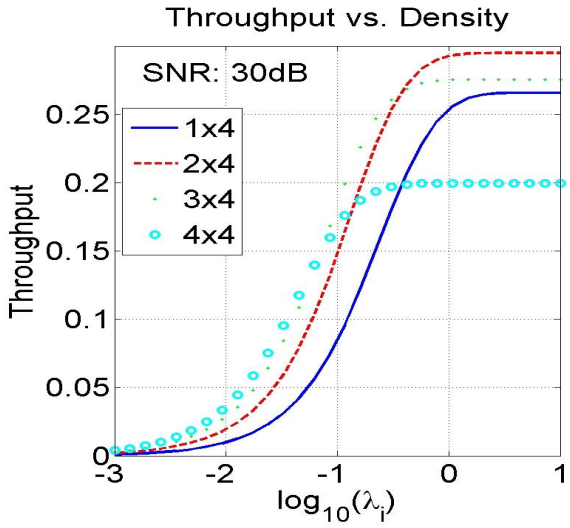

Figure 6.3: Comparison of throughput for CSMA at a high base SNR. Note that no outage constraints are imposed. Parameters were $R = 1, \alpha = 4, \theta_S = 0$dB.

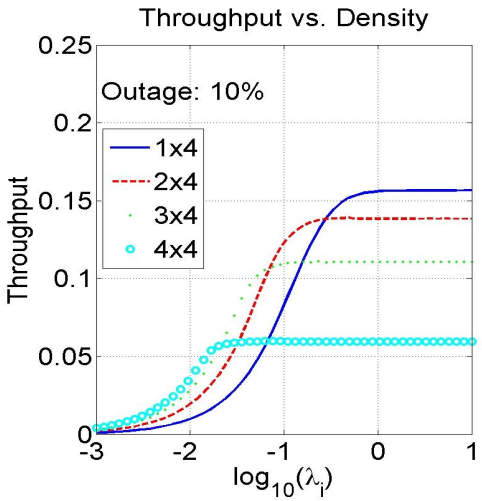

Figure 6.4: Throughput vs. initial density for 4-antenna systems with optimized CSMA and an outage constraint of 10% Parameters were $R = 1, \alpha = 4, \theta_S = 0$dB, SNR= 10dB.

6.6 Conclusion

This chapter advanced the framework to a parameterized model for CSMA and explored the optimization of MIMO techniques in it. Alternative expressions were derived for SINR distributions applicable to the Gamma approximation of standard fading forms. This enables much of the prior analysis to be carried out.

Chapter 7

Conclusion

This work advanced the shot noise interference model for packet radio networks in the realm of multi-antenna physical layers. A consistent framework was developed and applied to the major, representative MIMO techniques, permitting careful and fair comparison. Tools were also developed for incorporating other salient features that could be distilled into a change in the effective decoding SNR. In brief the conclusions could be stated as: (*i*) significant gain factors could be reaped by the use of multiple antennas in large distributed networks; (*ii*) MIMO techniques with spatially random interference and high QoS constraints can be optimized in a manner not too dissimilar to point-to-point settings, and under normal operating parameters have a rich set of solutions (i.e., they are not degenerate, as for example, "use one antenna or one spatial mode all the time"); (*iii*) receive diversity, apart from being practical, is a major contributor to gains, and transmit diversity techniques in the absence of CSI are self-defeating; and, (*iv*) simple distributed algorithms can achieve substantial gains from multiple antennas.

7.1 Impact of the Work

The framework developed here has already borne some fruit elsewhere in the analysis of distributed wireless systems, some of which is listed briefly here. The work of R. H. Y. Louie, *et al.* [66] and [103], built directly on the original presentation of the framework [38] and [37], but brought another rich set of mathematical tools to attack the problem. They have made substantial extensions and refinements, some of which were incorporated in this thesis (see for example Sec. 2.5 and Sec. 4.3.1). The foray into SDMA analysis by Kountouris [55] used the framework as the basis for relating multiuser transmission SINR statistics to network performance. The framework also inspired Chandrasekhar [10] to develop MIMO analysis for cellular systems with mobile users and hotspots. The work of Stamatiou, *et al.* [85, 84, 86], was initially parallel to the present work, but eventually also took the Laplace transform approach for alpha-stable processes to tackle MIMO signal distributions.

7.2 Future Work

As multiple antenna PHY layers proliferate, the extension of any given architecture to the MIMO case becomes a common question for the system designer. Several interesting developments of the Poisson shot noise model with multiple antennas are already underway, such as SDMA and successive interference cancellation and interference alignment. However, there are system level pursuits for which extension to MIMO would be both enlightening and difficult such as:

SINR-Aware Scheduling with Multiple Antennas. The work of Liu [62] developed a variety of bounds on the transmission capacity of networks in which SINR-aware scheduling is possible. Extending these results to the MIMO case opens up a large set of design and analysis questions. In addition, many transmission capacity results rely on the Poisson process for tractability, but SINR-aware decision making among multiple nodes tends to violate the assumptions of such a model. Developing a tractable model for interaction of this kind that had the flexibility of the framework developed here would have tremendous value, and may well find applications beyond the scope of ad hoc networks.

7.3 Parting Thoughts

Multiple antenna technology has been become mature in many ways, and enshrined in standards and delivered in ubiquitous commercial products. By contrast, historically large peer-to-peer wireless networks have not performed according to expectations, though expectations are in the eye of the beholder, despite a colossal sum expended in research and development. It is unlikely that multiple antenna physical layers alone will make up the difference, but they are likely to be an integral part of the solution in any case.

Assuming expenditures on research and development correspond roughly to a latent demand for unavailable technology, it is worth considering the effort by the U.S. military to make flexible, high-throughput, mobile ad hoc networks a reality. The cost of the Department of Defense programs Joint Tactical Radio System for Ground Mobile Radio (JTRS and GMR, respectively), begun in 1997,

have now run into the tens of billions of dollars [15], while the end products have not matched expectations. Theoretical analysis has helped put some of the expectations in perspective, but the demand is unlikely to subside.

This work has focused on a "traditional" view of what wireless devices are capable, most notably in the form of the central place of the communicating pair. A number of alternative architectures have been suggested, including the concepts of interference alignment and hierarchical MIMO. In general these require a level of cooperation and/or channel state awareness that is unknown to contemporary systems, though not wholly out of the question. Another promising, and less ambitious, architecture is that of fully SINR-aware scheduling. While this has been studied in the abstract often, it became a publicly demonstrated prototype, incarnated as Qualcomm's FlashLinQ [102].

There are other reasons as well to suggest a non-traditional architecture may be desirable. In 2005-2007, MIMO channel measurement campaigns were conducted in both Manhattan and semi-rural New Jersey [60]. Each case happily confirmed that MIMO channels with significant degrees of freedom for modest numbers of antennas (2-10) were common. But one result was rather unexpected. In the rural setting, log-normal shadow fading standard deviation was measured in excess of 20 dB and averaged 17.5 dB for some areas. This spread is 8-12 dB higher than typical outdoor models. This kind of variability in channel strength could lead to very different conclusions about the nature of spatial interactions in ad hoc networks. In this sense, the fundamental model of propagation, interference, and spatial interaction is still, in the opinion of the author, an open question in the

case of ad hoc networks, awaiting further verification from field-tested systems.

Lastly, though the framework developed here has considered a node in the midst of a large network, generally performance is limited by a node's nearest neighbors. As a result many of the methods and intuition developed here related to SINR distribution are analogous to the performance of other system designs such as cityscapes with many overlapping microcell hotspots. Thus there is promise that the transmission capacity framework will continue to provide a point of comparison and suggest analysis tools for many systems to come.

Bibliography

[1] N. Abramson. The throughput of packet broadcasting channels. *IEEE Transactions on Communications*, COM-25(1):117–128, Jan. 1977.

[2] J. G. Andrews, R. K. Ganti, M. Haenggi, N. Jindal, and S. Weber. A primer on spatial modeling and analysis in wireless networks. *IEEE Communications Magazine*, 48:156–163, Nov. 2010.

[3] F. Baccelli and B. Błaszczyszyn. Stochastic geometry and wireless networks – Volume I: Theory. *Foundations and Trends® in Networking*, 3(3–4):249–449, 2009.

[4] F. Baccelli and B. Błaszczyszyn. Stochastic geometry and wireless networks – Volume II: Applications. *Foundations and Trends® in Networking*, 4(1–2):1–312, 2009.

[5] F. Baccelli, B. Blaszczyszyn, and P. Muhlethaler. An ALOHA protocol for multihop mobile wireless networks. *IEEE Trans. on Inf. Theory*, 52(2):421–436, Feb. 2006.

[6] F. Baccelli, B. Blaszczyszyn, and P. Muhlethaler. Stochastic analysis of spatial and opportunistic aloha. *IEEE Journal on Sel. Areas in Comm.*, 27(7):1105–1119, Sept. 2009.

[7] C. A. Balanis. *Antenna Theory: Analysis and Design*. New York: Harper and Row Publishers, 1982.

[8] R. S. Blum. MIMO capacity with interference. *IEEE Journal on Sel. Areas in Comm.*, 21(5):793–801, June 2003.

[9] G. Caire and D. Tuninetti. The throughput of hybrid-ARQ protocols for the Gaussian collision channel. *IEEE Trans. on Inf. Theory*, 47(5):1971–1988, July 2001.

[10] V. Chandrasekhar and J. G. Andrews. Coverage in multi-antenna two-tier networks. *IEEE Trans. on Wireless Comm.*, 8(10):5314–5327, Oct. 2009.

[11] B. Chen and M. J. Gans. MIMO communications in ad hoc networks. *IEEE Trans. on Signal Processing*, 54(7):2773–2783, July 2006.

[12] W. Choi, N. Himayat, S. Talwar, and M. Ho. The effect of co-channel interference on spatial diversity techniques. *IEEE Wireless Comm. and Net. Conf.*, pages 1936–1941, March, 2007.

[13] R. R. Choudhury, X. Yang, R. Ramanathan, and N. H. Vaidya. On designing MAC protocols for wireless networks using directional antennas. *IEEE Trans. Mobile Comp.*, 5(5):477–491, May 2006.

[14] R. A. Comroe and D. J. Costello. ARQ schemes for data transmission in mobile radio systems. *IEEE Journal on Sel. Areas in Comm.*, 2(4):473–481, July 1984.

[15] Department of Defense. Selected Acquisition Report: JTRS GMR. Website: Oct. 2012. www.dod.mil/pubs/foi/logistics_material_readiness/ acq_-bud_fin/SARs.html.

[16] A. Edelman. *Eigenvalues and Condition Numbers of Random Matrices*. PhD Thesis, Massachusetts Institute of Technology, 1989.

[17] R. H. Etkin, D. Tse, and H. Wang. Gaussian interference channel capacity to within one bit. *IEEE Trans. on Inf. Theory*, 54(12):5534–5562, 2008.

[18] L. R. Ford and D. R. Fulkerson. *Flows in Networks*. USA: Princeton University Press, 1962.

[19] H. E. Gamal, G. Caire, and M. O. Damen. The MIMO ARQ channel: diversity-multiplexing-delay tradeoff. *IEEE Trans. on Inf. Theory*, 52(8):3601–3621, Aug. 2006.

[20] R. K. Ganti and J. G. Andrews. A new method for computing the transmission capacity of non-Poisson wireless networks. In *Proc., IEEE Intl. Symposium on Information Theory*, Austin, TX, 2010.

[21] R. K. Ganti, J. G. Andrews, and M. Haenggi. High-SIR transmission capacity of wireless networks with general fading and node distribution. *IEEE Transactions on Information Theory*, 57(5):3100–3116, May 2011.

[22] R. K. Ganti, F. Baccelli, and J. G. Andrews. Series expansion for interference in wireless networks. *IEEE Trans. on Inf. Theory*, 58(4):2194–2205, Apr. 2012.

[23] R. K. Ganti and M. Haenggi. Interference and outage in clustered wireless ad hoc networks. *IEEE Trans. on Inf. Theory*, 55(9):4067–4086, Sept. 2009.

[24] A. J. Goldsmith. *Wireless Communications*. Cambridge University Press, 2005.

[25] S. Govindasamy. *Multiple-Antenna Systems in Ad-Hoc Wireless Networks*. PhD Thesis, Massachusetts Institute of Technology, 2008.

[26] S. Govindasamy, D. W. Bliss, and D. H. Staelin. Spectral efficiency in single-hop ad-hoc wireless networks with interference using adaptive antenna arrays. *IEEE Journal on Sel. Areas in Comm.*, 25(7):1358–1369, Sept. 2007.

[27] S. Govindasamy, D. W. Bliss, and D. H. Staelin. Asymptotic spectral efficiency of multiantenna links in wireless networks with limited Tx CSI. *IEEE Trans. on Inf. Theory*, 58(8):5375–5387, Aug. 2012.

[28] I. S. Gradshteyn and I. M. Ryzhik. *Table of Integrals, Series, and Products*. London: Academic Press, 6th edition, 2000.

[29] M. Grossglauser and D. Tse. Mobility increases the capacity of ad-hoc wireless networks. *IEEE/ACM Trans. on Networking*, 10:477–486, Aug. 2002.

[30] P. Gupta and P. R. Kumar. The capacity of wireless networks. *IEEE Trans. on Inf. Theory*, 46(2):388–404, Mar. 2000.

[31] M. Haenggi. Analysis and design of diversity schemes for ad hoc wireless networks. *IEEE Journal on Sel. Areas in Comm.*, 23(1):19–27, Jan. 2005.

[32] M. Haenggi, J. G. Andrews, F. Baccelli, O. Dousse, and M. Franceschetti. Stochastic geometry and random graphs for the analysis and design of wireless networks. *IEEE Journal on Sel. Areas in Comm.*, 27:1029–1046, Sept. 2009.

[33] M. Haenggi and R. K. Ganti. Interference in large wireless networks. *Foundations and Trends® in Networking*, 3(2):127–248, 2008.

[34] A. Hasan and J. G. Andrews. The guard zone in wireless ad hoc networks. *IEEE Trans. on Wireless Comm.*, 6(3):897–906, Mar. 2007.

[35] R. A. Horn and C. R. Johnson. *Matrix Analysis*. Cambridge: Cambridge University Press, 1985.

[36] K. Huang, J. G. Andrews, R. W. Heath, Jr., D. Guo, and R. Berry. Spatial interference cancelation for mobile ad hoc networks. *IEEE Trans. on Inf. Theory*, 58(3):1660–1676, Mar. 2012.

[37] A. M. Hunter and J. G. Andrews. Adaptive rate control over multiple spatial channels in ad hoc networks. In *Proc., Workshop on Spatial Stoch. Models for Wireless Net. (SpaSWiN)*, Berlin, Germany, Apr. 2008.

[38] A. M. Hunter, J. G. Andrews, and S. Weber. Transmission capacity of wireless ad hoc networks with spatial diversity. *IEEE Trans. on Wireless Comm.*, 7(12):5058–5071, Dec. 2008.

[39] H. Inaltekin, S. B. Wicker, M. Chiang, and H. V. Poor. On unbounded path-loss models: effects of singularity on wireless network performance. *IEEE Journal on Selected Areas in Communications (JSAC)*, 27(7):1078–1092, Sept. 2009.

[40] S. A. Jafar and M. Fakhereddin. Degrees of freedom for the MIMO interference channel. *IEEE Trans. on Inf. Theory*, 53(7):2637–2642, July 2007.

[41] L. Jiang and J. Walrand. A distributed CSMA algorithm for throughput and utility maximization in wireless networks. *IEEE/ACM Trans. on Networking*, 18(3):960–972, June 2010.

[42] L. Jiang and J. Walrand. Approaching throughput-optimality in distributed CSMA scheduling algorithms with collisions. *IEEE/ACM Trans. on Networking*, 19(3):816–829, June 2011.

[43] N. Jindal, J. G. Andrews, and S. Weber. Bandwidth partitioning in decentralized wireless networks. *IEEE Transactions on Wireless Communications*, 7(12):5408–5419, Dec. 2008.

[44] N. Jindal, J. G. Andrews, and S. Weber. Multi-antenna communication in ad hoc networks: achieving MIMO gains with SIMO transmission. *IEEE Transactions on Communications*, 59(2):529–540, Feb. 2011.

[45] N. Jindal, S. Weber, and J. G. Andrews. Fractional power control for

decentralized wireless networks. *IEEE Transactions on Wireless Communications*, 7(12):5482–5492, Dec. 2008.

[46] W. P. Johnson. The curious history of Faà di Bruno's formula. In *Amer. Math. Monthly*, volume 109, pages 217–234, 2002.

[47] M. Kang and M.-S. Alouini. Largest eigenvalue of complex Wishart matrices and performance analysis of MIMO MRC systems. *IEEE Journal on Sel. Areas in Comm.*, 21(3):418–426, Apr. 2003.

[48] M. Kang and M.-S. Alouini. A comparative study on the performance of MIMO MRC systems with and without cochannel interference. *IEEE Trans. on Comm.*, 52(8):1417–1425, Aug. 2004.

[49] M. Kaynia, G. Oien, and N. Jindal. Impact of fading on the performance of ALOHA and CSMA. In *Proc., IEEE Signal Proc. Adv. in Wireless Comm. (SPAWC)*, Italy, June 2009.

[50] C. G. Khatri. Distribution of the largest or the smallest characteristic root under null hypothesis concerning complex multivariate normal populations. *Ann. Math. Stat.*, 35:1807–1810, Dec. 1964.

[51] Y. Kim, F. Baccelli, and G. de Veciana. Spatial reuse and fairness of mobile ad-hoc networks with channel-aware CSMA protocols. *IEEE Trans. on Inf. Theory*, 58(12), Dec. 2012.

[52] J. F. C. Kingman. *Poisson Processes.* USA: Oxford University Press, 1993.

[53] L. Kleinrock and J. Silvester. Spatial reuse in packet radio networks. *Proc. of the IEEE*, 75(1):156–167, Jan. 1987.

[54] L. Kleinrock and F. Tobagi. Packet switching in radio channels: Part I - carrier sense multiple-access models and their throughput-delay characteristics. *IEEE Trans. on Comm.*, 23(12):1400–1416, Dec. 1975.

[55] M. Kountouris and J. G. Andrews. Transmission capacity scaling of SDMA in wireless ad hoc networks. In *IEEE Information Theory Workshop (ITW)*, pages 534–538, Taormina, Italy, Oct. 2009.

[56] M. Kountouris and J. G. Andrews. Capacity bounds on multiuser MIMO transmission in random wireless networks. *under revision, IEEE Transactions on Information Theory*, 2010.

[57] E. G. Larrsson and P. Stoica. *Space-Time Block Coding for Wireless Communications*. Cambridge: Cambridge University Press, 2003.

[58] O. Leveque and I. E. Telatar. Information-theoretic upper bounds on the capacity of large extended ad hoc wireless networks. *IEEE Trans. on Inf. Theory*, 51(3):858–865, Mar. 2005.

[59] X. Lin, N. Shroff, and R. Srikant. A tutorial on cross-layer optimization in wireless networks. *IEEE Journal on Sel. Areas in Comm.*, 24(8):1452–1463, Aug. 2006.

[60] J. Ling, D. Chizhik, D. Samardzija, and R. Valenzuela. Peer-to-peer MIMO radio channel measurements in a rural area. *IEEE Trans. on Wireless Comm.*, 6(9):3229–3237, Sept. 2007.

[61] C. H. Liu and J. G. Andrews. Multicast capacity scaling of wireless networks with multicast outage. In *Proc., IEEE Intl. Symposium on Information Theory*, Austin, Texas, June 2010.

[62] C. H. Liu and J. G. Andrews. Distributed SIR-aware scheduling in large-scale wireless ad hoc networks. *submitted to IEEE Transactions on Information Theory*, 2011.

[63] X. Liu and M. Haenggi. Throughput analysis of fading sensor networks with regular and random topologies. *EURASIP J. of Wireless Comm. and Net.*, 4:554–564, Aug. 2005.

[64] R. Louie, M. McKay, N. Jindal, and I. Collings. Spatial multiplexing with MMSE receivers in ad hoc networks. In *IEEE International Conference on Communications (ICC)*, Kyoto, Japan, June 2011.

[65] R. H. Y. Louie, M. McKay, and I. B. Collings. Spatial multiplexing with zero-forcing receivers in ad hoc networks. *Proc., IEEE Intl. Conf. on Communications*, June 2009.

[66] R. H. Y. Louie, M. R. McKay, and I. B. Collings. Open-loop spatial multiplexing and diversity communications in ad hoc networks. *IEEE Trans. on Inf. Theory*, 57(1):317–344, Jan. 2011.

[67] A. Lozano and N. Jindal. Transmit diversity vs. spatial multiplexing in modern MIMO systems. *IEEE Trans. on Comm.*, 9(1):186–197, Jan. 2010.

[68] M. L. Mehta. *Random Matrices*. Kluwer Academic Press, 3rd edition, 2003.

[69] M. J. Neely and E. Modiano. Capacity and delay tradeoffs for ad-hoc mobile networks. *IEEE Trans. on Inf. Theory*, 51(6):1917–1937, June 2005.

[70] R. Nelson and L. Kleinrock. The spatial capacity of a slotted ALOHA multihop packet radio network with capture. *IEEE Trans. on Comm.*, 32(6):684–694, June 1984.

[71] J. Ni, B. Tan, and R. Srikant. Q-CSMA: queue-length based CSMA/CA algorithms for achieving maximum throughput and low delay in wireless networks. *IEEE/ACM Trans. on Networking*, 20(3):825–836, June 2012.

[72] B. Nosrat-Makouei, J. G. Andrews, and R. W. Heath, Jr. User admission in MIMO interference alignment networks. In *Proc., IEEE Intl. Conf. on Acoustics, Speech, and Sig. Proc. (ICASSP)*, Prague, May 2011.

[73] A. Ozgur, R. Johari, D. Tse, and O. Leveque. Information theoretic operating regimes of large wireless networks. *IEEE Trans. on Inf. Theory*, 56(1):427–437, Jan. 2010.

[74] A. Ozgur, O. Leveque, and D. Tse. Hierarchical cooperation achieves optimal capacity scaling in ad hoc networks. *IEEE Trans. on Inf. Theory*, 12(53), Dec. 2007.

[75] A. Ozgur, O. Leveque, and D. Tse. Throughput-delay tradeoff for hierarchical cooperation in ad hoc wireless networks. *Proc. IEEE Intl. Conf. on Comm.*, June 2008.

[76] A. Paulraj, R. Nabar, and D. Gore. *Introduction to Space-Time Wireless Communications*. Cambridge: Cambridge University Press, 2003.

[77] R. Ramanathan, J.Redi, C. Santivanez, D. Wiggins, and S. Polit. Ad hoc networking with directional antennas: a complete solution. *IEEE Journal on Sel. Areas in Comm.*, 23(3):496–506, Mar. 2005.

[78] S. Ray, J. Carruthers, and D. Starobinski. RTS/CTS-induced congestion in ad-hoc wireless LANs. *Proc., IEEE Wireless Networking and Comm. Conf.*, pages 1516–1521, 2003.

[79] F. Rosas. Nakagami-m approximations for MIMO SVD transmissions. *Intl. Workshop on Smart Antennas*, Mar. 2012.

[80] A. Shah and A. M. Haimovich. Performance analysis of maximal ratio combining and comparison with optimum combining for mobile radio communications with co-channel interference. *IEEE Trans. on Veh. Tech.*, 49(4):1454–1463, July 2000.

[81] J. Silvester and L. Kleinrock. On the capacity of multihop slotted ALOHA networks with regular structure. *IEEE Trans. on Comm.*, 31(8):974–982, Aug. 1983.

[82] P. S. Sindhu. A retransmission error-control technique for packet broadcasting channels. *IEEE Trans. on Comm.*, 25:473–479, May 1977.

[83] M. R. Souryal, B. R. Vojcic, and R. L. Pickholtz. Adaptive modulation in ad hoc DS/CDMA packet radio networks. *IEEE Trans. on Comm.*, 54(4):714–725, Apr. 2006.

[84] K. Stamatiou, J. G. Proakis, and J. R. Zeidler. Evaluation of MIMO techniques in frequency hopped-multi-access ad hoc networks. *Proc. IEEE Globecom*, Nov. 2007.

[85] K. Stamatiou, J. G. Proakis, and J. R. Zeidler. Information efficiency of ad hoc networks with FH-MIMO receivers. *Proc. IEEE Intl. Conf. on Comm.*, June 2007.

[86] K. Stamatiou, J. G. Proakis, and J. R. Zeidler. Spatial multiplexing in random wireless networks. *Adv. in Electr. and Telecomm.*, 1(1):5–12, Apr. 2010.

[87] D. Stoyan, W. Kendall, and J. Mecke. *Stochastic Geometry and Its Applications*. John Wiley and Sons, 2nd edition, 1996.

[88] G. L. Stuber. *Principles of Mobile Communication*. Boston: Kluwer Academic Publishers, 2nd edition, 2001.

[89] I. E. Telatar. Capacity of multi-antenna Gaussian channels. *Eur. Trans. Telecomm. ETT*, 10(6):585–596, Nov. 1999.

[90] F. Tobagi and L. Kleinrock. Packet switching in radio channels: Part II - the hidden terminal problem in carrier sense multiple-access and the busy-tone solution. *IEEE Trans. on Comm.*, 23(12):1417–1433, Dec. 1975.

[91] F. Tobagi and L. Kleinrock. Packet switching in radio channels: Part III - polling and (dynamic) split-channel reservation multiple access. *IEEE Trans. on Comm.*, 24(8):832–844, Aug. 1976.

[92] S. Toumpis and A. J. Goldsmith. Capacity regions for wireless ad hoc networks. *IEEE Trans. on Wireless Comm.*, 2(4):736–748, July 2003.

[93] R. Vaze. Throughput-delay-reliability tradeoff with ARQ in wireless ad hoc networks. *IEEE Transactions on Wireless Communications*, 10(7):2142–2149, July 2011.

[94] R. Vaze and R. W. Heath, Jr. Transmission capacity of ad-hoc networks with multiple antennas using transmit stream adaptation and interference cancellation. *IEEE Trans. on Inf. Theory*, 58(2):780–792, Feb. 2012.

[95] S. Vishwanath, N. Jindal, and A. Goldsmith. Duality, achievable rates and sum rate capacity of the Gaussian MIMO broadcast channel. *IEEE Transactions on Information Theory*, 49(10):2658–2668, Oct. 2003.

[96] S. Weber, J. Andrews, and N. Jindal. The effect of fading, channel inversion, and threshold scheduling on ad hoc networks. *IEEE Trans. on Inf. Theory*, 53(11):4127–4149, Nov. 2007.

[97] S. Weber, J. G. Andrews, and N. Jindal. An overview of the transmission capacity of wireless networks. *IEEE Transactions on Communications*, 58(12):3593–3604, Dec. 2010.

[98] S. Weber, X. Yang, J. G. Andrews, and G. de Veciana. Transmission capacity of wireless ad hoc networks with outage constraints. *IEEE Trans. on Inf. Theory*, 51(12):4091–4102, Dec. 2005.

[99] S. P. Weber and J. G. Andrews. Transmission capacity of wireless networks. *Foundations and Trends® in Wireless Networks*, 5(2-3):109–281, 2012.

[100] P. W. Wolniansky, G. J. Foschini, G. D. Golden, and R. A. Valenzuela. V-BLAST: an architecture for realizing very high data rates over the rich-scattering wireless channel. *URSI Intl. Symp. on Sig., Sys., and Electr.*, pages 295–300, Oct. 1998.

[101] P. Wu and N. Jindal. Coding versus ARQ in fading channels: how reliable should the PHY be? *IEEE Trans. on Comm.*, 59(12):3363–3374, Dec. 2011.

[102] X. Wu, S. Tavildar, S. Shakkottai, T. Richardson, L. Junyi, R. Laroia, and A. Jovicic. FlashLinQ: A synchronous distributed scheduler for peer-to-peer ad hoc networks. *Proc., Allerton Conf. on Comm., Control, and Computing*, Oct. 2012.

[103] Y. Wu, R. H. Y. Louie, M. R. McKay, and I. B. Collings. Generalized framework for the analysis of linear MIMO transmission schemes in de-

centralized wireless ad hoc networks. *IEEE Trans. on Wireless Comm.*, 11(8):2815–2827, Aug. 2012.

[104] L. Xie and P. R. Kumar. A network information theory for wireless communication: scaling laws and optimal operation. *IEEE Trans. on Inf. Theory*, 50(5):748–767, May 2004.

[105] S. Ye and R. S. Blum. On the rate regions for wireless MIMO ad hoc networks. In *IEEE Fall Vehicular Technology Conference (VTC)*, volume 3, pages 1648–1652, Los Angeles, CA, Sept. 2004.

[106] X. Yu, R. de Moraes, H. Sadjadpour, and J. J. Garcia-Luna-Aceves. Capacity of MIMO mobile wireless ad hoc networks. *Wirelesscomm, Maui, HI*, 2:1053–1058, June 2005.

[107] H. Zheng, A. Lozano, and M. Haleem. Multiple ARQ processes for MIMO systems. *EURASIP Journal on Appl. Sig. Proc.*, (5):772–782, 2004.

[108] L. Zheng and D. Tse. Diversity and multiplexing: A fundamental tradeoff in multiple antenna channels. *IEEE Trans. on Inf. Theory*, 49(5):1073–1096, May 2003.